DISSERTATION

PUMP-FREE MAGNETOPHORESIS FOR IMPROVED POINT-OF-CARE DIAGNOSTICS

Submitted by

Zachary D. Call

Department of Chemistry

In partial fulfillment of the requirements

For the Degree of Doctor of Philosophy

Colorado State University

Fort Collins, Colorado

Summer 2022

Doctoral Committee:

Advisor: Charles S. Henry

Melissa M. Reynolds
David S. Dandy
Christopher D. Snow

ABSTRACT

PUMP-FREE MAGNETOPHORESIS FOR IMPROVED POINT-OF-CARE DIAGNOSTICS

Infectious diseases are one of the largest health burdens for low-income countries and claim millions of lives every year. The loss of life in low-income countries is largely due to the lack of access to preventative healthcare and appropriate diagnostic testing. Several health agencies have recognized the need for improved diagnostics to reduce the burden of infectious diseases. The following works described in this thesis are focused on improving the capabilities of point-of-care (POC) testing to improve patient healthcare.

Microfluidic devices are a popular approach for diagnostics because they offer reduced assay times, reduced sample volume, and are small (<10 cm). Additionally, microfluidic devices can be used with magnetophoresis to improve sensitivity and specificity. However, traditional microfluidic devices have difficulty translating to the POC because of tedious and expensive fabrication. Microfluidic paper-based analytical devices (μPADs) are a popular alternative to traditional microfluidics due to the natural capillary action through cellulose fibers and simple fabrication. μPADs are portable, low-cost, and do not require external instrumentation, making them ideal for POC settings. However, μPADs often suffer from poor analytical performance resulting in failing to translate to POC testing. In Chapters 2, 3 and 4 of this thesis, I described combining μPADs with magnetophoresis to improve the analytical performance without sacrificing the advantages of μPADs. Coupling magnetophoresis with μPADs is a novel approach and was not reported until the publication of chapter two.

Chapter 2 of this thesis describes the first reported example of paper-based magnetophoresis. Magnetophoresis has always needed external pumps to drive flow, however we demonstrate the ability to perform magnetophoresis completely pump-free in a μPAD. We demonstrated the ability to detect *E. coli* at 10^5 colony forming units (CFU)/mL with a fluorescent label in a pooled human urine sample. Chapter 3, describes improvements to the device described in chapter 2. The limit of detection was improved by three orders of magnitude and calculated at 4.67×10^2 CFU/mL in pooled human urine, which is below detection limits for commercial urinary tract infection tests. Colorimetric detection was used instead of fluorescence detection to eliminate any instrumentation needed and create an easy read-by-eye assay. Additionally, the device design was modified to incorporate a burst valve to generate more consistent laminar flow and simplify user-end steps. We envision this technology to be used a platform for future paper-based devices incorporating magnetophoresis for improved POC devices.

In Chapter 4 of this thesis, we describe a new platform for microfluidic magnetophoresis that simplifies user-end steps further through a simple magnet sliding operation. Here we introduce a Magnetophoresis Slider Assay (MeSA) for sequential binding and washing steps without the need for any external instrumentation. A competitive biotin assay and a sandwich immunoassay are demonstrated to display the functionality of this new platform. The limit of detection was calculated at 1.62×10^3 CFU/mL using colorimetric detection. The MeSA is extremely user-friendly, provides sensitive and rapid results (<15 min), and can be applied to a wide range of applications.

ACKNOWLEDGEMENTS

First, I would like to thank my family for their support throughout my Ph.D: My father, David Call, for his unconditional guidance and support; my brother, Brandon Call, for his constant support and for coming to visit me here in Colorado even when I couldn't make it back to Maryland; my stepmother and stepsisters for their support and good time when I go back to visit Maryland.

Secondly, I would like to thank my advisor, Dr. Chuck Henry, for his constant support, guidance, and mentorship. I could not have asked for a better advisor during graduate school and I feel very fortunate to have been accepted into his group. I am very thankful for the countless brainstorming sessions, group meetings, and social events. Chuck has a created a great culture in his lab and that stems from his hard-work and dedication to his students. Chuck allowed me to travel to Hong Kong to present my research at Gordon Research Conference and that trip will always be a highlight of my Ph.D. Chuck cares deeply about his student's development and I know I have become a better scientist, writer, and public speaker because of it. The Henry group has been an amazing place to work and I will always be thankful for my time at CSU. I only hope that my next boss will be half as good as Chuck.

Finally, I would like to thank the members of the Henry group for their support over the last five years. Everyone was always willing to help, edit papers, improve presentations, and help each other become a better scientist. I will miss the group lunches, fishing trips, and golf trips. Specifically, I would like to thank Dr. Cody Carrell, for his constant support, friendship, and mentorship. Cody has been the best friend and mentor that I could have asked for.

TABLE OF CONTENTS

CHAPTER 1. INTRODUCTION

1.1 Global Health and Current Diagnostics

The Global Burden of Disease (GBD) project provides a tool to measure health loss by estimating the number of health life years lost globally.[1] GDB is commonly measured in terms of disability-adjusted life years (DALYs) that accounts for the years of healthy years lost due to mortality and disability as a result of disease. Globally, non-communicable diseases are the largest health burden, where cardiovascular diseases alone accounted for loss of almost 400 million DALYs in 2019. In comparison, communicable diseases (tuberculosis, HIV, malaria, etc.) accounted for the loss of 320 million DALYs in 2019.[2] Non-communicable diseases account for largest loss of DALYs in high income countries. However, communicable-diseases such as infectious diseases are the major cause of loss of DALYs in lower-income countries with the largest burden on Africa (Figure 1.1).[2-4] Moreover, in just the last two decades, pandemics such as the Ebola virus in 2013, cholera in 2015, zika virus in 2015, and most recently the corona virus pandemic in 2020 have claimed millions of lives.[5]

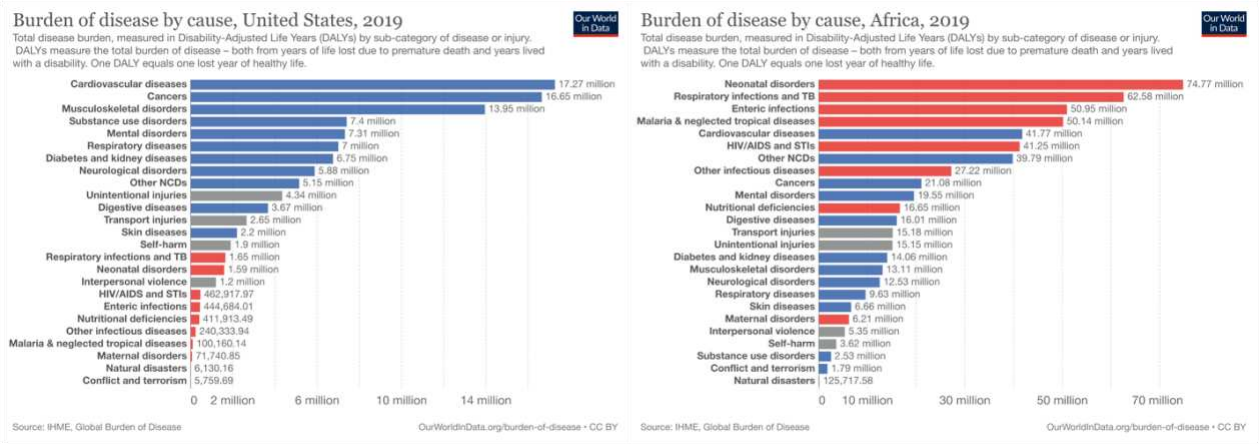

Figure 1.1 Comparison of the burden of disease in the United States to Africa in 2019 outlined by DALYs, where non-communicable diseases are shown in red and communicable diseases shown in blue with injuries shown in grey. One DALY equals one lost year of healthy life.[2]

The lack of appropriate access to healthcare accounts for large loss of DALYs in low income countries.[6] High income countries have access to current gold standard pathogen detection methods including culturing, western-blot (WB), polymerase chain reaction (PCR) or enzyme-linked immunosorbent assay (ELISA). [7] Culturing, PCR, and ELISA are highly sensitive methods but are expensive, time-consuming, and require trained personnel. However, low-income countries do not have access to these expensive laboratory techniques, and current low-cost diagnostic tools are inadequate creating a large health-care gap. Consequently, to prevent severe outcomes from infectious diseases in low-income countries, improved diagnostic tools are needed. The World Health Organization (WHO), Centers for Disease Control, and the Bill and Melissa Gates Foundation all recognize the need for improved and appropriate diagnostics to reduce DALYs resulting from infectious diseases in low-income countries.[8-10]

Point-of-Care (POC) testing is defined as testing that is performed near or at the site of the patient with result leading to improved quality of patient care.[11] In 2003, the WHO published criteria for the ideal diagnostic that can be applied to all levels of the healthcare system in developing and developed countries.[8, 12] These criteria is known as ASSURED and states tests should be **A**ffordable, **S**ensitive, **S**pecific, **U**ser-friendly, **R**apid and Robust, **E**quipment-free, and **D**eliverable to end users.[12, 13] The first POC tests for diagnosing malaria became commercially available in the early 1990s.[14] Since then, researchers have dedicated significant effort into the development of POC assays for infectious disease.[15] It is difficult for tests to meet all of the ASSURED criteria, so researchers focus on the most important for the given assay dependent upon the end goal. For example, tests that are the most accurate and sensitive (culturing, PCR,ELISA,WB) trade-off affordability and accessibility.[12, 16] In contrast, rapid diagnostic tests (e.g. lateral flow assays) are the most affordable and accessible but often trade-off sensitivity and

specificity.[12, 17, 18] A popular alternative is to combine microfluidic technology with laboratory based tests to meet the ASSURED criteria.[19] The development of improved diagnostics that meet these criteria are critical to reducing DALYs from infectious diseases in low-income countries.

1.2 Microfluidic Devices

The first microfluidic device was created in 1970 by Terry et al. for rapid gas analysis using a silicon wafer.[20] Microfluidic devices since then have expanded to using glass, quartz, poly(methylmethacrylate) (PMMA), and poly(dimethylsiloxane) (PDMS).[21, 22] Microfluidic devices are often small (< 10 cm x 10 cm), easy to operate, offer rapid detection, and have the ability to transport small volumes (μL, nL, pL) making them ideal for POC testing.[22-24] Since 1970, microfluidics have become a popular approach for pathogen detection because of these advantages.[22, 25] Immunoassays are a common pathogen detection method based on antibody and antigen interactions that allows for highly sensitive and specific detection.[9, 26, 27] The combination of immunoassays and microfluidics is popular for rapid and sensitive POC diagnostics. However, inconsistencies with antibody purity, low affinities, and binding site recognition result in decreased sensitivity and specificity.[28] To improve sensitivity, one method researchers use for signal amplification is to use enzyme/substrate systems.[29] Antibodies can be conjugated to enzymes through covalent cross-linkage to serve as detection antibodies. The substrate is converted into a colored product that can be turned over thousands of times by the enzyme, enhancing color formation and increasing sensitivity. Consequentially, this is why ELISA is such a popular method for pathogen detection. Enzymes such as horseradish peroxidase (HRP), alkaline phosphatase (AP), and beta-galactosidase (B-Gal) are some of the most common enzymes.[30] Each enzyme has numerous substrates available that need to be selected based on selectivity, color, and visualization for the given assay.[31] One of the most common enzyme/substrate pairing is HRP and 3,3',5,5' -

Tetramethylbenzidine (TMB) because of the availability of HRP and the enhanced sensitivity of TMB. Additionally, to increase sensitivity and specificity for enzyme/substrate systems, the use of magnetic beads is a popular approach. Primary or secondary antibodies can be conjugated to magnetic particles which then capture the target analyte. The magnetic complex can then be magnetically isolated to remove any unbound species.[32, 33] Microfluidic manipulation of magnetic particles can be used for a wide range of applications and is referred to magnetophoresis.[34]

1.2.1 Microfluidic Magnetophoresis

Microfluidic magnetophoresis is the process of using an external magnetic field to remove magnetic species from a sample a matrix during flow.[34] Microfluidic magnetophoresis has been used for a wide range of applications and is popular for biological assays because it is a gentle manipulation technique for whole cells, proteins, and large magnetic complexes.[34] To fully understand magnetophoresis we must recognize the parameters that govern the magnetic manipulation. Magnetism in materials is caused by the spin of electrons and their orbital motion around the nucleus.[35] Materials can be classified into three categories based on their number of unpaired electrons and their response to an external magnetic field, including diamagnetic, paramagnetic, and ferromagnetic. Diamagnetic materials do not have any unpaired electrons and are non-magnetic. Copper, zinc, gold, and water are some of the most common diamagnetic materials.[36] Paramagnetic materials have a small number of unpaired electrons and are weakly magnetic, examples are tungsten, chromium, and aluminum.[37] Ferromagnetic materials have a large number of unpaired electrons and are strongly magnetic, examples are iron, cobalt, and nickel.[35, 38] In the presence of a magnetic field, electrons of diamagnetic materials will become slightly unbalanced and small magnetic dipoles will be created that oppose the applied field. Inversely, electrons of paramagnetic and ferromagnetic materials will align with the applied field

and will be attracted toward the field.[34, 35, 39, 40] Upon removal of the applied field, electrons in paramagnetic materials will return to original orientation, whereas, electrons of ferromagnetic materials will remain aligned with the applied field. In this case, ferromagnetic materials such iron are referred to as permanent magnets because they will retain their magnetization.[35, 38] Some of the strongest permanent magnets can be made with alloys such as neodymium iron boron (NdFeB) being the most common permanent magnet. Magnetic susceptibility (χ) is a dimensionless measure of a materials degree of magnetization to an applied field. Diamagnetic materials have negative susceptibilities, and paramagnetic and ferromagnetic materials will have positive susceptibilities. However, Magnetic susceptibility is only one parameter we must consider to understand microfluidic magnetophoresis and the force acting on each magnetic particle during flow.[25, 35, 38-41] The following sections will describe the flow and magnetic forces that govern microfluidic magnetophoresis.

1.2.2 Magnetic Force

The magnetic field lines of a given magnet can only reach a certain density with a material and is quantified by the materials magnetic permeability (μ) and the number of field lines per area is given by the magnetic flux density (B). The flux density is inversely proportional to distance and so will decrease rapidly as distance increases. After taking the applied field into account, the force on a particle within a magnetic field depends on the volume of the particle (Vp) and the difference in magnetic susceptibilities between the particle itself and the surround medium ($\chi_p - \chi_m = \Delta\chi$). By combining these parameters the equation for magnetic force (F_{mag}) experienced by a particle can be expressed with Equation 1 shown below.[34, 39, 42]

$$F_{mag} = \frac{V_p \times \Delta\chi}{\mu_0} (\nabla \mathrm{B}) B \qquad (1)$$

B and ∇B are the magnetic flux density and the gradient respectively. A difference in magnetic susceptibilities is required to induce a magnetic force on a particle and can be either positive or negative. Magnetophoresis can be then classified into two categories, positive and negative. For positive magnetophoresis, the magnetization of the microparticles is greater than the magnetization of the surrounding media resulting in the microparticles migrating toward the magnetic field maxima. Positive magnetophoresis is the most common form and is used for particles with intrinsically magnetic properties such as red blood cells, magnetic microbeads, and magnetotactic bacteria. Negative magnetophoresis is a label-free technique where diamagnetic particles are suspended in a paramagnetic medium and migrate away from a high magnetic field. Negative magnetophoresis can be used to sort, focus, trap or mix diamagnetic particles by varying magnet placement through the flow cell.[25, 34, 43-45]

1.2.3 Microfluidics and Magnetic Particles

In microfluidic devices operating under laminar flow with a low Reynolds number the dominant force acting upon a magnetic microparticle is hydrodynamic drag force F_d which can be estimated from the stokes law and the relative velocity given by Equation 2.[34]

$$F_d = 6\pi\eta r\left(U_f - U_p\right) \times C_w \tag{2}$$

Where η (kg/ms) is the viscosity of the medium, r (m) is the radius of the microparticle, and U_f (m/s) and U_p (m/s) are the velocities of the fluid and the microparticles, respectively. C_w is a constant accounting for the effect the channel wall has on the drag force of the microparticle. The magnetic field is typically applied perpendicular to the flow channel where paramagnetic particles will become magnetized in the presence of the applied field and dragged into the field. The deflection of the magnetic particles, U_{defl} (m/s), can be described by the sum of the magnetically

induced flow velocity, U_{mag} (m/s) and F_d given by Equation 3.[34, 39, 42]

$$U_{defl} = U_{mag} + F_d \tag{3}$$

U_{mag} is the ratio of the magnetic force exerted on the microparticle by the magnetic field to the hydrodynamic drag force shown in Equation 4.[46]

$$U_{mag} = \frac{F_{mag}}{F_d} \tag{4}$$

When we insert Equation 1 into Equation 4, providing a consistent magnetic field and medium viscosity, U_{mag} becomes dependent upon the size of the microparticle and magnetic susceptibility. U_{mag} is proportional to the radius of the microparticle squared, and to the magnetic susceptibility of the given particle shown by Equation 5. Following this relationship, particles of different sizes and magnetic properties will be deflected from the laminar flow differently.[42, 46]

$$U_{mag} \propto r^2 \chi_p \tag{5}$$

1.2.4 Magnetophoresis Applications

By selecting magnetic microparticles of different sizes susceptibilities, complex separations are possible using microfluidics. The Pamme group pioneered the field of microfluidic magnetophoresis and developed multiple assays for pathogen detection. In 2004, Pamme et al. showed the ability to separate magnetic beads based on size and magnetic susceptibility, allowing for the possibility of multiplexed detection using varying magnetic beads sizes.[46] Nagasom et al. then used this technique to multiplex the assay to sort *S. typhimurium* and *E. coli* 0157 from spiked food broths.[47] Additionally in 2014, Phurimsak et al. demonstrated the ability to sequentially bind a capture antibody, analyte, and detection antibody to a magnetic bead to form immunomagnetic complex during automated flow in a glass microchip (Figure 1.2).[48] They demonstrated the ability

to perform a sandwich immunoassay during flow with magnetic beads to eliminate the need for tedious pipetting steps.[45, 49] However, traditional microfluidic devices require external pumps to drive flow, trained personnel, and are difficult to fabricate, limiting their portability to the POC and failing to meet the ASSURED criteria.[19, 34]

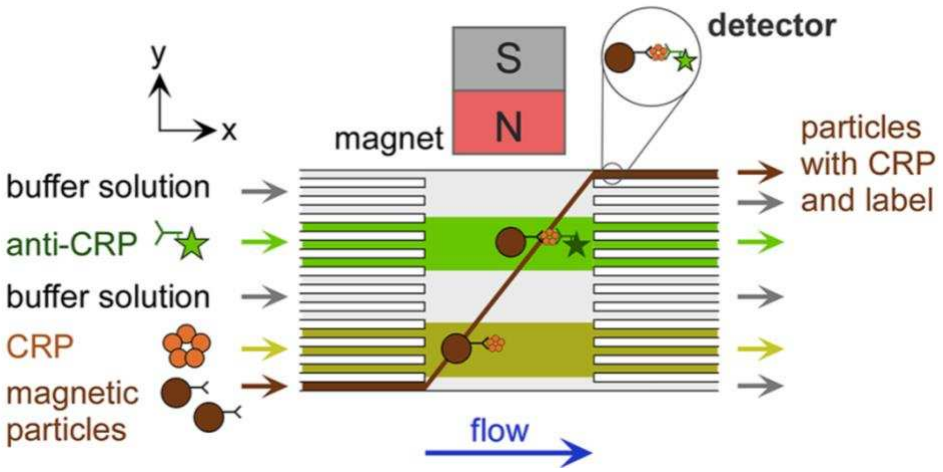

Figure 1.2. Schematic of microfluidic magnetophoresis used for sequential binding of magnetic immunocomplex for the detection of CRP.[48]

1.3 Paper-Based Microfluidics (Contents of this section were taken and combined from a published review article, in which I was listed as an author, with edits and modifications.)[29]

Paper-based microfluidics have been developed to address limitations of traditional microfluidic devices.[50, 51] Researchers have developed paper-based microfluidics for a wide range of applications resulting in tens of thousands of publications with point-of-care diagnostics remaining at the center for motivation.[9, 52, 53] Paper offers natural capillary action, a high surface to area ratio, and the ability to store reagents within the cellulose fibers making paper a popular choice for low-cost diagnostics.[13, 54] As a result, paper has long been used for chemical measurements, with the first example dating to the 1700s when litmus paper was invented using pH sensitive chromophores.[29] More recently, paper-based microfluidics have been developed for medical diagnostics, environmental testing, and food-based testing.[29, 55, 56]

Paper-based microfluidics for POC testing have shown tremendous potential for health monitoring. Paper diagnostics have been developed to detect biomarkers, proteins, pathogens, DNA, glucose, and several other analytes.[57-59] Additionally, paper-based devices are popular for environmental testing because they are portable where testing can be performed on-site without the need to transport sample to centralized laboratories.[29, 60, 61] The Henry group developed two distance-based paper-based microfluidics to quantify aluminum concentration in water samples without the for need pretreatment or preconcentration.[62] In that work a chemometer and radial device were developed using a ligand to treat the paper fibers to produce a fluorescent signal in the presence of Al (III).[62] Screening of chemical contaminants, bacteria, and whole viruses are a major concern for the food industry.[63] The WHO reports over 600 million people are diagnosed with foodborne illnesses with 420,000 deaths each year globally.[64] Paper-based devices for food safety are advantageous for low-cost, robust, and rapid on-site screening.[65, 66] Developing paper-based devices for bacteria detection is the most popular because *E. coli* and *Salmonella* cause over a million foodborne illnesses each year in the United States.[67, 68] The following sections will review paper-based technologies will corresponding fabrication and detection methods.

1.3.1 Lateral Flow Assays

The first Lateral flow assay (LFA) first appeared in 1959 and LFAs remain the most common form of paper-based devices for diagnostic testing.[29, 69, 70] LFAs have been developed to detect a wide range of analytes including antibodies, pathogens, nucleic acids, and biomarkers.[29, 71] LFAs operate using the natural capillary action of cellulose with the use of capture and detection antibodies for a colorimetric or fluorescent readout. Figure 1.3 shows a schematic of the basic operation of a traditional LFA using antibody coated nanoparticles. After sample is added to the

sample pad, flow initiates via capillary action and then flows into the capture membrane where the capture antibodies are stored.[29, 69, 71]

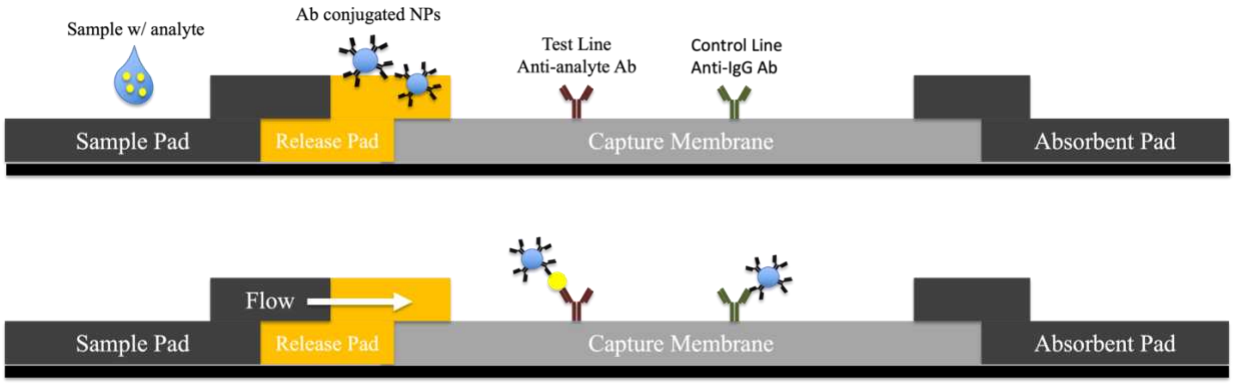

Figure 1.3. Schematic of traditional lateral flow assay assembly and binding operation.

The home pregnancy test and more recently the COVID-19 home test kits are possibly the most impactful LFAs that have been developed.[72] However, arguably the most impactful POC device is the blood glucose monitor initially developed in the 1970s.[73] It operates using the same technology as a LFA with immobilized reagents on a test strip, however, electrodes are incorporated into the strips to improve sensitivity and specificity.[29, 57] A small drop is blood is added and then reacts with an immobilized enzyme (glucose oxidase) and the electrodes measure the current produced from the oxidation of glucose and provides a rapid readout of current glucose levels.[57, 74] The test strips are inexpensive (< $0.10) and are stable for up to a year.[75] Millions of these tests are used daily all over the world and represent the gold standard for POC testing.[29, 60] Flow generated in these test strips are all non-directed, meaning that once sample is added flow initiates and stays in a singular flow path. To create more complex POC testing able of detecting for multiple analytes at once with stored reagents, researchers needed to be able to direct flow in paper with defined channels as in traditional microfluidics.

1.3.2 Microfluidic Paper-Based Analytical Devices

In 2007, the Whitesides group introduced the first example of paper-based microfluidics fabricated using a photoresist able to detect glucose and presence of proteins simultaneously.[76] This allowed fluid to be directed to multiple detection zones to where associated reagents were stored in the cellulose. In 2009, Carrilho et al. demonstrated the use of wax printing to create hydrophobic channel barriers to replace the more complicated fabrication of photoresist.[50] Herein they showed that wax printing is a cheap and simple fabrication to create paper-based microfluidics and coined the term microfluidic paper-based analytical devices (μPADs).

1.3.3 Fabrication

The first example of paper with a fluidic channel was introduced in 1949 by Müller and Clegg.[77] They created paraffin-patterned paper by melting paraffin and then transferring it to filter paper. The transferred paraffin created a hydrophobic channel to direct flow for automated paper chromatography. Then in 2007, the Whitesides' group mainstreamed the ability of paper-based microfluidics using photolithography with a photoresist to create fluid channels. Photolithography involves complex fabrication and expensive equipment and reagents limiting the application for mass production and translating to the POC.[78] This led them to move to cheaper fabrication with wax-printing and since then many fabrication techniques have been introduced.

μPADs can fabricated by either using patterned hydrophobic barriers to define fluid channels or to cut the paper to the fluid channel design desired.[79] These methods include, photolithography, wax printing, screen-printing, inkjet printing, laser toner printing, stamping, wax-dipping, drawing, and laser etching and are outlined in Table 1.1.[78, 80] Wax printing has been the most common fabrication method since 2009, however the commercial printer used for this

technique was discontinued in 2017.[80, 81] These printers are now hard to come by and the wax for the printers either has to molded independently or bought from a third party. Thus, wax printing has seen a decline since 2017 and alternative fabrication methods are needed. Two of the most popular alternatives to wax printing are inkjet and laser toner printing.[78, 81] Multiple ink materials such as, alkenyl ketene dimer (AKD) and UV curable acrylates have used with μPADs.[29, 60, 80] Laser toner printing is a faster method than inkjet and is advantageous for large scale fabrication but requires high temperatures that can damage the paper. Other non-printing techniques such as stamping, wax dipping or drawing are excellent for rapid prototyping of μPADs. However, these fabrication techniques suffer from poor resolution when compared to other methods. Lateral spreading of the patterning reagents within the paper also creates large variability in channel dimensions.[29, 60, 82] Laser cutting using a CO_2 laser is often used with commercial hydrophobic coated paper (parchment paper/wax paper). Laser cutting can also be used with standard hydrophilic paper but backings are required to enhance device capability.[80]

Table 1.1 Overview of paper-based microfluidic fabrication techniques and advantages and disadvantages associated to each method.

Fabrication Technique	Patterning Agent	Advantages	Disadvantages
Photolithography	Photoresist	High resolution	Requires organic solvents Expensive Tedious fabrication
Inkjet printing	Permanent marker ink Alkenyl ketene dimer (AKD)	Prototyping Inexpensive High resolution	Not suitable for mass production
Laser toner printing	Powder composite toner	Rapid Robust Simple	Low resolution High temperatures
Wax printing	Wax	Inexpensive Rapid Simple process	Low resolution Discontinued commercial printers
Laser cutting	Hydrophobic paper	High resolution Versatile	Complicated fabrication
Screen printing	Varnish paint solutions Wax	Inexpensive	Need a patterned mesh Not suitable for prototyping
Wax dipping	Wax	Circumvents need for discontinued wax printer	Not compatible with organic solvents/surfactants
Stamping	PDMS Ink	Inexpensive	Low resolution Not suitable for prototyping

1.3.4 Detection Methods

With the wide range of fabrication techniques there is also a wide range of detection methods used for μPADs. Since the introduction of μPADs by the Whitesides group with colorimetric detection, other groups have investigated alternative detection methods including, electrochemical, and fluorescence.[62, 83-85]

1.3.4.1 Colorimetry

Colorimetric detection remains the most common method for paper-based devices due to several advantages for POC diagnostics.[86, 87] Paper offers a white background for high contrast to color change for good signal-to-noise ratio.[88] Colorimetric detection can be used for qualitative or quantitative measurements to avoid the use of any external instrumentation. Color changes can be achieved by pH sensitive probes, enzymatic conversion of substrates, and aggregation of NPs.[87] Litmus paper using pH sensitive dyes, either weak acids or bases are cheap, and relatively stable but do not provide a quantitative readouts.[89] Enzymatic conversion of substrates provide sensitive and quantitative results and allow for correlation of analyte concentration to signal intensity.[90] Multiple enzyme-substrate pairs are readily available and can be selected based on optimal pH and specific activity.[31, 90] However, enzymes are susceptible to degradation and therefore not preferred for long term stability.[91] Nanoparticles are an alternative and have been widely used in lateral flow assays and μPADs and can be tuned based on size, shape and color of the NPs.[92] Anfossi et al. demonstrated the ability to use multicolored gold and silver NPs (AuNPs/AgNPs) in a multiplexed assay for the detection of food allergens.[93] Colorimetric detection methods can be used to detect a wide range of analytes making them ideal for POC diagnostics.[94]

1.3.4.2 Electrochemistry

Electrochemical detection is an alternative that offers improved sensitivity and specificity over colorimetry. In 2009, the Henry group published the first demonstration of electrochemical detection integrated with paper-based analytical devices. The detection of glucose, lactate, and uric acid in biological samples was demonstrated.[95] Since this electrochemical paper-based analytical devices (ePADs) have been integrated for the detection of multiple analytes from heavy metals to cardiovascular biomarkers.[56] Most ePADs consist of three-electrode systems with a working, counter and reference electrode. However, many techniques exist to incorporate the electrodes into paper-based devices including screen printing, stencil printing, heat-pressing, and microwires.[96-98] Various types of electrode materials have been used with ePADs such as gold, silver, platinum, and carbon. Electrodes can be surface modified with functional groups and antibodies increasing selectivity of assays. For example, Channon et al. demonstrated dithiol functionalized Au microwires for detection of intact Zika virus particles incorporated into a μPAD. However, the easiest electrochemical detection is the direct detection of electrochemically active analytes such as metals and redox active molecules.[99, 100]

1.3.4.3 Fluorescence

Fluorescence is another detection approach that can improve sensitivity over traditional colorimetric techniques.[101] Fluorescence occurs by a molecule absorbing energy and promoting electrons to a higher energy level and then the electron relaxes back to its ground state and emits a photon. The emitted photons can then be measured for intensity and correlated to the conjugated target analyte concentration. Fluorescence has highly sensitive emission profiles, spatial resolution, and high specificity making it a popular approach for detection.[102, 103] Fluorescence can be applied to qualitative or quantitative measurements making it a diverse detection method.

µPADs using fluorescence have ranged from heavy metals to pathogens.[85, 104, 105] There are several types of fluorescent probes that can be incorporated including fluorescent dyes (fluorophores), quantum dots, and other types of fluorescent small molecules.[29, 103] Fluorescent probes offer the ability to be quenched providing a "on" or "off" signal for simple qualitative measurements.[56, 106] Liang et al. reported a 3D paper-based microfluidic device using nitrogen-doped quantum dots as the fluorescence reporter for the highly sensitive "turn on" detection of H_2O_2 released from living cancer.[107] Fluorescence is a highly sensitive detection method but is often difficult to translate to the POC because external instrumentation is needed.[101] Additionally, some paper has autofluorescence properties that can interfere with detection of an analyte by increasing background signal.[108]

1.3.5 Shortcomings of Paper-Based Microfluidics

Paper has a long history for chemical analysis with a wide range of applications.[51] Paper-based microfluidics have had a large impact on diagnostic testing since the 1970s with the commercialization of LFAs.[71, 76, 109] Paper-based microfluidic technology has shown great potential, however paper devices are difficult to get commercialized because of inherent shortcomings. Poor detection limits, degradation of reagents, difficulty for multiplexed detection, and complicated user steps all limit these devices from becoming successful outside of laboratories.[22, 29] Focusing on improving sensitivity, multiplexed detection, and simplifying user steps are critical to create improved paper-based technologies to overcome the difficulty of commercialization.[16, 29, 56, 80] Improved paper-based devices need to be cost-effective, rapid and portable to translate to the POC. We believe that by combining the advantages of paper with other inexpensive materials such as transparency films and adhesives improved devices can be achieved.

1.4 Hybrid Paper-Based Microfluidic Devices

The natural capillary action of paper allows for fluid transport through cellulose fibers, however, it limits the transport of large objects such as bacteria or magnetic beads to flow freely.[110, 111] Multilayered paper-based devices to create hollow fluid channels was first reported in 2013 by Renault et al.[110] Here, fluid travels through hollow channels rather than through a cellulose network providing the ability for large particles to flow freely.[110] In 2018, Channon et al. expanded upon this with the development of multilayered µPADs fabricated using double-sided tape to create different hollow channel heights.[112] They demonstrated a 145-fold increase in flow rate when compared to single layer µPADs. Here, they reported the correlation between channel height and flow rate the ability to tune flow rate without the use of any external pumps. [112, 113] However, these multilayered devices still use the cellulose network of paper to drive flow as well as capillary action of the hollow channel. Particles and analytes can become trapped in the cellulose fibers reducing signal. To overcome this, recent work by the Henry group has reported multilayered devices fabricated using transparency film with double-sided adhesive (DSA) (Figure 1.4).[114]

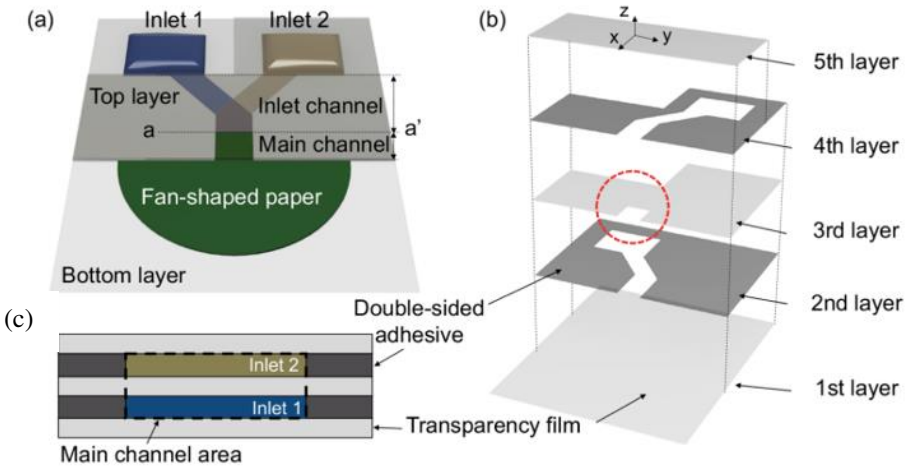

Figure 1.4. Schematic of hybrid µPADs. (a) Assembly of device with sample inlets and an inserted paper pump at the end of the device. (b) Device assembly with each layer outlined with alternating transparency and DSA layers. (c) Cross-sectional view from a-a' shown in (a).

These devices use DSA layers to define fluid channels that can be designed in computer aided design (CAD) software for highly accurate dimensions. By using transparency and DSA, the device channels do not become saturated with excess volume as in traditional μPADs. Paper waste pads can be inserted at the outlet of the channels to act as pumps to continuously wick fluid through the channel so large sample volumes can be used. Paper pads with stored reagents can be inserted into the devices to perform sequential reagent delivery opening the possibility for complex assays. The use of these improved hybrid devices will be described in detail in the following sections. Complex microfluidic magnetophoresis assay are described using these devices to demonstrate capability of hybrid μPADs. It is our hope with these devices to overcome long-term shortcomings of paper-based devices to create a new platform for POC devices.

1.5 Improved Devices Using Magnetophoresis

The following works describe improved devices that address existing gaps in the field of POC diagnostics. Currently, centralized laboratories, trained personnel and expensive instrumentation are needed for gold standard diagnostic testing. However, low-income countries do not have appropriate healthcare access causing a high mortality rate from infectious diseases. Here, we describe devices that take a step towards creating ideal diagnostic testing to meet the ASSURED criteria.

First, we demonstrate the first example of paper-based magnetophoresis free of any external pumps to drive flow. Magnetophoresis is a powerful tool for isolating and concentrating target analytes and has always needed external pumps to drive flow making it difficult to translate to the POC. We first demonstrated the ability to use pump-free magnetophoresis to detect *E. coli* from a human urine sample through fluorescence detection. We believe this is a pivotal step to make more sensitive and specific diagnostic testing available to low-resource settings.

Second, we improved the initial device to further refine this technology to the POC. Here we improved the limit of detection my three orders of magnitude for the detection of *E .coli* while also improving upon the device design to create a more user-friendly assay. We incorporated a capillary driven device free of any wax printing with several key features. A colorimetric enzyme/substrate system was used for easy read-by-eye analysis and making the device completely free of any instrumentation. Also, as will be described, a burst valve was created by tuning the device design to create more consistent generation of laminar flow. Additionally, we added a wash buffer reservoir behind the sample inlet to ensure all magnetic beads would reach the high magnetic field and thereby improving signal.

Third, we describe a new platform for microfluidic magnetophoresis that simplifies user-end steps through a simple magnet sliding operation. Here we introduce a magnetophoresis slider assay for sequential binding and washing steps without the need for any external instrumentation. A competitive biotin assay and a sandwich immunoassay are demonstrated to display the functionality of this new platform. The assay is extremely user-friendly and provides sensitive and rapid results (<15 min).

Since µPADs were established in 2007, there have been thousands of publications on µPADs but very few have been implemented into resource-limited settings. The lack of success for µPADs is attributed to the lack of sensitivity and complicated user-end steps. Here, we believe we have made critical progress in creating improved diagnostic tests to be used in low-resource settings.

REFERENCES

1. Vos, T.; Lim, S. S.; Abbafati, C.; Abbas, K. M.; Abbasi, M.; Abbasifard, M.; Abbasi-Kangevari, M.; Abbastabar, H.; Abd-Allah, F.; Abdelalim, A., Global burden of 369 diseases and injuries in 204 countries and territories, 1990–2019: a systematic analysis for the Global Burden of Disease Study 2019. *The Lancet* **2020,** *396* (10258), 1204-1222.
2. Roser, M.; Ritchie, H., Burden of disease. *Our world in data* **2021**.
3. Lopez, A. D.; Murray, C. C., The global burden of disease, 1990–2020. *Nature medicine* **1998,** *4* (11), 1241-1243.
4. Murray, C. J.; Lopez, A. D., Measuring the global burden of disease. *New England Journal of Medicine* **2013,** *369* (5), 448-457.
5. Zumla, A.; Hui, D. S., Emerging and reemerging infectious diseases: global overview. *Infectious Disease Clinics* **2019,** *33* (4), xiii-xix.
6. Yager, P.; Domingo, G. J.; Gerdes, J., Point-of-care diagnostics for global health. *Annu. Rev. Biomed. Eng.* **2008,** *10*, 107-144.
7. Yager, P.; Domingo, G. J.; Gerdes, J., Point-of-care diagnostics for global health. *Annual Review of Biomedical Engineering* **2008,** *10*, 107-144.
8. Organization, W. H., *First WHO Model List of Essential In Vitro Diagnostics: Volume 1017*. World Health Organization: 2019; Vol. 1017.
9. Nasseri, B.; Soleimani, N.; Rabiee, N.; Kalbasi, A.; Karimi, M.; Hamblin, M. R., Point-of-care microfluidic devices for pathogen detection. *Biosensors and Bioelectronics* **2018,** *117*, 112-128.
10. Enserink, M., Gates invests in diagnostics. *Science* **2003,** *300* (5624), 1355.
11. Briggs, C.; Guthrie, D.; Hyde, K.; Mackie, I.; Parker, N.; Popek, M.; Porter, N.; Stephens, C., Guidelines for point-of-care testing: haematology. *British Journal of Haematology* **2008,** *142* (6), 904-915.
12. Land, K. J.; Boeras, D. I.; Chen, X.-S.; Ramsay, A. R.; Peeling, R. W., REASSURED diagnostics to inform disease control strategies, strengthen health systems and improve patient outcomes. *Nature Microbiology* **2019,** *4* (1), 46-54.
13. Nilghaz, A.; Guan, L. Y.; Tan, W. R.; Shen, W., Advances of Paper-Based Microfluidics for Diagnostics-The Original Motivation and Current Status. *Acs Sensors* **2016,** *1* (12), 1382-1393.
14. Cunningham, J.; Jones, S.; Gatton, M. L.; Barnwell, J. W.; Cheng, Q.; Chiodini, P. L.; Glenn, J.; Incardona, S.; Kosack, C.; Luchavez, J., A review of the WHO malaria rapid diagnostic test product testing programme (2008–2018): performance, procurement and policy. *Malaria journal* **2019,** *18* (1), 1-15.
15. Chin, C. D.; Linder, V.; Sia, S. K., Commercialization of microfluidic point-of-care diagnostic devices. *Lab on a Chip* **2012,** *12* (12), 2118-2134.
16. Cate, D. M.; Adkins, J. A.; Mettakoonpitak, J.; Henry, C. S., Recent Developments in Paper-Based Microfluidic Devices. *Analytical Chemistry* **2015,** *87* (1), 19-41.
17. Smith, S.; Korvink, J. G.; Mager, D.; Land, K., The potential of paper-based diagnostics to meet the ASSURED criteria. *RSC advances* **2018,** *8* (59), 34012-34034.
18. Bissonnette, L.; Bergeron, M. G., Diagnosing infections--current and anticipated technologies for point-of-care diagnostics and home-based testing. *Clinical Microbiology and Infection* **2010,** *16* (8), 1044-1053.

19. Mairhofer, J.; Roppert, K.; Ertl, P., Microfluidic systems for pathogen sensing: a review. *Sensors* **2009,** *9* (6), 4804-4823.
20. Terry, S. C.; Jerman, J. H.; Angell, J. B., A gas chromatographic air analyzer fabricated on a silicon wafer. *IEEE transactions on electron devices* **1979,** *26* (12), 1880-1886.
21. Zhu, P.; Wang, L., Passive and active droplet generation with microfluidics: a review. *Lab on a Chip* **2017,** *17* (1), 34-75.
22. Whitesides, G. M., The origins and the future of microfluidics. *nature* **2006,** *442* (7101), 368-373.
23. Myers, F. B.; Lee, L. P., Innovations in optical microfluidic technologies for point-of-care diagnostics. *Lab on a Chip* **2008,** *8* (12), 2015-2031.
24. Bhagat, A. A. S.; Bow, H.; Hou, H. W.; Tan, S. J.; Han, J.; Lim, C. T., Microfluidics for cell separation. *Medical & Biological Engineering & Computing* **2010,** *48* (10), 999-1014.
25. Xia, N.; Hunt, T. P.; Mayers, B. T.; Alsberg, E.; Whitesides, G. M.; Westervelt, R. M.; Ingber, D. E., Combined microfluidic-micromagnetic separation of living cells in continuous flow. *Biomedical Microdevices* **2006,** *8* (4), 299-308.
26. Dye, C., After 2015: infectious diseases in a new era of health and development. *Philosophical Transactions of the Royal Society B-Biological Sciences* **2014,** *369* (1645).
27. Foudeh, A. M.; Didar, T. F.; Veres, T.; Tabrizian, M., Microfluidic designs and techniques using lab-on-a-chip devices for pathogen detection for point-of-care diagnostics. *Lab on a Chip* **2012,** *12* (18), 3249-3266.
28. Byrne, B.; Stack, E.; Gilmartin, N.; O'Kennedy, R., Antibody-based sensors: principles, problems and potential for detection of pathogens and associated toxins. *Sensors* **2009,** *9* (6), 4407-4445.
29. Carrell, C.; Kava, A.; Nguyen, M.; Menger, R.; Munshi, Z.; Call, Z.; Nussbaum, M.; Henry, C., Beyond the lateral flow assay: A review of paper-based microfluidics. *Microelectronic Engineering* **2019,** *206*, 45-54.
30. Volpe, G.; Draisci, R.; Palleschi, G.; Compagnone, D., 3, 3′, 5, 5′-Tetramethylbenzidine as electrochemical substrate for horseradish peroxidase based enzyme immunoassays. A comparative study. *Analyst* **1998,** *123* (6), 1303-1307.
31. Blake, C.; Gould, B. J., Use of enzymes in immunoassay techniques. A review. *Analyst* **1984,** *109* (5), 533-547.
32. Pappert, G.; Rieger, M.; Niessner, R.; Seidel, M., Immunomagnetic nanoparticle-based sandwich chemiluminescence-ELISA for the enrichment and quantification of E. coli. *Microchimica Acta* **2010,** *168* (1-2), 1-8.
33. Srisa-Art, M.; Boehle, K. E.; Geiss, B. J.; Henry, C. S., Highly Sensitive Detection of Salmonella typhimurium Using a Colorimetric Paper-Based Analytical Device Coupled with Immunomagnetic Separation. *Analytical Chemistry* **2018,** *90* (1), 1035-1043.
34. Alnaimat, F.; Dagher, S.; Mathew, B.; Hilal-Alnqbi, A.; Khashan, S., Microfluidics Based Magnetophoresis: A Review. *Chem. Rec.* **2018,** *18* (11), 1596-1612.
35. Reis, M., *Fundamentals of magnetism*. Elsevier: 2013.
36. Tarn, M. D.; Elders, L. T.; Peyman, S. A.; Pamme, N., Diamagnetic repulsion of particles for multilaminar flow assays. *Rsc Advances* **2015,** *5* (126), 103776-103781.
37. Spaldin, N. A., *Magnetic materials: fundamentals and applications*. Cambridge university press: 2010.
38. Lacroix, C.; Mendels, P.; Mila, F., *Introduction to frustrated magnetism: materials, experiments, theory*. Springer Science & Business Media: 2011; Vol. 164.

39. Pamme, N., Magnetism and microfluidics. *Lab on a Chip* **2006,** *6* (1), 24-38.
40. Peyman, S. A.; Iwan, E. Y.; Margarson, O.; Iles, A.; Pamme, N., Diamagnetic repulsion-A versatile tool for label-free particle handling in microfluidic devices. *Journal of Chromatography A* **2009,** *1216* (52), 9055-9062.
41. Yaman, S.; Anil-Inevi, M.; Ozcivici, E.; Tekin, H. C., Magnetic Force-Based Micro fluidic Techniques for Cellular and Tissue Bioengineering. *Front. Bioeng. Biotechnol.* **2018,** *6*, 29.
42. Pamme, N.; Wilhelm, C., Continuous sorting of magnetic cells via on-chip free-flow magnetophoresis. *Lab on a Chip* **2006,** *6* (8), 974-980.
43. Zborowski, M.; Ostera, G. R.; Moore, L. R.; Milliron, S.; Chalmers, J. J.; Schechter, A. N., Red blood cell magnetophoresis. *Biophysical journal* **2003,** *84* (4), 2638-2645.
44. Hejazian, M.; Nguyen, N. T., Negative magnetophoresis in diluted ferrofluid flow. *Lab on a Chip* **2015,** *15* (14), 2998-3005.
45. Deman, A.-L.; Le Roy, D., Magnetophoresis in Bio-Devices. In *Engineering of Micro/Nano Biosystems*, Springer: 2020; pp 309-361.
46. Pamme, N.; Manz, A., On-chip free-flow magnetophoresis: Continuous flow separation of magnetic particles and agglomerates. *Analytical Chemistry* **2004,** *76* (24), 7250-7256.
47. Ngamsom, B.; Esfahani, M. M.; Phurimsak, C.; Lopez-Martinez, M. J.; Raymond, J.-C.; Broyer, P.; Patel, P.; Pamme, N., Multiplex sorting of foodborne pathogens by on-chip free-flow magnetophoresis. *Analytica Chimica Acta* **2016,** *918*, 69-76.
48. Phurimsak, C.; Tarn, M. D.; Peyman, S. A.; Greenman, J.; Pamme, N., On-Chip Determination of C-Reactive Protein Using Magnetic Particles in Continuous Flow. *Analytical Chemistry* **2014,** *86* (21), 10552-10559.
49. Peyman, S. A.; Iles, A.; Pamme, N., Rapid on-chip multi-step (bio)chemical procedures in continuous flow - manoeuvring particles through co-laminar reagent streams. *Chemical Communications* **2008,** (10), 1220-1222.
50. Carrilho, E.; Martinez, A. W.; Whitesides, G. M., Understanding Wax Printing: A Simple Micropatterning Process for Paper-Based Microfluidics. *Analytical Chemistry* **2009,** *81* (16), 7091-7095.
51. Martinez, A. W.; Phillips, S. T.; Whitesides, G. M.; Carrilho, E., Diagnostics for the Developing World: Microfluidic Paper-Based Analytical Devices. *Analytical Chemistry* **2010,** *82* (1), 3-10.
52. Lei, K. F., Microfluidic systems for diagnostic applications: A review. *Journal of laboratory automation* **2012,** *17* (5), 330-347.
53. Pandey, C. M.; Augustine, S.; Kumar, S.; Kumar, S.; Nara, S.; Srivastava, S.; Malhotra, B. D., Microfluidics based point-of-care diagnostics. *Biotechnology journal* **2018,** *13* (1), 1700047.
54. Akyazi, T.; Basabe-Desmonts, L.; Benito-Lopez, F., Review on microfluidic paper-based analytical devices towards commercialisation. *Analytica Chimica Acta* **2018,** *1001*, 1-17.
55. Aimeida, M. I. G. S.; Jayawardane, B. M.; Kolev, S. D.; McKelvie, I. D., Developments of microfluidic paper-based analytical devices (mu PADs) for water analysis: A review. *Talanta* **2018,** *177*, 176-190.
56. Noviana, E.; Ozer, T.; Carrell, C. S.; Link, J. S.; McMahon, C.; Jang, I.; Henry, C. S., Microfluidic Paper-Based Analytical Devices: From Design to Applications. *Chemical Reviews* **2021**.

57. Gabriel, E. F. M.; Garcia, P. T.; Lopes, F. M.; Coltro, W. K. T., Based colorimetric biosensor for tear glucose measurements. *Micromachines* **2017,** *8* (4), 104.
58. Zhao, C.; Liu, X., A portable paper-based microfluidic platform for multiplexed electrochemical detection of human immunodeficiency virus and hepatitis C virus antibodies in serum. *Biomicrofluidics* **2016,** *10* (2), 024119.
59. Li, X.; Scida, K.; Crooks, R. M., Detection of hepatitis B virus DNA with a paper electrochemical sensor. *Analytical chemistry* **2015,** *87* (17), 9009-9015.
60. Noviana, E.; Ozer, T.; Carrell, C. S.; Link, J. S.; McMahon, C.; Jang, I.; Henry, C. S., Microfluidic paper-based analytical devices: From design to applications. *Chemical Reviews* **2021,** *121* (19), 11835-11885.
61. Quinn, C. W.; Cate, D. M.; Miller-Lionberg, D. D.; Reilly III, T.; Volckens, J.; Henry, C. S., Solid-phase extraction coupled to a paper-based technique for trace copper detection in drinking water. *Environmental science & technology* **2018,** *52* (6), 3567-3573.
62. Nguyen, M. P.; Kelly, S. P.; Wydallis, J. B.; Henry, C. S., Read-by-eye quantification of aluminum (III) in distance-based microfluidic paper-based analytical devices. *Analytica Chimica Acta* **2020,** *1100*, 156-162.
63. Scallan, E.; Hoekstra, R. M.; Angulo, F. J.; Tauxe, R. V.; Widdowson, M. A.; Roy, S. L.; Jones, J. L.; Griffin, P. M., Foodborne Illness Acquired in the United States-Major Pathogens. *Emerging Infectious Diseases* **2011,** *17* (1), 7-15.
64. Organization, W. H. *COVID-19 and food safety: guidance for food businesses: interim guidance, 07 April 2020*; World Health Organization: 2020.
65. Velusamy, V.; Arshak, K.; Korostynska, O.; Oliwa, K.; Adley, C., An overview of foodborne pathogen detection: In the perspective of biosensors. *Biotechnology advances* **2010,** *28* (2), 232-254.
66. Kant, K.; Shahbazi, M.-A.; Dave, V. P.; Tien Anh, N.; Chidambara, V. A.; Linh Quyen, T.; Dang Duong, B.; Wolff, A., Microfluidic devices for sample preparation and rapid detection of foodborne pathogens. *Biotechnology Advances* **2018,** *36* (4), 1003-1024.
67. Scallan, E.; Hoekstra, R. M.; Angulo, F. J.; Tauxe, R. V.; Widdowson, M.-A.; Roy, S. L.; Jones, J. L.; Griffin, P. M., Foodborne illness acquired in the United States—major pathogens. *Emerging infectious diseases* **2011,** *17* (1), 7.
68. Carrell, C. S.; Wydallis, R. M.; Bontha, M.; Boehle, K. E.; Beveridge, J. R.; Geiss, B. J.; Henry, C. S., Rotary manifold for automating a paper-based Salmonella immunoassay. *RSC Advances* **2019,** *9* (50), 29078-29086.
69. Kasetsirikul, S.; Shiddiky, M. J. A.; Nguyen, N.-T., Challenges and perspectives in the development of paper-based lateral flow assays. *Microfluidics and Nanofluidics* **2020,** *24* (2), 17.
70. Andryukov, B. G., Six decades of lateral flow immunoassay: from determining metabolic markers to diagnosing COVID-19. *AIMS microbiology* **2020,** *6* (3), 280.
71. Sajid, M.; Kawde, A.-N.; Daud, M., Designs, formats and applications of lateral flow assay: A literature review. *Journal of Saudi Chemical Society* **2015,** *19* (6), 689-705.
72. Mak, W. C.; Beni, V.; Turner, A. P., Lateral-flow technology: From visual to instrumental. *TrAC Trends in Analytical Chemistry* **2016,** *79*, 297-305.
73. Krouwer, J. S.; Cembrowski, G. S., A review of standards and statistics used to describe blood glucose monitor performance. *Journal of Diabetes Science and Technology* **2010,** *4* (1), 75-83.
74. Petryayeva, E.; Algar, W. R., Toward point-of-care diagnostics with consumer electronic devices: the expanding role of nanoparticles. *Rsc Advances* **2015,** *5* (28), 22256-22282.

75. Turner, A. P., Biosensors: sense and sensibility. *Chemical Society Reviews* **2013,** *42* (8), 3184-3196.
76. Martinez, A. W.; Phillips, S. T.; Butte, M. J.; Whitesides, G. M., Patterned paper as a platform for inexpensive, low-volume, portable bioassays. *Angewandte Chemie-International Edition* **2007,** *46* (8), 1318-1320.
77. Müller, R.; Clegg, D., Automatic paper chromatography. *Analytical Chemistry* **1949,** *21* (9), 1123-1125.
78. Xia, Y.; Si, J.; Li, Z., Fabrication techniques for microfluidic paper-based analytical devices and their applications for biological testing: A review. *Biosensors & Bioelectronics* **2016,** *77*, 774-789.
79. Sher, M.; Zhuang, R.; Demirci, U.; Asghar, W., Paper-based analytical devices for clinical diagnosis: recent advances in the fabrication techniques and sensing mechanisms. *Expert Review of Molecular Diagnostics* **2017,** *17* (4), 351-366.
80. Ozer, T.; McMahon, C.; Henry, C. S., Advances in paper-based analytical devices. *Annual Review of Analytical Chemistry* **2020,** *13*, 85-109.
81. Nishat, S.; Jafry, A. T.; Martinez, A. W.; Awan, F. R., based microfluidics: Simplified fabrication and assay methods. *Sensors and Actuators B: Chemical* **2021,** *336*, 129681.
82. Qin, X.; Liu, J.; Zhang, Z.; Li, J.; Yuan, L.; Zhang, Z.; Chen, L., Microfluidic paper-based chips in rapid detection: Current status, challenges, and perspectives. *TrAC Trends in Analytical Chemistry* **2021,** *143*, 116371.
83. Adkins, J. A.; Boehle, K.; Friend, C.; Chamberlain, B.; Bisha, B.; Henry, C. S., Colorimetric and electrochemical bacteria detection using printed paper-and transparency-based analytic devices. *Analytical chemistry* **2017,** *89* (6), 3613-3621.
84. Rattanarat, P.; Dungchai, W.; Cate, D.; Volckens, J.; Chailapakul, O.; Henry, C. S., Multilayer Paper-Based Device for Colorimetric and Electrochemical Quantification of Metals. *Analytical Chemistry* **2014,** *86* (7), 3555-3562.
85. Chen, X.; Chen, S.; Ma, Q., Fluorescence detection of dopamine based on nitrogen-doped graphene quantum dots and visible paper-based test strips. *Analytical Methods* **2017,** *9* (15), 2246-2251.
86. Yang, Y.; Noviana, E.; Nguyen, M. P.; Geiss, B. J.; Dandy, D. S.; Henry, C. S., Paper-Based Microfluidic Devices: Emerging Themes and Applications. *Analytical Chemistry* **2017,** *89* (1), 71-91.
87. Morbioli, G. G.; Mazzu-Nascimento, T.; Stockton, A. M.; Carrilho, E., Technical aspects and challenges of colorimetric detection with microfluidic paper-based analytical devices (mu PADs) - A review. *Analytica Chimica Acta* **2017,** *970*, 1-22.
88. Byrnes, S.; Thiessen, G.; Fu, E., Progress in the development of paper-based diagnostics for low-resource point-of-care settings. *Bioanalysis* **2013,** *5* (22), 2821-2836.
89. Walpole, G. S., The use of litmus paper as a quantitative indicator of reaction. *Biochemical Journal* **1913,** *7* (3), 260.
90. Laidler, K. J., Theory of the transient phase in kinetics, with special reference to enzyme systems. *Canadian Journal of Chemistry* **1955,** *33* (10), 1614-1624.
91. Daniel, R. M.; Dines, M.; Petach, H. H., The denaturation and degradation of stable enzymes at high temperatures. *Biochemical journal* **1996,** *317* (1), 1-11.
92. Quesada-González, D.; Merkoçi, A., Nanoparticle-based lateral flow biosensors. *Biosensors and Bioelectronics* **2015,** *73*, 47-63.

93. Anfossi, L.; Di Nardo, F.; Russo, A.; Cavalera, S.; Giovannoli, C.; Spano, G.; Baumgartner, S.; Lauter, K.; Baggiani, C., Silver and gold nanoparticles as multi-chromatic lateral flow assay probes for the detection of food allergens. *Analytical and bioanalytical chemistry* **2019,** *411* (9), 1905-1913.
94. Zhou, W.; Gao, X.; Liu, D.; Chen, X., Gold nanoparticles for in vitro diagnostics. *Chemical reviews* **2015,** *115* (19), 10575-10636.
95. Dungchai, W.; Chailapakul, O.; Henry, C. S., Electrochemical detection for paper-based microfluidics. *Analytical chemistry* **2009,** *81* (14), 5821-5826.
96. Noviana, E.; Klunder, K. J.; Channon, R. B.; Henry, C. S., Thermoplastic Electrode Arrays in Electrochemical Paper-Based Analytical Devices. *Analytical chemistry* **2019,** *91* (3), 2431-2438.
97. Noviana, E.; Henry, C. S., Simultaneous Electrochemical Detection in Paper-Based Analytical Devices. *Current Opinion in Electrochemistry* **2020**.
98. Boonkaew, S.; Jang, I.; Noviana, E.; Siangproh, W.; Chailapakul, O.; Henry, C. S., Electrochemical paper-based analytical device for multiplexed, point-of-care detection of cardiovascular disease biomarkers. *Sensors and Actuators B: Chemical* **2021,** *330*, 129336.
99. Kokkinos, C.; Economou, A.; Giokas, D., based device with a sputtered tin-film electrode for the voltammetric determination of Cd (II) and Zn (II). *Sensors and Actuators B: Chemical* **2018,** *260*, 223-226.
100. Costa-Rama, E.; Nouws, H.; Delerue-Matos, C.; Blanco-López, M. d. C.; Fernández-Abedul, M. T., Preconcentration and sensitive determination of the anti-inflammatory drug diclofenac on a paper-based electroanalytical platform. *Analytica Chimica Acta* **2019,** *1074*, 89-97.
101. Obahiagbon, U.; Smith, J. T.; Zhu, M.; Katchman, B. A.; Arafa, H.; Anderson, K. S.; Christen, J. M. B., A compact, low-cost, quantitative and multiplexed fluorescence detection platform for point-of-care applications. *Biosensors and Bioelectronics* **2018,** *117*, 153-160.
102. Lichtman, J. W.; Conchello, J.-A., Fluorescence microscopy. *Nature methods* **2005,** *2* (12), 910-919.
103. Lakowicz, J. R., Introduction to fluorescence. In *Principles of fluorescence spectroscopy*, Springer: 1999; pp 1-23.
104. Taylor, J. R.; Fang, M. M.; Nie, S. M., Probing specific sequences on single DNA molecules with bioconjugated fluorescent nanoparticles. *Analytical Chemistry* **2000,** *72* (9), 1979-1986.
105. Schultz, N. M.; Kennedy, R. T., Rapid immunoassays using capillary electrophoresis with fluorescence detection. *Analytical Chemistry* **1993,** *65* (21), 3161-3165.
106. Ko, K. C.; Wu, J.-S.; Kim, H. J.; Kwon, P. S.; Kim, J. W.; Bartsch, R. A.; Lee, J. Y.; Kim, J. S., Rationally designed fluorescence 'turn-on'sensor for Cu 2+. *Chemical communications* **2011,** *47* (11), 3165-3167.
107. Liang, L.; Lan, F.; Li, L.; Su, M.; Ge, S.; Yu, J.; Liu, H.; Yan, M., Fluorescence "turn-on" determination of H2O2 using multilayer porous SiO2/NGQDs and PdAu mimetics enzymatic/oxidative cleavage of single-stranded DNA. *Biosensors and Bioelectronics* **2016,** *82*, 204-211.
108. Shah, K. G.; Yager, P., Wavelengths and Lifetimes of Paper Autofluorescence: A Simple Substrate Screening Process to Enhance the Sensitivity of Fluorescence-Based Assays in Paper. *Analytical Chemistry* **2017,** *89* (22), 12023-12029.

109. Koczula, K. M.; Gallotta, A., Lateral flow assays. *Essays in biochemistry* **2016,** *60* (1), 111-120.
110. Renault, C.; Li, X.; Fosdick, S. E.; Crooks, R. M., Hollow-Channel Paper Analytical Devices. *Analytical Chemistry* **2013,** *85* (16), 7976-7979.
111. Renault, C.; Anderson, M. J.; Crooks, R. M., Electrochemistry in hollow-channel paper analytical devices. *Journal of the American Chemical Society* **2014,** *136* (12), 4616-4623.
112. Channon, R. B.; Nguyen, M. P.; Scorzelli, A. G.; Henry, E. M.; Volckens, J.; Dandy, D. S.; Henry, C. S., Rapid flow in multilayer microfluidic paper-based analytical devices. *Lab on a Chip* **2018,** *18* (5), 793-802.
113. Robert B. Channon, M. P. N., Charles S. Henry, David S. Dandy, Multilayered Microfluidic Paper-Based Devices: Characterization,
Modeling, and Perspectives. 2019.
114. Jang, I.; Carrão, D. B.; Menger, R. F.; Moraes de Oliveira, A. R.; Henry, C. S., Pump-free microfluidic rapid mixer combined with a paper-based channel. *ACS sensors* **2020,** *5* (7), 2230-2238.

CHAPTER 2. PAPER-BASED PUMP-FREE MAGNETOPHORESIS

Microfluidic magnetophoresis is a powerful technique that is used to separate and/or isolate cells of interest from complex matrices for analysis. However, mechanical pumps are required to drive flow, limiting portability, and making translation to point-of-care (POC) settings difficult. Microfluidic paper-based analytical devices (μPADs) offer an alternative to traditional microfluidic devices that do not require external pumps to generate flow. However, μPADs are not typically used for particle analysis because they are slow and particles become trapped in the porous fiber network. Here we report newly developed fast-flow microfluidic paper-based analytical devices (ffPADs) to perform magnetophoresis. ffPADs use capillary action in a gap between stacked layers of paper and transparency sheets to drive flow at higher velocities than traditional μPADs. The multi-layer ffPADs allow particles and cells to move through the gap without being trapped in the paper layers. We first demonstrate that ffPADs enable magnetic particle separations in a μPAD with a neodymium permanent magnet and study key factors that affect performance. To demonstrate utility, *E. coli* was used as a model analyte and was isolated from human urine before detection with a fluorescently labeled antibody. A capture efficiency of 61.5% was then obtained for *E. coli* labeled magnetic beads in human urine. Future studies will look at the improvement of the capture efficiency and to make this assay completely off-chip without the need of a fluorescent label. The assay and device described here demonstrate the first example of magnetophoresis in a paper based, pump free microfluidic device. This chapter was published in *Analytical Methods.*[32] I was the first author and was the sole writer of the published work. All experiments were conducted by myself or one of the other listed authors with assistance from Dr. Ilhoon Jang and Dr. Cody Carrell.

2.1 Introduction

Improving medical diagnostics is a key need to reduce the 15 million deaths a year worldwide from infectious diseases.[1] While significant improvement has been made in the field, patients in many parts of the world still cannot access early diagnosis which is crucial for adequate care.[2-5] For example, sepsis patients treated within one day of showing symptoms had a 10% mortality rate, while those treated after three days had a 50% mortality rate.[6] Current infectious disease detection methods include culturing, polymerase chain reaction (PCR), and enzyme-linked immunosorbent assay (ELISA).[1, 7] These methods are widely accepted because of their ability to identify bacteria with low limits of detection.[8-10] However, all require trained personnel, can take hours to days to complete, and cost at least $10 per test.[11] Consequently, a simple, rapid, and reliable point-of-care (POC) diagnostic for the detection of infectious diseases that is both sensitive and selective is needed. Land et al. recently recommended POC technologies to meet a REASSURED criteria.[12] These criteria are defined as real-time connectivity, ease of specimen collection, affordable, sensitive, specific, user-friendly, rapid and robust, and equipment-free. μPADs are one technology that meets many of these requirements but suffers from slow fluid velocity and poor limits of detection.[2, 13] One technique known to improve detection limits and selectivity of an assay is to separate target analytes from the sample matrix.[14]

In this work, we are focused on isolating bacteria from complex matrices to remove interferents, concentrate the target cells, and improve detection performance. The cell separation/isolation process can be tedious, so microfluidic platforms have been developed to automate and simplify this process.[15] A popular microfluidic separation approach is magnetophoresis, which separates cells in continuous flow using a permanent magnet to move magnetically labeled cells from one flowing stream to another.[16] However, magnetophoresis

requires external pumps to drive flow, limiting their portability and usefulness for POC applications. μPADs transport fluid via capillary action, which eliminates the need for external pumps,[17] but are not currently used for magnetophoresis because particles and cells become trapped in the paper fibers and fluid velocities generated in μPADs are not fast enough for continuous separation.[18] In this work we address both challenges by creating fast flow in a modified multi-layer μPAD.[2, 13, 19-21] Fast-flow μPADs (ffPADs) are created by stacking two layers of wax-printed paper around laser cut double sided adhesive to create channels or gaps. The channels between paper layers enable fast flow without trapping particles. The velocities in the multi-layer μPAD increase by 145x or more compared to single-layer μPADs. The fast-flow phenomenon seen with this method of fabrication was characterized in depth previously in Channon et al.[19, 20] Taking advantage of this fast-flow phenomenon provides a way to make paper-based magnetophoresis possible.[19] Herein we describe the first example of a paper-based, pump-free magnetophoretic device and demonstrate its capabilities by detecting bacteria in urine. We envision the μPAD designed here for rapid detection of *E. coli* and other bacteria and viruses would benefit both food safety and human health diagnostics.

2.2 Materials and Methods

2.2.1 Materials

Whatman 1 chromatography paper was purchased from GE Healthcare Sciences. Wax patterns were printed using a Xerox ColorQube 8870 and an IsoTemp hot plate (Fisher Scientific) was used to melt the wax. A benchtop digital microscope (Dino-Lite AF4915) was used for laminar flow colorimetric experiments. Two fluorescent Dino-Lite digital microscopes with excitation wavelengths of 400 nm and 570 nm (Dino-Lite AM4115T-CFVW and Dino-Lite AM4115T-YFGW) were used for fluorescence detection and analysis. All videos were imported into ImageJ

for analysis. A cylindrical ¼" x ¼" Neodymium Iron Boron (NdFeB) permanent magnet, grade N52 (K&J Magnetics, INC.) was used to create an external magnetic field. Other magnet types and shapes were investigated; however, the cylindrical magnet was chosen because of the smaller size while maintaining strong field lines. All magnetic beads were purchased from Spherotech Inc. (Lake Forest, Illinois). *E. coli* antibodies (bs-2033R/bs-2033R-A555) were purchased from Bioss Antibodies. The buffers used in this work were 0.1 M phosphate-buffered saline (PBS) and 0.1 M PBS with 0.1% Tween-20 (PBST). The two antibodies were diluted in PBS. Human pooled urine was purchased from Lee BioSolutions (Maryland Heights, MO).

2.2.2 Device Design and Fabrication

The µPADs discribed here were designed in CorelDRAW X4 and then printed onto Whatman grade 1 chromatography paper and a cellulose acetate transparency sheet (3M PP2950). Next, the paper was placed on a hot plate at 150°C for 90 s to create hydrophobic barriers. Grade 467 and 468 double-sided adhesives were used to define the gap height, and the channel pattern was cut out using a CO_2 laser cutter (Epilog Zing Laser Cutter and Engraver). The multilayered device was then assembled in 8.5"x11" sheets by first applying the double-sided adhesive to the transparency and applying consistent pressure with a pouch laminator set at room temperature. Finally, the top paper layer was placed directly onto the double-sided adhesive using a guide to provide necessary alignment to create the ffPAD.

2.2.3 Magnetophoresis System Setup

A range of fluorescent carboxyl magnetic particles from 2.0 µm to 44.1 µm were purchased from Spherotech Inc. and diluted from 5 mg/mL to 1 mg/mL in phosphate buffered saline (PBS). All 44.1 µm diameter particles used in these and following studies were labeled with a yellow

fluorophore onto the surface of the particles with an excitation wavelength from 400-500 nm and emission from 450-550 nm. Imaging was done with the Dino-Lite microscope (400 nm). All dilutions of particles were made in phosphate-buffered saline, pH 7.2, kept at room temperature and protected from light. Solutions were vortexed for 30 s before use (Scientific Industries Vortex Genie 2). The Grade N52 permanent magnet was placed on top of the device and placement was optimized for consistent and ideal separation results based on magnetic field lines. Images of the fluorescent particles within the gap of the device were taken using the fluorescent DinoLite microscope.

2.2.4 E. coli Growth and Sample Preparation

E. coli DH5-α was used as the model bacteria in this work; it was grown in Universal PreEnrichment Broth (Sigma-Aldrich, pH 7) overnight in a shaker at 37°C and 220 rpm. The bacteria concentration was quantified by serial dilution and plating on lysogeny broth (LB) agar plates. Serial dilutions of this solution were made using PBS or human pooled urine.

2.2.5 E. coli Detection Using Immunomagnetic Separation and H-Cell Device in Human Urine

The enzymatic assay presented by Srisa-Art et al. was modified for DH5-α fluorescence detection (Figure A1.1).[22] The entire assay was performed on the benchtop at room temperature. First, 44.1 µm streptavidin coated paramagnetic beads (SpheroTech) were vortexed for 30 s at room temperature. Second, the beads were conjugated to a biotinylated anti-*E. coli* antibody in a microcentrifuge for 20 min on a rotator. Third, an immunomagnetic separation (IMS) was performed using a magnet (DynaMag-2 magnet, Thermo Fisher Scientific, Inc.) to isolate and concentrate the magnetic bead-antibody complex by removing the supernatant and resuspending the content in 100 µL of PBS. Fourth, the bead-antibody complex was added to 1 mL of *E. coli* spiked urine and incubated on a rotator for 20 min. Another IMS step was performed to

isolate/concentrate the sample and to remove the supernatant. The complex was washed twice with PBS-Tween (0.1%) to remove any unbound species. Finally, an anti-*E. coli* AlexaFluor-555 was conjugated to the bead complex for 20 min on a rotator. The final complex was then washed twice using IMS with PBS-Tween. The complex was then resuspended in 50 µL of urine. 30 µL of the complex was then added simultaneously to the device with 30 µL of PBS buffer to create capillary driven laminar flow. The permanent magnet was placed on the adjacent channel at the desired detection zone. After 30 s the fast flow has stopped and analysis of *E. coli* capture was performed.

2.2.6 Image Analysis

Videos of all experiments were taken with the DinoLite microscopes and pictures were then exported to be analyzed in NIH ImageJ. The images were split into red, green, and blue channels for elimination of background signal and analysis. Fluorescence intensity plots were created with proportional mean grey scale values.

2.3 Results and Discussion

2.3.1 Device Dimensions and Laminar Flow

An H-cell device was created from paper and transparency film to demonstrate capillary driven laminar flow was possible. The device was assembled by stacking packing tape, paper, double-sided adhesive, transparency together as shown in Figure 2.1a. Figure 2.1b shows the cross-sectional view of the channel once the device is assembled. ffPADs yield faster sustained flows than traditional µPADs, as demonstrated in Figure 2.1c, where the liquid 6 cm from the inlet in a ffPAD with 360 µm gap has a speed of 0.62 cm/s versus 0.0035 cm/s in traditional single-layer µPAD.[19] The gap height can be controlled by changing the number of double-sided adhesive layers placed between the paper and transparency layers. Modeling of this phenomenon recently

published by Channon et al. describes flow dominated by Laplace pressure for the first 1-2 cm.[20] Shown by a still image in the supplemental, the fluid flow in the gap of the device is dragging the liquid in the paper layer. The flow in the gap is then dominated by a "moving wall" of liquid, resulting in a shear flow within the paper and a linear velocity profile.[19, 20] The modeling described is confirmed by the experimental results shown in Figure 2.1c, where there are high initial velocities of over 4 cm/s for a 360 µm gap height that decay over distance.[20] The fluid velocities in the devices shown here have similar flow characteristics and show the same experimental results described by Channon et al.[19, 20] Although ffPADs have shown faster velocities as compared to traditional µPADs, the maximum Reynolds number (*Re*) in the multi-layer device was calculated to be 2.0, which occurred in the 360 µm gap configuration, confirming that flow is extremely laminar. Based on the studies showing sustained high velocities, we were led to hypothesize that magnetophoresis was possible because ffPADs have a large enough gap height for the majority of suspended particles to avoid being trapped in the cellulose fibers.[4, 19, 23]

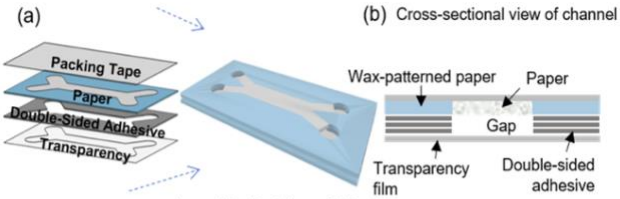

	Velocity at 3 cm [cm/s]	Velocity at 6 cm [cm/s]
360 µm gap	1.74	6.24×10^{-1}
240 µm gap	5.62×10^{-1}	2.77×10^{-1}
120 µm gap	4.17×10^{-2}	2.29×10^{-2}
single paper	6.70×10^{-3}	3.45×10^{-3}

Figure 2.1. Assembly and flow characteristics of microfluidic paper-based analytical devices (µPADs). (a) Schematic of fast flow µPAD assembly. (b) Cross-sectional view of channel of fast flow µPADs, with flow to-ward/away from the observer. (c) Plot showing flow velocities with respect to gap height.

We next sought to demonstrate laminar flow in the ffPAD configuration because consistent laminar flow is needed for magnetophoresis to avoid convective mixing between the two parallel flowing streams in the H-cell.[24] A ffPAD with two inlets containing red and green dyes showed a distinct interface between the two liquid streams, again confirming laminar flow was established in the device with only slight diffusional mixing (Figure 2.2a). Following the demonstration of fully developed laminar flow, the effect of inlet angle was quantified using the absolute mixing index (AMI) as a measure of total mixing. AMI indicates the extent of mixing and operates on a scale of 0-1, where 0 indicates a completely mixed state and 1 indicates a completely unmixed state. Photographs above each graph in Figure 2.2b show each device and the main channel where the analysis is performed. Devices I, II, and III were all consistent with a 3 mm wide channel with only changing the angle of the inlet. Where device I had a 90˚ angle, device II had a 180˚ angle and device III had a 15˚ angle. Devices I and II showed inconsistent flow with relatively large standard deviation of ±1 shown in blue. In device III a 15° angle between the two inlets led to less mixing and more reproducible laminar flow. Device IV was fabricated incorporating the optimal angle geometry with a 270° fan at end of the channels that produces steady flow in paper analytical devices.[21, 25] Inserting the fan decreased variability and increased AMI (Figure 2.2b). Device IV showed the most reproducible laminar flow along with the least mixing denoted by an AMI of 0.7 with only diffusional mixing occurring. As a result, the Device IV geometry was selected for subsequent studies.

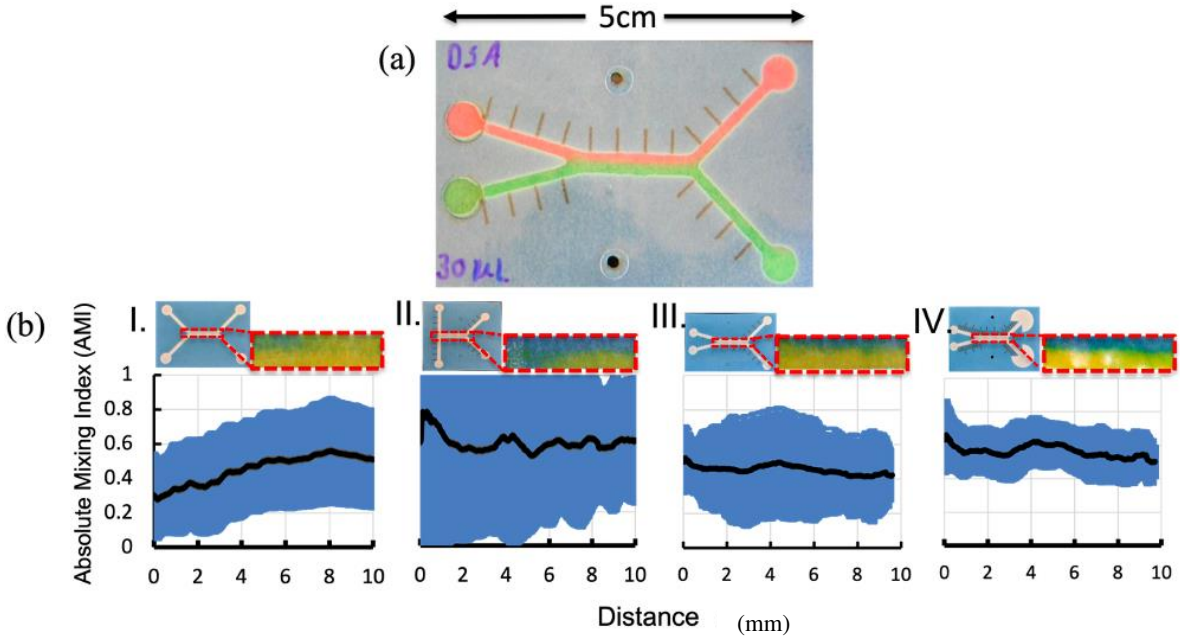

Figure 2.2. (a) Image taken of fast-flow µPAD with laminar flow. (b) Images taken of the middle channel to analyze AMI. The corresponding graphs show the effect the angle has on consistency of laminar flow by quantifying the amount of mixing of each device.

2.3.2 Understanding Particle Behavior

Once velocities and laminar flow parameters were characterized, particle separation via magnetophoresis was investigated. Since the bottom layer of the ffPADs was made from transparency film, it was possible to image the magnetic particles inside the gap. Figure 2.3a shows a qualitative schematic of expected particle trajectories, where magnetic particles move across the laminar flow interface and are trapped by a permanent magnet. The NdFeB permanent magnet was placed on the top side of the device on the edge of the channel. 2 µm, 8 µm, and 44.1 µm magnetic particles were tested. The sizes were selected based on commercial availability. 2 µm and 8 µm particles were retained within the paper fibers resulting in no observable movement across the parallel flowing streams and significant fluorescent background in the channel (Figure 2.3b and 2.3c). Whatman 1 chromatography paper has an average pore size of 11 µm, which resulted in trapping particles size smaller than 11 µm in the device. In addition to particle size, the magnetic

susceptibility changes proportionally with the size of the particles. As a result, the 44.1 µm particles remained in the gap area between paper and transparency film and could be moved across the laminar flow barrier with ease (Figure 2.3d). The 44.1 µm magnetic particles also accumulated near the magnet. As a control, the trajectories of the 44.1 µm particles were obtained in the absence of a magnetic field. Without the field present, the particles largely followed the liquid streamlines and did not cross the parallel streams' interface (Figure 2.3e). The ability to pull the 44.1 µm particles from one stream to another with the magnetic field under continuous flow is the first time magnetophoresis has been demonstrated in a pump-free device to the best of our knowledge.

After confirming magnetophoresis in ffPADs, the concentration dependent signal was evaluated by analyzing the fluorescence intensity of captured particles by taking the mean grey scale intensity of the area at magnet. Figure 2.3f shows the normalized fluorescence intensity variation as a function of particle concentration. The linear calibration curve shows the fluorescent signal increasing with increasing particle concentration with corresponding error bars taken from a standard deviation with an n of 3 for each concentration.

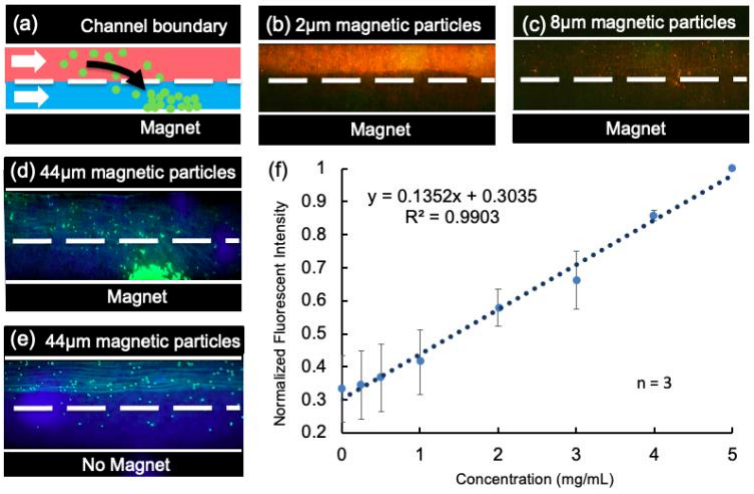

Figure 2.3. Magnetophoresis in µPAD (a) Overview of magnetophoresis concept where the white dashed lines indicate the laminar flow interface. (b) 2µm magnetic particles. (c) 8µm magnetic particles. (d) Control image of particles flowing in the absence of a magnetic field. (e) 44µm magnetic particles undergoing positive magnetophoresis. (f) Calibration curve of fluorescent intensity of particle capture via concentration.

2.3.3 Improvements in Device Design

The effect of gap height on particle capture was investigated. Pamme et al. showed in a glass microchip that if fluid velocities are above 0.2 cm/s then little to no deflection of magnetic particles occurs. Conversely, if velocities are lower than 0.04 cm/s the magnetic moment will be more pronounced and inherently influence the particle deflection trajectory.[26] Since the velocity and magnetic field vectors are orthogonal, faster flow decreases particle deflection caused by a constant magnetic field, as described by the equation shown in Figure 2.4. The fluid velocity in a ffPAD is controlled by the gap height between the layers, so the gap height was varied to study these competing effects.[19] ffPAD gap heights of 60, 70, 120, 230, 290, 360, and 500 µm were tested using 44.1 µm magnetic particles and the fluorescent intensity of captured particles analyzed. A gap height between 230 and 290 µm yielded the highest number of magnetic particles captured by the magnet (Figure 2.4a). In the ffPAD, a velocity exceeding ~1.5 cm/s prevented the particles from being captured. When the velocity was lower than ~0.5 cm/s the particles were retained in the paper fibers particle and accumulation at the magnet was not observed.

(a)

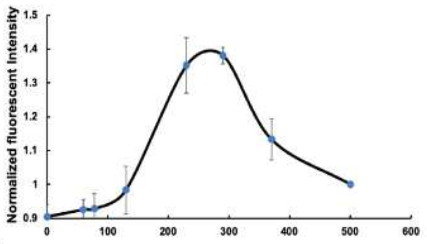

$$u_{res} = u_{flow} + u_{mag}$$

μ_{res} = velocity of particle
μ_{flow} = fluid velocity
μ_{mag} = magnetic velocity

(b)

# of Particles	# Particles Captured	# of Particles Left in Inlet	Actual Capture Efficiency	Theoretical Capture Efficiency
42 ± 5 (0.05 mg/mL)	25 ± 1	9 ± 2	62.5% ± 7.3	85.0%
90 ± 9 (0.1 mg/mL)	55 ± 3	22 ± 3	61.8% ± 6.3	85.5%
171 ± 18 (0.2 mg/mL)	108 ± 5	33 ± 4	63.5% ± 6.9	82.9%
399 ± 19 (0.3 mg/mL)	231 ± 14	124 ± 7	58.2% ± 3.0	89.1%

Figure 2.4. (a) Optimization of particle capture with respect to gap height characterized by fluorescent intensity. Correlated equation showing the relationship of the velocity of the particle with respect to the fluid and magnetic velocity. (b) Photograph and theoretical capture efficiency in the device with optimized gap height.

In addition to optimizing gap height, the shapes of the outlet channels were studied. The magnetic particles follow a curved deflection trajectory. To account for this trajectory and improve the efficiency of particle capture, the device geometry was modified to match the general shape of the trajectory. A thin wax line was also printed on the top paper layer directly down the center of the channel to improve flow reproducibility. The particles then deflect only in the gap of the device and mixing in the paper is minimized (Figure A1.3). Additionally, a larger fan with a 14 mm diameter was used with the upper channel versus a 9.5 mm diameter fan on the lower channel. The larger fan is used to continually wick the solution from the upper channel and particle inlet to transport more particles to the detection zone and improve capture efficiency (Figure 2.5a). The magnetic field is shown with an overlay of a schematic of the device and magnetic particles following the field lines and being attracted toward the high gradient (Figure 2.5b). The shape of the outlet channels were designed to match that of the magnet field lines to further improve capture of the magnetic particles. [27] After optimization of the device was completed the capture efficiency was then investigated yielding capture of 61.5% ± 5.8 (n=4) with similar efficiencies for increasing concentrations. Other studies have shown capture efficiencies anywhere from 44% to 100% with permanent magnets, however all previous studies were conducted in traditional microfluidic channels using pumps.[28] Concentrations from 0.05 mg/mL to 0.3 mg/mL were selected because of the ability to physically count the number of particles in a 30 µL sample. The lowest capture was reported for the highest concentration because particles will aggregate at higher concentrations. The calculated capture efficiency of 61.5% was further analyzed and it was determined that many of the large 44.1µm particles sediment to the bottom of the inlet and are trapped before reaching the capture magnet. If the particles left in the inlet were able to reach the capture zone, a theoretical yield of 85.6% would result (Figure 2.4c). This is calculated by counting

the number of particles left in the inlet versus the total number of particles added (n=4). A washing step of buffer immediately after the initial addition showed an increase of ~5%.

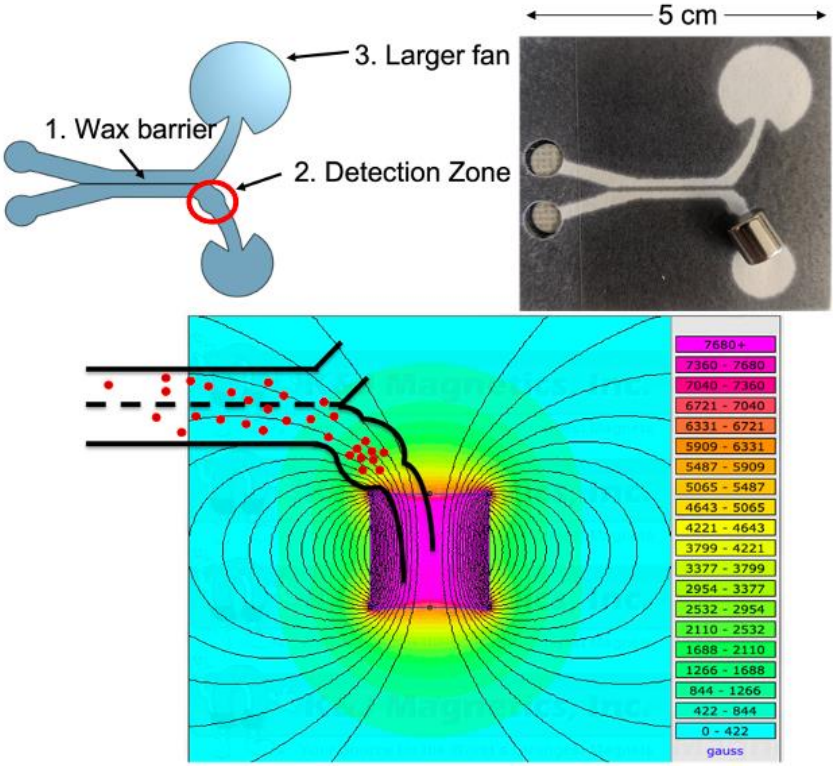

Figure 2.5. (a) CAD rendering of the device design and photograph of the fabricated µPAD. (b) Magnetic field gradient of a N52 cylindrical NdFeB permanent magnet overlay with fluid channel. Red spheres indicate magnetic particles. Magnetic flux density estimated to be 1300 gauss or 130 mT near the center of the channel.

2.3.4 E. coli Magnetophoresis in Urine

Escherichia coli (*E. coli)* is a common bacterium found in food and water that causes millions of infections per year in the US. *E. coli* accounts for 70-95% of all urinary tract infections (UTIs).[29] An immunomagnetic sandwich *E. coli* assay in urine was performed to demonstrate the ability to carry out analysis on real samples. To verify that the 44.1 µm beads would capture *E. coli,* the streptavidin coated beads were modified with biotinylated anti-*E. coli* and incubated with 10^7 CFU/mL *E. coli* labeled with a fluorescent secondary antibody. As shown in Figure 2.6c and Figure A1.2, fluorescently labeled bacteria are bound to the surface of the magnetic beads. To demonstrate that the device could process a complex sample matrix, the optimized

magnetophoresis assay was performed using human urine. 30 µL of the streptavidin magnetic bead antibody complex was incubated in a urine sample spiked with *E. coli* during the antibody conjugation. A full schematic of the conjugation process can be found in the supporting information. After conjugation was complete, the complex was resuspended in urine and the detection of the labeled *E. coli* was shown in the device via magnetophoresis along with a blank (Figure 2.6a and 2.6b). Next, serial dilutions from 10^7 CFU/mL to 10^1 CFU/mL were used to create a dose-response curve (Figure 2.6d). The LOD in the device of 10^5 CFU/mL is not as low as a colorimetric response seen previously by our group of 10^2 CFU/mL for IMS methods,[22] but still demonstrates proof-of-concept. Detection limits could be improved in a few ways. First, enzymatic amplification instead of a fluorescent tag has been shown to improve the LOD especially in µPADs. Second, if the lower concentrations of *E. coli* were cultured prior to conjugation it would improve the LOD as well.[30, 31] The final complex was introduced into the device and compared against the blank to see significant capture *E. coli* in the device in less than 30 s. Further investigation will be done to try to improve the capture efficiency with sequential washing steps to fully wash any complexes left in the inlet, and by adding a surfactant to the buffer to decrease particle-transparency interactions. Fluorescence detection is convenient for rapid detection of the complex, however we found it was limited by intensity when trying to record the entire channel.

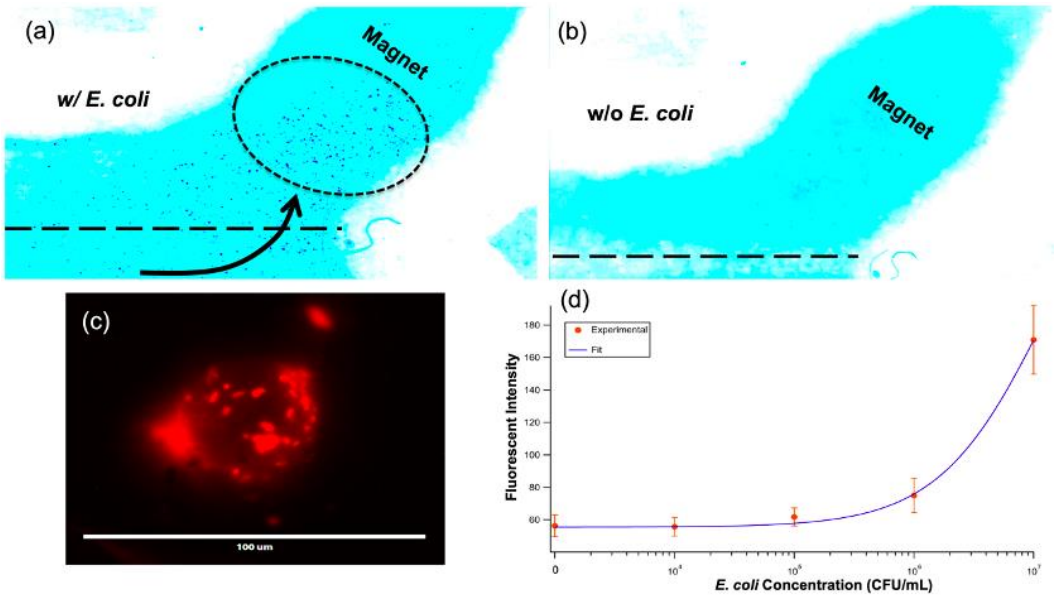

Figure 2.6. Detection of fluorescently labeled bacteria in µPAD magnetophoresis. (a) Inverted image of positive magnetophoresis of E. coli complex. (b) Negative control assay (without *E. coli*). False color has been applied for visualization (c) Fluorescent microscope image taken of bound E. coli to bead. (d) Dose-response curve of *E. coli* in urine in the device.

2.4 Conclusions and Future Directions

In this work, the first example of a pump-free paper-based magnetophoresis device is demonstrated. The novel design shows efficient capture and detection of magnetic particles made possible by the fast flow system with sustained high velocities. Device dimensions, particle size, gap height, and magnet placement and strength were all studied to improve particle capture and reduce convective and diffusional mixing between the two flow streams. A capture efficiency of 61.5% was obtained and further investigation is being done to improve this as described above. Even though this capture efficiency is not as high as other magnetophoretic devices, this device represents a novel approach to a technique that has not previously been demonstrated in paper. The current method for this assay involves several off-chip steps, but future work will also seek to integrate all steps to minimize assay complexity. We envision additional new potential diagnostic platforms possible because of the technique described. Future work will target adapting the system to incorporate the off-chip manipulations onto the device and to detect multiple pathogens at once.

REFERENCES

1. Dye, C., After 2015: infectious diseases in a new era of health and development. *Philosophical Transactions of the Royal Society B-Biological Sciences* **2014,** *369* (1645).
2. Carrell, C.; Kava, A.; Nguyen, M.; Menger, R.; Munshi, Z.; Call, Z.; Nussbaum, M.; Henry, C., Beyond the lateral flow assay: A review of paper-based microfluidics. **2019,** *206*, 4554.
3. Petryayeva, E.; Algar, W. R., Toward point-of-care diagnostics with consumer electronic devices: the expanding role of nanoparticles. *Rsc Advances* **2015,** *5* (28), 22256-22282. 4.
Martinez, A. W.; Phillips, S. T.; Whitesides, G. M.; Carrilho, E., Diagnostics for the Developing World: Microfluidic Paper-Based Analytical Devices. *Analytical Chemistry* **2010,** *82* (1), 3-10.
5. Yager, P.; Domingo, G. J.; Gerdes, J., Point-of-care diagnostics for global health. *Annual Review of Biomedical Engineering* **2008,** *10*, 107-144.
6. Dellinger, R. P.; Levy, M. M.; Rhodes, A.; Annane, D.; Gerlach, H.; Opal, S. M.; Surviving Sepsis Campaign, G., Surviving Sepsis Campaign: International Guidelines for Management of Severe Sepsis and Septic Shock: 2012. *Crit. Care Med.* **2013,** *41* (2), 580-637.
7. Chin, C. D.; Linder, V.; Sia, S. K., Commercialization of microfluidic point-of-care diagnostic devices. *Lab on a Chip* **2012,** *12* (12), 2118-2134.
8. Myers, F. B.; Lee, L. P., Innovations in optical microfluidic technologies for point-of-care diagnostics. *Lab on a Chip* **2008,** *8* (12), 2015-2031.
9. Mahony, J. B.; Blackhouse, G.; Babwah, J.; Smieja, M.; Buracond, S.; Chong, S.; Ciccotelli, W.; O'Shea, T.; Alnakhli, D.; Griffiths-Turner, M.; Goeree, R., Cost Analysis of Multiplex PCR Testing for Diagnosing Respiratory Virus Infections. *Journal of Clinical Microbiology* **2009,** *47* (9), 2812-2817.
10. Bissonnette, L.; Bergeron, M. G., Diagnosing infections--current and anticipated technologies for point-of-care diagnostics and home-based testing. *Clinical Microbiology and Infection* **2010,** *16* (8), 1044-1053.
11. Wormser, G. P.; Levin, A.; Soman, S.; Adenikinju, O.; Longo, M. V.; Branda, J. A., Comparative Cost-Effectiveness of Two-Tiered Testing Strategies for Serodiagnosis of Lyme Disease with Noncutaneous Manifestations. *Journal of Clinical Microbiology* **2013,** *51* (12), 4045-4049.
12. Land, K. J.; Boeras, D. I.; Chen, X.-S.; Ramsay, A. R.; Peeling, R. W., REASSURED diagnostics to inform disease control strategies, strengthen health systems and improve patient outcomes. *Nature Microbiology* **2019,** *4* (1), 46-54.
13. Osborn, J. L.; Lutz, B.; Fu, E.; Kauffman, P.; Stevens, D. Y.; Yager, P., Microfluidics without pumps: reinventing the T-sensor and H-filter in paper networks. *Lab on a Chip* **2010,** *10* (20), 2659-2665.
14. Bhagat, A. A. S.; Bow, H.; Hou, H. W.; Tan, S. J.; Han, J.; Lim, C. T., Microfluidics for cell separation. *Medical & Biological Engineering & Computing* **2010,** *48* (10), 999-1014.
15. Yaman, S.; Anil-Inevi, M.; Ozcivici, E.; Tekin, H. C., Magnetic Force-Based Micro fluidic Techniques for Cellular and Tissue Bioengineering. *Front. Bioeng. Biotechnol.* **2018,** *6*, 29.
16. Zborowski, M.; Ostera, G. R.; Moore, L. R.; Milliron, S.; Chalmers, J. J.; Schechter, A. N., Red blood cell magnetophoresis. *Biophysical journal* **2003,** *84* (4), 2638-2645.

17. Cate, D. M.; Adkins, J. A.; Mettakoonpitak, J.; Henry, C. S., Recent Developments in Paper-Based Microfluidic Devices. *Analytical Chemistry* **2015,** *87* (1), 19-41.
18. Kasetsirikul, S.; Shiddiky, M. J. A.; Nguyen, N.-T., Challenges and perspectives in the development of paper-based lateral flow assays. *Microfluidics and Nanofluidics* **2020,** *24* (2), 17.
19. Channon, R. B.; Nguyen, M. P.; Scorzelli, A. G.; Henry, E. M.; Volckens, J.; Dandy, D. S.; Henry, C. S., Rapid flow in multilayer microfluidic paper-based analytical devices. *Lab on a Chip* **2018,** *18* (5), 793-802.
20. Robert B. Channon, M. P. N., Charles S. Henry, David S. Dandy, Multilayered Microfluidic Paper-Based Devices: Characterization, Modeling, and Perspectives. 2019.
21. Adkins, J. A.; Boehle, K.; Friend, C.; Chamberlain, B.; Bisha, B.; Henry, C. S., Colorimetric and Electrochemical Bacteria Detection Using Printed Paper- and TransparencyBased Analytic Devices. *Analytical Chemistry* **2017,** *89* (6), 3613-3621.
22. Srisa-Art, M.; Boehle, K. E.; Geiss, B. J.; Henry, C. S., Highly Sensitive Detection of Salmonella typhimurium Using a Colorimetric Paper-Based Analytical Device Coupled with Immunomagnetic Separation. *Analytical Chemistry* **2018,** *90* (1), 1035-1043.
23. Pamme, N.; Manz, A., On-chip free-flow magnetophoresis: Continuous flow separation of magnetic particles and agglomerates. *Analytical Chemistry* **2004,** *76* (24), 7250-7256.
24. Choban, E. R.; Markoski, L. J.; Wieckowski, A.; Kenis, P. J. A., Microfluidic fuel cell based on laminar flow. *J. Power Sources* **2004,** *128* (1), 54-60.
25. Mendez, S.; Fenton, E. M.; Gallegos, G. R.; Petsev, D. N.; Sibbett, S. S.; Stone, H. A.; Zhang, Y.; Lopez, G. P., Imbibition in Porous Membranes of Complex Shape: Quasi-stationary Flow in Thin Rectangular Segments. *Langmuir* **2010,** *26* (2), 1380-1385.
26. Pamme, N.; Wilhelm, C., Continuous sorting of magnetic cells via on-chip free-flow magnetophoresis. *Lab on a Chip* **2006,** *6* (8), 974-980.
27. K&J magnetics, I. Magnetic Field Visualization Single Magnet in Free Space. https://www.kjmagnetics.com/magfield.asp?pName=D22-N52 (accessed 01-11-20).
28. Alnaimat, F.; Dagher, S.; Mathew, B.; Hilal-Alnqbi, A.; Khashan, S., Microfluidics Based Magnetophoresis: A Review. *Chem. Rec.* **2018,** *18* (11), 1596-1612.
29. Flores-Mireles, A. L.; Walker, J. N.; Caparon, M.; Hultgren, S. J., Urinary tract infections: epidemiology, mechanisms of infection and treatment options. *Nature Reviews Microbiology* **2015,** *13* (5), 269-284.
30. Shih, C. M.; Chang, C. L.; Hsu, M. Y.; Lin, J. Y.; Kuan, C. M.; Wang, H. K.; Huang, C. T.; Chung, M. C.; Huang, K. C.; Hsu, C. E.; Wang, C. Y.; Shen, Y. C.; Cheng, C. M., Paper-based ELISA to rapidly detect Escherichia coli. *Talanta* **2015,** *145*, 2-5.
31. Aspevall, O.; Osterman, B.; Dittmer, R.; Stén, L.; Lindbäck, E.; Forsum, U., Performance of Four Chromogenic Urine Culture Media after One or Two Days of Incubation Compared with Reference Media. *Journal of Clinical Microbiology* **2002,** *40* (4), 1500-1503.
32. Call, Z. D.; Carrell, C. S.; Jang, I.; Geiss, B. J.; Dandy, D. S.; Henry, C. S., Paper-based pump-free magnetophoresis. *Analytical Methods* **2020,** *12* (43), 5177-5185.

CHAPTER 3. PROGRESS TOWARD A SIMPLIFED UTI DIAGNOSTIC: PUMP-FREE MAGNETOPHORESIS FOR *E. COLI* DETECTION

Urinary tract infections (UTIs) are one of the most common infections across the world and can lead serious complications such as sepsis if not treated in a timely manner. Uropathogenic *E. coli* (UPEC) represent 75% of all UTIs. Early diagnosis is crucial to help control UTIs, but current culturing methods are expensive, time-consuming, and can lack sensitivity. Existing point-of-care (POC) methods fall short because they rely on indirect detection from elevated nitrates in urine rather than detecting the actual bacteria causing the infection. Magnetophoresis is a powerful method used to separate and/or isolate cells of interest from complex matrices for analysis. However, magnetophoresis typically requires complex and expensive instrumentation to control flow in microfluidic devices. Coupling magnetophoresis with microfluidic paper-based analytical devices (μPADS) enables pump free flow control, simple operation, and low cost. Early magnetophoresis μPADs showed detection limits competitive to traditional methods but higher than targets for clinical use. Here, we demonstrate magnetophoresis using hybrid μPADs that rely on capillary action in hydrophilic polyethylene terephthalate (PET) channels combined with paper pumps. We were able to detect *E. coli* with a calculated limit of detection of 2.40×10^2 Colony Forming Units per mL (CFU/mL). This chapter has been submitted to *Analytical Chemistry* and accepted with revisions. I was the first author and was the sole writer of this work. All experiments were conducted by myself or one of the other listed authors with assistance from Dr. Ilhoon Jang on the initial device design.

3.1 Introduction

UTIs occur when microbial pathogens infect the urinary tract of the urethra, bladder, ureters, and/or kidneys. UTIs are the one of the most common bacterial infections accounting for

more than 200,000 deaths worldwide per year.[1] UTIs are most prevalent in women with up to 50% of women experiencing at least one UTI during their life, and one in five women experiencing recurring UTIs.[2, 3] Another major concern is catheter-associated UTIs (CAUTIs), most commonly found in nursing homes and hospitals.[4] Catheters are prone to infection and commonly lead to complications such as sepsis, bladder stones and endotoxic stock.[5] CAUTIs develop in over 80% of patients with even higher rates for elderly patients.[4-6] Finally, a recent study found that in 2019 there were more than 404.6 million UTI cases resulting in 236,786 deaths and UTIs contributed to 5.2 million disability-adjusted life years (DALYs) worldwide.[7]

Early detection is crucial to help control UTI cases and related deaths. The ideal UTI diagnostic assay needs to be less than 10 min, inexpensive, portable, and applicable at the point-of-care (POC) to enable rapid, and effective treatment.[8] Current diagnostics fail to reach patients at the POC due to cost, the need for trained personnel, and controlled temperature, which requires that they be performed in a laboratory setting. The few diagnostics used at the POC fail to test for the pathogenic bacteria that cause UTIs.[2] Nitrate diagnostic tests are the most common, in the form of dipsticks, have been used since the 1970s. Instead of testing for Uropathogenic *E. coli* (UPEC), which accounts for 75-90% of all UTIs, nitrate dipsticks test for elevated nitrate levels.[2-6, 8] Which can be caused from numerous bacteria that are present in urine even without a UTI reducing the test accuracy.[6, 9, 10] While dipstick nitrate tests are inexpensive and readily available, an improved diagnostic is needed that can detect UPEC at low levels to diagnose UTIs earlier and more accurately. By creating a diagnostic that can accurately detect UPEC, doctors can provide the correct antibiotic rather than a general antibiotic that leads to reduced recovery times and antibiotic resistance.[11]

μPADs consisting of porous materials are a popular format for POC diagnostics because they are not only generating a fluid flow by capillary action but also are portable and cost effective sensors.[12-15] The home pregnancy test is the most popular example of an influential POC diagnostic.[12, 16] In recent years, μPADs have been used to detect metals in water, foodborne pathogens, virus and bacterial infections with success.[16-21] In these studies, immunoassays, enzymatic, electrochemical and magnetophoresis assays were used in the μPADs with success. However, μPADs are often criticized for poor sensitivity and specificity when compared to traditional laboratory assays (e.g. ELISA and PCR) where tests can detect 10^2 CFU/mL.[21] To improve sensitivity and limits of detection to similar levels, sample concentration and washing steps are needed.[16, 22] However, this is challenging to do in μPADs without substantial manual user intervention, decreasing ease-of-use.

One solution for improving UTI detection is magnetophoresis. Magnetophoresis is the process of manipulating a magnetic particle bound to an analyte of interest in the presence of an external magnetic field and has shown promise for diagnostic assays.[23, 24] Traditional microfluidics using glass chips and polydimethylsiloxane (PDMS) have dominated magnetophoreisis.[19, 20, 23] For example, Phurimsak *et al*, demonstrated enzymatic magnetophoresis with traditional microfluidics using a glass chip to sequentially bind reagents while washing sample during flow, reducing the amount of user steps needed for detection.[20] However, until recently, magnetophoresis has required external pumps to drive flow, limiting the portability and usefulness for POC applications. Although μPADs transport fluid via capillary action, which eliminates the need for external pumps, but was only recently used for magnetophoresis,[25] because particles and cells become trapped in the paper fibers during flow, limiting their ability to be separated.

Magnetophoresis coupled with μPADs presents an alternative POC method for UTI detection by automating the concentration and washing steps, while improving sensitivity relative to other μPAD methods. The Henry lab recently adapted a magnetophoresis-based assay into a μPAD to demonstrate the first example of a paper-based pump-free magnetophoretic device.[25] In this work, DH5-alpha *E. coli*, a model for UPEC, was immunomagnetically labeled and fluorescence was used for detection. The device created was free of any external pumps and total assay time from sample addition to detection was less than one minute. However, the use of fluorescence provided a limit of detection of 10^5 CFU/mL in human pooled urine, which is higher than target clinical levels.

Although an important step towards a promising technology, several improvements are needed to translate pump-free magnetophoresis into an effective POC device. First, in paper devices, only a portion of the conjugated magnetic beads make it through the device, reducing sensitivity. Second, multiple user steps were required, impacting ease-of-use. To meet the detection limits needed for easy, sensitive detection at the POC both needs must be addressed. We report an updated pump-free system here that addresses these challenges and achieves simplified operation and significant improvements in detection limit.

3.2 Material and Methods

3.2.1 Materials

Hydrophilic transparency 9984 sheets were purchased from 3M. Double-sided adhesive sheets (3M9726-ND) were purchased through DigiKey. A cylindrical ¼" x ¼" Neodymium Iron Boron (NdFeB) permanent magnet, grade N52 (K&J Magnetics, INC.) was used to create an external magnetic field. Other magnet types and shapes were investigated; however, the cylindrical

magnet was chosen because of the smaller size while maintaining strong field lines. All magnetic beads were purchased from Spherotech Inc. (Lake Forest, Illinois). *E. coli* antibodies (bs-2033R/bs-2033R-A555) were purchased from Bioss Antibodies (Woburn, Massachusetts). The buffers used in this work were 0.1 M phosphate-buffered saline (PBS) and 0.1 M PBS with 0.1% Tween-20 (PBST). The two antibodies were diluted in PBS. 1-step Ultra 3,3',5,5'-tetramethylbenzidine (TMB)-ELISA substrate solution (34028) was purchased from ThermoFischer Scientific (Waltham, Massachusetts). Human pooled urine was purchased from Lee BioSolutions (Maryland Heights, MO).

3.2.2 Magnetophoresis System Setup

A housing was designed using CAD software (OnShape) and incorporated alignment features, inlet sample ports, and a magnet holder. The housing was 3D printed using a FormLabs Form3 SLA printer. The NdFeB permanent magnet placement was optimized for efficient positive magnetophoresis, and the housing was designed to hold the magnet in the correct position and orientation.

3.2.3 Device Construction and Operation

The device consists of five alternating layers of 9984 transparency and 467 double-sided adhesive. The double-sided adhesive layers are laser cut to outline the fluid channels. To create more reproducible results and consistent magnetophoresis, we needed to generate consist laminar flow through the main channel in the device. To accomplish this, both flow streams need to enter the main channel simultaneously. We accomplished this goal using recently described burst valves.[122]The device is first assembled with a bottom layer 9984 transparency (layer 1) followed by the first double sided adhesive layer cut for the lower fluid channel shown in Figure 3.1a. The

third layer is transparency film cut out to create a burst valve between the top and bottom double sided adhesive channels (layers 2 and 4). The fourth layer is double-sided adhesive with the top fluid layer cut out incorporating a sample addition inlet and a buffer wash inlet. Placing a wash buffer inlet behind the sample inlet ensures all the sample gets washed through the device. The fifth layer is a transparency layer cut to fit the inlet holes and seal the device.

Operation of the device starts with addition of blue dye at stage 1. Then at stage 2, yellow dye is added and both blue and yellow dyes meet at a junction point. Once both fluids meet at a junction point flow is then initiated into the main channel (Figure 3.1c). Stages 1-5 in Figure 3.1c demonstrate how fluid is added and remains laminar while completely washing the sample through the device (red dye) with only small diffusional mixing. At stage 1 and 2, the blue and yellow dyes are added and laminar flow begins once both reach the junction point. At stage 3 and 4 the red dye is added to simulate the sample where it is completely washed through the device while maintaining laminar flow. At stage 5, the red dye has been completely washed through

ensuring the maximum amount of sample reaches the detection zone, improving the detection limit.

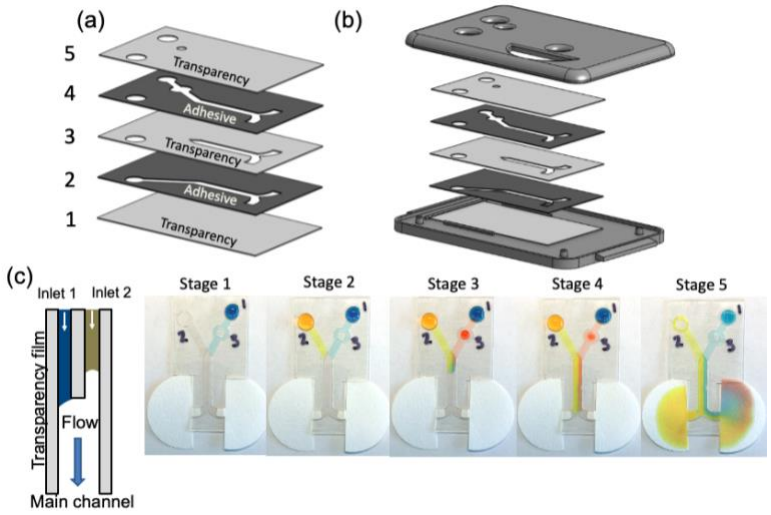

Figure 3.1. (a) CAD rendering of assembly of the device with alternating layers of transparency film and double-sided adhesive with layer assembly 1-5. (b) Device construction with 3D printed housing. (c) Demonstration of laminar flow with simultaneous delivery of reagents into the main channel with food dye. Stage 1-5 shows the addition of each reagent (blue, yellow, and red) while maintaining laminar flow.

3.2.4 E. coli Growth and Sample Preparation

E. coli DH5-Alpha was used as the model bacteria in this work; it was grown in Universal Enrichment Broth (Sigma-Aldrich, pH 7) overnight (12-16hr) in a shaker at 37°C and 220 rpm. The bacteria concentration was quantified by serial dilution and plating on lysogeny broth (LB) agar plates. Serial dilutions of this solution were made using PBS or human pooled urine.

3.2.5 E. coli Detection Using Immunomagnetic Separation

The enzymatic assay presented by Srisa-Art et al. was modified for DH5-Alpha detection.[22] The entire assay was performed on the benchtop at room temperature and displayed in Figure 3.2. First, 100 µL of 2.5mg/mL 8µm streptavidin coated paramagnetic beads (SpheroTech) were vortexed for 30 s at room temperature. Second, the beads were conjugated to 5 µg/mL of biotinylated anti-*E. coli* in a microcentrifuge tube for 20 min on a rotator. Third,

an immunomagnetic separation (IMS) was performed using a magnet (DynaMag-2 magnet, Thermo Fisher Scientific, Inc.) to isolate and concentrate the magnetic bead-antibody complex by removing the supernatant and resuspending the content in 100 µL of PBS. Fourth, the bead-antibody complex was added to 1 mL of *E. coli* spiked urine and incubated on a rotator for 30 min. Another IMS step was performed to isolate/concentrate the sample and to remove the supernatant. The complex was washed twice with PBS-Tween (0.1%) to remove any unbound species and blocked with 5% bovine serum albumin (BSA). Finally, 5 µg/mL of anti-*E. coli* horseradish peroxidase (HRP) was conjugated to the bead complex for 20 min on a rotator. The final complex was then washed twice using IMS with PBS-Tween and blocked with 5% BSA. The complex was then resuspended in 100 µL of urine to give a bead concentration of 2.5 mg/mL. 10 µL of the complex was then added to the device with 30 µL of PBS buffer and 65 µL of Ultra-TMB to create capillary driven laminar flow. The permanent magnet was placed on the adjacent channel at the desired detection zone. After 30 s the fast flow has stopped, and analysis of *E. coli* capture was analyzed by mean grey scale intensity with ImageJ from a smartphone picture.

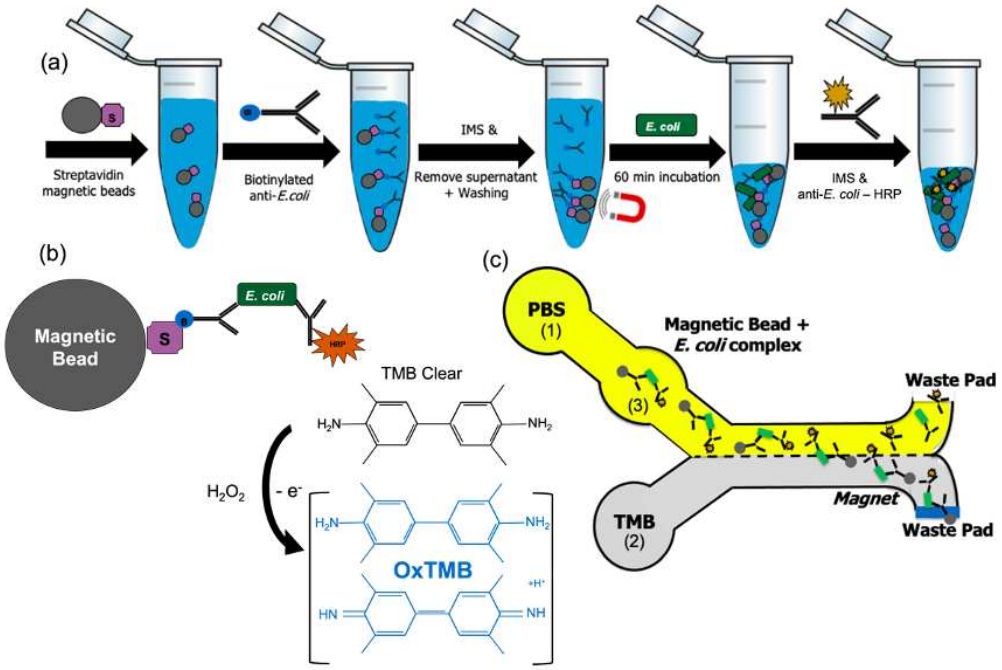

Figure 3.2. Schematic of immunomagnetic separation process of sequential binding of magnetic complex. (a) Binding schematic of immunomagnetic separation process of conjugating the magnetic bead sandwich complex. (b) Schematic of the enzyme-substrate reaction of TMB with HRP. (c) Flow schematic of reagent additions into the device with the full sandwich *E. coli* complex, where PBS is added first, then TMB is added second, and finally the magnetic bead complex is added last.

3.2.6 Image Analysis

Images were taken using a smartphone of the paper waste pads where the color develops. Images were imported into ImageJ, inverted, converted to 8-bit and intensity measurements were taken following published protocols. A consistent area where the blue color forms in the detection zone was measured (Figure A2.1). Mean grey scale intensity plots were created using a 4-parameter logistical (4PL) regression curve.

3.2.7 Paramagnetic Magnetic Beads

Commercially available 8µm paramagnetic streptavidin labeled beads were purchased from SpheroTech Inc (Lake Forrest, Illinois). The beads were purified through immunomagnetic

separation washes of PBST to remove any unbound streptavidin molecules before use. The beads were then resuspended in PBS at 2.5 mg/mL and store at 4˚C before use.

3.3 Results and Discussion

3.3.1 Immunomagnetic Conjugation

To address sensitivity issues with the original magnetophoresis device, we transferred from a fluorescent label to an enzymatic label for visual color formation. Enzymatic labels such as horseradish peroxidase (HRP) are commonly used to label target analytes in traditional ELISAs.[27, 28] Colorimetric reactions between enzymes and specific substrates provide fast reaction rates with easy-to-read signals.[27-29] HRP and TMB are a well-known enzyme-substrate pair that produce a strong color change from colorless to bright blue in the presence of peroxide (Figure 3.2b). HRP is readily available, inexpensive, stable and has a high turnover rate, making it an ideal enzyme for POC diagnostics.[28] Using a colorimetric system allows for easier read-by-eye detection for a simple qualitative test if desired. Furthermore, smartphone apps have been used in the past to take a picture of the detection zone, perform a color intensity measurement and then provide a concentration dependence.[30, 31] The magnetic complex was washed after each labeling step to ensure all supernatant is removed before the next labeling step. Off-chip conjugation requires multiple pipetting steps and user manipulation which is not ideal for a POC assay. However, the complex was shown to be stable after two weeks at 4˚C, indicating that the magnetic bead complex can be shipped with the capture antibody already labeled. Future iterations of this system will be aimed at reducing the number of off-chip steps to include the washing and incubation steps being performed on-chip with little user-manipulation.

3.3.2 Device Design and Assembly

In a previous publication we demonstrated the first paper-based pump-free magnetophoresis device.[25] However, the first version of the device did not provide sufficiently low detection limits to be of significant use clinically and require very precise control of sample addition to establish laminar flow. To solve the laminar flow challenge, we changed the device design to take out user error associated with sample addition to generate laminar flow. In 2019 Jang *et al,* introduced burst valves into paper-based microfluidics to control flow by controlling the geometry channel intersections in an assembled multi-layer device.[26] Building on this concept, we incorporated a burst valve into the working device to establish laminar flow more reproducibly. The burst valve works by controlling the geometry of the 3rd layer of transparency as shown in Figure 3.3a. The pointed geometry of the 3rd layer allows the user to add one sample at a time without flow being initiated into the main channel until both fluids meet at the junction point in layer 3 as shown in Figure 3.1c.

Secondly, we observed in the first version of the device magnetic beads were left in the sample inlet after flow stopped. To solve this, we added a sample inlet in between the wash buffer reservoir and the junction area to wash the magnetic beads completely out of the sample inlet (Figure 3.3b). In order to make a buffer flow consistently, a flow channel is designed around the inlet hole. Another advantage of the sample inlet is that the sample could be added in the middle of the operation without an air bubble problem. The wash buffer reservoir successfully washes the magnetic beads from the inlet to the detection zone as shown by red food dye in Figure 3.3c. Once the fluid reaches the paper waste pad at the end of the device flow is driven by wicking through the cellulose. Flow features of the developed device are achieved without usinga complicated pump or valve system. For stages 1 through 4, the flow is driven by the capillary acting on a

hydrophilic film. However, once the fluid reaches the paper waste pad at the end of device is driven by wicking through the cellulose (Figure 3.1).

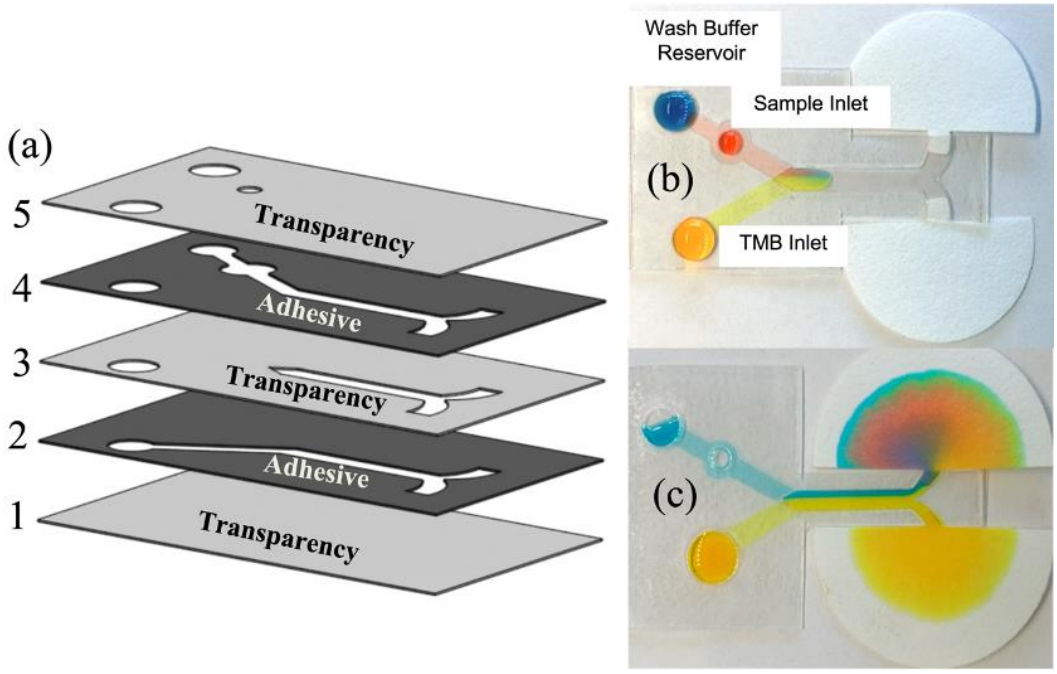

Figure 3.3. (a) CAD assembly rendering of the current paper-magnetophoresis model. (b) Photography of fully assembled device from 3b while undergoing flow using food dye. (c) Photography of a device undergoing flow after the red food dye has been washed through.

3.3.3 Flow Optimization

It is crucial to establish consistent laminar flow in this device to avoid mixing of the sample containing secondary-HRP antibody and TMB. The use of valves is common practice to control fluids by controlling the geometry and design of the channels.[32, 33] By establishing consistent parallel flow from the two fluid inlets, we can control parallel flow with only diffusional mixing of the TMB and sample. Optimal sample volumes were investigated to determine which conditions allowed for reproducible laminar flow without unintended mixing. Volume ranges from 10-40 µL of wash buffer were investigated, along with 30-70 µL of Ultra-TMB and 5-20 µL of bead-sample. 30 µL of buffer with 65 µL of Ultra-TMB were chosen as they gave the most reproducible flow results. If too much fluid was added to the device, the burst

valve initiated before both flow streams reached the junction point due to increased Laplace pressure. 10 µL of bead-sample was chosen because it was the smallest amount of sample that would still give strong enough signal for analysis while conserving sample. Additionally, the order of the sample and reagent addition was investigated to determine flow success rate to ensure the device can be operated by untrained users at a POC settings. It was determined that the optimal order of sample additions to generate the most consistent flow was to add 30 µL of wash buffer and then 65 µL of Ultra-TMB. After the first two steps were completed, flow reached the burst valve and flow in the main channel was initiated. 10 µL of the sample containing magnetic particles was then added to the sample inlet. The 30 µL of wash buffer loaded behind the 10 µgµL sample addition washed all the magnetic beads through while flow remained laminar through the main channel as shown in Figure 3.1c. Paper waste pads were inserted at the end of the capillary device to continuously wick fluid through the device while laminar flow was maintained.

3.3.4 Device Operation with Housing Assembly

A 3D printed housing was designed for the device to improve assay operation. An integrated magnet holder keeps the magnet in the correct orientation during the assay, while a window is included to visualize color formation of the blue oxidized TMB. A sample inlet port keeps all reagents contained during the assay for improved ease-of-use. Finally, alignment and friction boss features keep the capillary device in place and the top and bottom parts of the housing held securely together. Operation of the device is outlined in Figure 3.4. Once conjugation of the urine sample to the magnetic beads has been completed, the full assay can be broken down into three steps: (1) 30 µL of PBS wash buffer into the top sample port, (2) 65 µL of TMB substrate solution is loaded into the bottom sample port, (3) 10 µL of magnetic bead complex is added to

the sample inlet. After 10 min from sample addition, the device can be read for either a positive or negative *E. coli* sample. Presence of blue color indicates a positive sample, while no blue color being present indicates a negative sample. The photograph taken in Figure 3.4 of the blue color formation resulted from the processing of a urine sample with 10^6 CFU/mL *E. coli.*

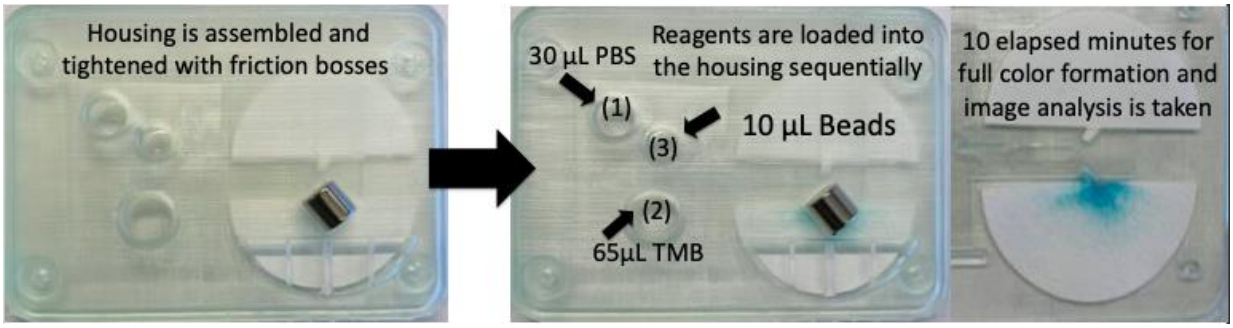

Figure 3.4. Photographs of device assembly and operation to color formation of a positive *E. coli* sample. Sample shown in picture was from 10^6 CFU/mL 14-day old conjugation.

3.3.5 Colorimetric E. coli Detection

Colorimetric *E. coli* detection was conducted initially using phosphate buffered saline (PBS) as a sample matrix and was then conducted in human pooled urine to mock a real urine sample. Here, *E. coli* cultured in universal growth medium was diluted to concentrations from 10^2 to 10^7 CFU/mL. Results for *E. coli* diluted in PBS and urine are shown in Figure 3.5a and 3.5b, respectively. The data was fit to a 4-parameter logistic curve (4PL) commonly used for immunoassays because of the antibody binding limiting kinetics of the sandwich immunoassay.[17, 34] LODs of 2.40 x 10^2 CFU/mL (PBS) and 4.67 x 10^2 CFU/mL (urine) were calculated using the 4PL ($3\sigma + \bar{\mu}$). In the urine-based assay, the conjugation of the immunomagnetic sandwich, as well as the final complex were both conducted in urine. Future iterations of this assay will be aimed at performing the conjugation and washing steps on-chip so showing the assay is still functional in urine is crucial moving forward. An LOD of 4.67 x 10^2 CFU/mL was calculated for the human urine assay. By creating a wash-through style device while also using an enzyme substrate

detection system we were able to improve our limit of detection by 3-fold from the previous work, which demonstrates the capability of this device to detect bacteria from complex samples in the early stages of infection.

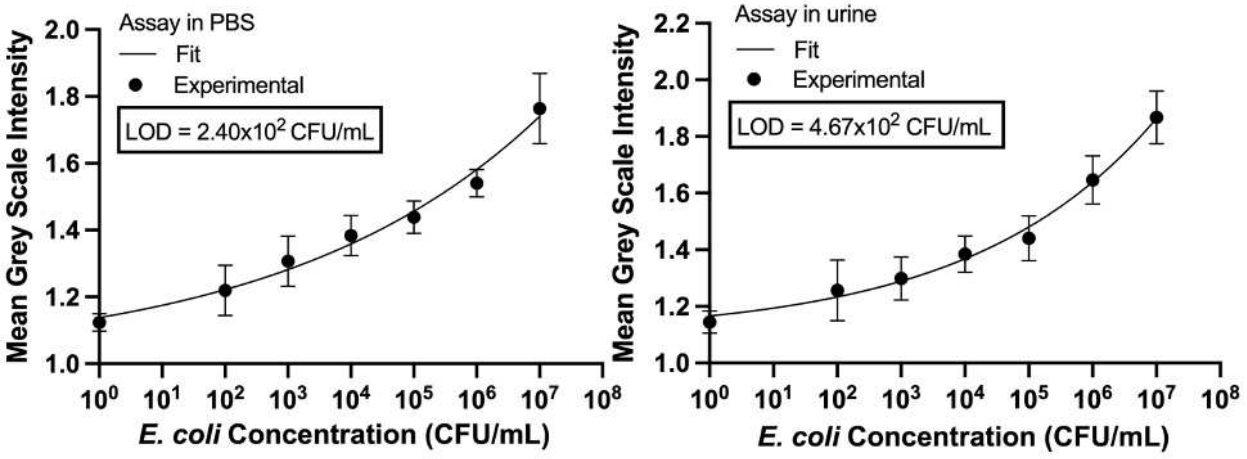

Figure 3.5. 4PL regression curve for the *E. coli* immunoassay. (a) Immunoassay curve with the conjugation of *E. coli* in PBS. (b) Immunoassay curve with the conjugation of *E. coli* in the presence of human pooled urine and then resuspended in urine to run the assay.

3.4 Conclusions and Future Work

UTIs remain one of the most common infections and current UTI diagnostics fall short. A rapid, inexpensive, sensitive, and easy to use assay is urgently needed. Early detection of UTIs in health-care settings such as hospitals and nursing homes is crucial to prevent serious infection and reduce misuse of antibiotics in these settings. Here we have shown the capability of μPADs coupled with magnetophoresis as a powerful POC device that rivals traditional laboratory methods. In this work we developed a power-free capillary driven device that detects *E. coli* from a complex matrix with detection limits of 10^2 CFU/mL in buffer and 4.67 x 10^2 CFU/mL in urine. The device could generate laminar flow consistently as well as transport magnetic particles to the detection area completely. Importantly, this device can be used for many analytes other than *E. coli.* By simply changing the specific antibodies, other organisms, biomarkers, and DNA could also be

detected. The assay described is an easy-to-read test that can provide feedback for patients in 10 min or less. Quick assay times will help control UTIs in the community and healthcare settings. Future work for this project will involve transferring conjugation and washing steps to be conducted on-chip with little to no user intervention. We believe a one-step magnetophoresis UTI assay would impact patient care in at home settings and healthcare. In future iterations of this device, we will be working with local hospitals and nursing homes to start to test this platform with patient samples.

REFERENCES

1. Lallukka, T.; Millear, A.; Pain, A.; Cortinovis, M.; Giussani, G., GBD 2015 mortality and causes of death collaborators. Global, regional, and national life expectancy, all-cause mortality, and cause-specifi c mortality for 249 causes of death, 1980-2015: a systematic analysis for the global burden of disease study 2015 (vol 388, pg 1459, 2016). *Lancet* **2017,** *389* (10064), E1-E1.
2. Medina, M.; Castillo-Pino, E., An introduction to the epidemiology and burden of urinary tract infections. *Therapeutic advances in urology* **2019,** *11*, 1756287219832172.
3. Flores-Mireles, A. L.; Walker, J. N.; Caparon, M.; Hultgren, S. J., Urinary tract infections: epidemiology, mechanisms of infection and treatment options. *Nature Reviews Microbiology* **2015,** *13* (5), 269-284.
4. Control, C. f. D. Catheter-Associated Urinary Tract Infection. https://www.cdc.gov/hai/pdfs/uti/ca-uti_tagged.pdf.
5. Cortese, Y. J.; Wagner, V. E.; Tierney, M.; Devine, D.; Fogarty, A., Review of catheter-associated urinary tract infections and in vitro urinary tract models. *Journal of healthcare engineering* **2018,** *2018*.
6. Arinzon, Z.; Peisakh, A.; Shuval, I.; Shabat, S.; Berner, Y. N., Detection of urinary tract infection (UTI) in long-term care setting: Is the multireagent strip an adequate diagnostic tool? *Archives of gerontology and geriatrics* **2009,** *48* (2), 227-231.
7. Zeng, Z.; Zhan, J.; Zhang, K.; Chen, H.; Cheng, S., Global, Regional, and National Burden of Urinary Tract Infections from 1990-2019: an Analysis of the Global Burden of Disease Study 2019. **2021**.
8. Davenport, M.; Mach, K. E.; Shortliffe, L. M. D.; Banaei, N.; Wang, T.-H.; Liao, J. C., New and developing diagnostic technologies for urinary tract infections. *Nature Reviews Urology* **2017,** *14* (5), 296-310.
9. Scheifele, D. W.; Smith, A. L., Home-testing for recurrent bacteriuria, using nitrite strips. *American Journal of Diseases of Children* **1978,** *132* (1), 46-48.
10. Ouslander, J. G.; Schapira, M.; Fingold, S.; Schnelle, J., Accuracy of rapid urine screening tests among incontinent nursing home residents with asymptomatic bacteriuria. *Journal of the American Geriatrics Society* **1995,** *43* (7), 772-775.
11. Butler, C. C.; Dunstan, F.; Heginbothom, M.; Mason, B.; Roberts, Z.; Hillier, S.; Howe, R.; Palmer, S.; Howard, A., Containing antibiotic resistance: decreased antibiotic-resistant coliform urinary tract infections with reduction in antibiotic prescribing by general practices. *British Journal of General Practice* **2007,** *57* (543), 785-792.
12. Carrell, C.; Kava, A.; Nguyen, M.; Menger, R.; Munshi, Z.; Call, Z.; Nussbaum, M.; Henry, C., Beyond the lateral flow assay: A review of paper-based microfluidics. *Microelectronic Engineering* **2019,** *206*, 45-54.
13. Martinez, A. W.; Phillips, S. T.; Whitesides, G. M.; Carrilho, E., Diagnostics for the Developing World: Microfluidic Paper-Based Analytical Devices. *Analytical Chemistry* **2010,** *82* (1), 3-10.
14. Yamada, K.; Shibata, H.; Suzuki, K.; Citterio, D., Toward practical application of paper-based microfluidics for medical diagnostics: state-of-the-art and challenges. *Lab on a chip* **2017,** *17* (7), 1206-1249.

15. Martinez, A. W.; Phillips, S. T.; Butte, M. J.; Whitesides, G. M., Patterned paper as a platform for inexpensive, low-volume, portable bioassays. *Angewandte Chemie-International Edition* **2007,** *46* (8), 1318-1320.
16. Aimeida, M. I. G. S.; Jayawardane, B. M.; Kolev, S. D.; McKelvie, I. D., Developments of microfluidic paper-based analytical devices (mu PADs) for water analysis: A review. *Talanta* **2018,** *177*, 176-190.
17. Carrell, C. S.; Wydallis, R. M.; Bontha, M.; Boehle, K. E.; Beveridge, J. R.; Geiss, B. J.; Henry, C. S., Rotary manifold for automating a paper-based Salmonella immunoassay. *RSC Advances* **2019,** *9* (50), 29078-29086.
18. Akyazi, T.; Basabe-Desmonts, L.; Benito-Lopez, F., Review on microfluidic paper-based analytical devices towards commercialisation. *Analytica Chimica Acta* **2018,** *1001*, 1-17.
19. Pamme, N.; Manz, A., On-chip free-flow magnetophoresis: Continuous flow separation of magnetic particles and agglomerates. *Analytical Chemistry* **2004,** *76* (24), 7250-7256.
20. Phurimsak, C.; Tarn, M. D.; Peyman, S. A.; Greenman, J.; Pamme, N., On-Chip Determination of C-Reactive Protein Using Magnetic Particles in Continuous Flow. *Analytical Chemistry* **2014,** *86* (21), 10552-10559.
21. Bhardwaj, J.; Devarakonda, S.; Kumar, S.; Jang, J., Development of a paper-based electrochemical immunosensor using an antibody-single walled carbon nanotubes bio-conjugate modified electrode for label-free detection of foodborne pathogens. *Sensors and Actuators B: Chemical* **2017,** *253*, 115-123.
22. Kasetsirikul, S.; Shiddiky, M. J. A.; Nguyen, N.-T., Challenges and perspectives in the development of paper-based lateral flow assays. *Microfluidics and Nanofluidics* **2020,** *24* (2), 17.
23. Pamme, N.; Wilhelm, C., Continuous sorting of magnetic cells via on-chip free-flow magnetophoresis. *Lab on a Chip* **2006,** *6* (8), 974-980.
24. Alnaimat, F.; Dagher, S.; Mathew, B.; Hilal-Alnqbi, A.; Khashan, S., Microfluidics Based Magnetophoresis: A Review. *Chem Rec* **2018,** *18* (11), 1596-1612.
25. Call, Z. D.; Carrell, C. S.; Jang, I.; Geiss, B. J.; Dandy, D. S.; Henry, C. S., Paper-based pump-free magnetophoresis. *Analytical Methods* **2020,** *12* (43), 5177-5185.
26. Jang, I.; Kang, H.; Song, S.; Dandy, D. S.; Geiss, B. J.; Henry, C. S., Flow control in a laminate capillary-driven microfluidic device. *Analyst* **2021,** *146* (6), 1932-1939.
27. Shih, C. M.; Chang, C. L.; Hsu, M. Y.; Lin, J. Y.; Kuan, C. M.; Wang, H. K.; Huang, C. T.; Chung, M. C.; Huang, K. C.; Hsu, C. E.; Wang, C. Y.; Shen, Y. C.; Cheng, C. M., Paper-based ELISA to rapidly detect Escherichia coli. *Talanta* **2015,** *145*, 2-5.
28. Overview of detection probes. *thermofisher*.
29. Volpe, G.; Draisci, R.; Palleschi, G.; Compagnone, D., 3, 3′, 5, 5′-Tetramethylbenzidine as electrochemical substrate for horseradish peroxidase based enzyme immunoassays. A comparative study. *Analyst* **1998,** *123* (6), 1303-1307.
30. Shen, L.; Hagen, J. A.; Papautsky, I., Point-of-care colorimetric detection with a smartphone. *Lab on a Chip* **2012,** *12* (21), 4240-4243.
31. Gul, I.; Bogale, T. F.; Deng, J.; Chen, Y.; Fang, R.; Feng, J.; Tang, L., Enzyme-based detection of epoxides using colorimetric assay integrated with smartphone imaging. *Biotechnology and applied biochemistry* **2020,** *67* (4), 685-692.
32. Cho, H.; Kim, H.-Y.; Kang, J. Y.; Kim, T. S., How the capillary burst microvalve works. *Journal of colloid and interface science* **2007,** *306* (2), 379-385.

33. Bauer, M.; Ataei, M.; Caicedo, M.; Jackson, K.; Madou, M.; Bousse, L., Burst valves for commercial microfluidics: A critical analysis. *Microfluidics and Nanofluidics* **2019,** *23* (7), 1-12.
34. Gottschalk, P. G.; Dunn, J. R., The five-parameter logistic: a characterization and comparison with the four-parameter logistic. *Analytical biochemistry* **2005,** *343* (1), 54-65.

CHAPTER 4. MAGNETOPHORESIS SLIDER ASSAY (MeSA): A SIMPLE PLATFORM FOR POINT-OF-CARE DIAGNOSTICS

Infectious diseases account for millions of deaths each year worldwide. To reduce the number of infectious disease related deaths, diagnostic testing needs to be more accessible to patients in low-income countries as well as developed countries. Current diagnostic methods rely on centralized laboratories, trained personnel, and are time intensive, limiting translation to the point-of-care (POC). Microfluidic devices are a popular alternative for diagnostics due to reduced assay times, reduced sample volume, and lower cost. Microfluidic devices are small (<10 cm) and can perform complex assays. Microfluidic paper-based analytical devices (μPADs) are a popular approach to help translate diagnostics to the POC but historically suffer from poor sensitivity when compared to established laboratory methods. Magnetically labeling analytes allows samples to be sorted resulting in improved sensitivity and specificity. Microfluidic magnetophoresis is the process of manipulating magnetic particles in a magnetic field and offers the ability to wash and concentrate a sample during flow. However, until recently, magnetophoresis has not been used in conjunction with μPADs because magnetophoresis requires complex and expensive instrumentation to control flow. Coupling magnetophoresis with μPADs enables pump-free flow control, simple operation, and low cost. Early magnetophoresis μPADs showed detection limits similar to traditional methods, but higher than targets for clinical use. In this work, we demonstrate a novel, simple Magnetophoresis Slider Assay (MeSA) that is free of any external instrumentation and offers a new platform for POC diagnostics. We demonstrate the assay's capability through biotin competitive assays and a sandwich immunoassay for *E. coli* detection. The calculated limit of detection for *E. coli* was 1.62×10^3 colony forming units per mL (CFU/mL). The work described is a novel and simple microfluidic platform that has potential for a wide range of future

applications. This chapter is in preparation for submission. I was the first author and was the sole writer of this work. All experiments were conducted by myself with this assistance of Alli Dolence and Jason Boes.

4.1 Introduction

Infectious diseases account for millions of deaths each year globally, and approximately one third of all annual deaths.[1] In 2020 alone, 10 million people were diagnosed with tuberculosis and 1.5 million people died from their infections.[2] The World Health Organization (WHO) states that Point-of-Care (POC) diagnostics are critical to reducing the number of infectious disease related deaths each year.[3, 4] POC testing is performed at or near the location of the patient, reducing the time needed to obtain a result.[5] However, current diagnostics are not accessible to all patients at the point of care, especially for those in low resource settings.[6, 7] To make current diagnostics more accessible to patients in need, assays need to be rapid, simple, and field-deployable.[8] The COVID-19 pandemic demonstrated the need for accessible diagnostics effective for pathogen detection.[9] Coupling existing laboratory techniques with microfluidic technology is a popular approach to improve sensitivity, specificity, and ease of use while making diagnostic testing more accessible.[10]

Microfluidic devices are able to handle small sample volumes precisely without tedious user intervention making them ideal for POC testing.[3, 10] Microfluidic devices have been developed to detect bacteria, viruses, heavy metals in water, and other infectious agents.[3, 10-13] Traditional microfluidic devices have been fabricated using photolithography with silicon wafers, glass, quartz, and/or poly(dimethylsiloxane) (PDMS) using methods that are expensive, time intensive, and use harsh chemicals.[14-17] An alternative to traditional microfluidics is microfluidic paper-based analytical devices (µPADs). µPADs are paper-based microfluidic devices with patterned

hydrophobic barriers to define fluid channels. There are several techniques to fabricate hydrophobic channels including; wax printing/dipping, photoresist, parafilm stamping, or as simple as drawing with a crayon.[18] μPADs are cheap, portable, and easy to fabricate in resource-limited settings.[15, 19] However, μPADs historically suffer from poor sensitivity and specificity when compared to traditional microfluidic techniques and established laboratory practices such as PCR and ELISA.[20, 21] To improve sensitivity and specificity of μPADs, sample washing and concentration steps are needed.[15, 22, 23]

Magnetophoresis is the process of manipulating magnetic particles using a magnetic field. It allows magnetic particles to be moved through a sample matrix so that the captured targets can be concentrated and pulled through wash buffers to remove any non-specifically bound substances, improving assay sensitivity and specificity.[24, 25] The Pamme group pioneered the field of magnetophoresis using PDMS and glass chip systems and external pumps to drive flow.[24, 26, 27] They have demonstrated the ability to conjugate magnetic particles during flow, detect multiple analytes such as C-reactive protein, *E. coli* and *Salmonella*, and to multiplex assays. Their work demonstrates the ability of magnetophoresis to simplify tedious laboratory techniques. However, traditional magnetophoresis is difficult to translate to the POC because of the need for external pumps, limiting portability.[24-28] Immiscible filtration assisted by surface tension (IFAST) is a magnetophoresis technique that eliminates the need for external pumps. IFAST is a process to wash a magnetic complex by using a permanent magnet to drag the complex through an immiscible phase.[29] While these methods address some of the problems with magnetophoresis, they still require complex fabrication and/or use of external pumps.

Recent work demonstrated the first example of magnetophoresis in μPADs without the need for external pumps for the detection of *E. coli*.[30] The limit of detection (LOD) was 10^5

CFU/mL of *E. coli* with no need for external pumps.[30] Even though this work demonstrated a proof of concept for magnetophoretic μPADs, several improvements were identified to make the method viable for POC settings. First, the reported LOD in human pooled urine is at the upper limits of clinically relevant levels. Second, several manual pipetting steps were required. Third, along with the motivation to transfer away from wax printing, magnetic particles can become trapped in the cellulose fibers, making magnetophoresis difficult.[31]

In this work, we report a hybrid magnetophoresis μPAD building off the previous magnetophoresis and IFAST work to simplify user manipulation without the need for external pumps. In this assay, a solution containing magnetic particles is added to the center of a capillary flow microfluidic device. A magnet under the inlet traps particles but allows sample to flow to outlets where reagents are rehydrated. To perform the assay, particles are pulled between reservoirs by translating the device relative to a fixed magnet. We refer to the assay as the Magnetophoresis Slider Assay (MeSA) based on the manipulation of particles by sliding the device. As proof of principle, we demonstrate a competitive assay for biotin and sandwich immunoassay for *E. coli*. To our knowledge this is the first example of this type of system coupled with μPADs. The MeSA described is a novel and simple platform that shows potential for a wide range of applications that can advance the microfluidic diagnostics.

4.2 Materials and Methods

4.2.1 Materials

Hydrophilic transparency 9984 sheets were purchased from 3M. 467 and 468 Double-sided adhesive (DSA) sheets (467-MP-ND/468-MP-ND) were purchased through DigiKey. Glass fiber membrane (GFDX203000) was purchased Millipore Sigma (Burlington, MA). A cylindrical ¼" x

¼” Neodymium Iron Boron (NdFeB) permanent magnet, grade N52 (K&J Magnetics, INC.) was used to create an external magnetic field. Other magnet types and shapes were investigated; however, the cylindrical magnet was chosen because of the smaller size while maintaining strong field lines. The DynaMag Magnet was used for magnetic separations and purchased from Thermo Fisher Scientific (Waltham, MA). Streptavidin-coated paramagnetic beads (SVM-05-5H) were purchased from Spherotech Inc. (Lake Forest, Illinois). Biotin-HRP (29139) and 1-step Ultra TMB-ELISA (34028) were purchased from Thermo Fisher Scientific. Biotin (58-85-5) and 55K Polyvinylpyrrolidone (PVP) were purchased from Sigma-Aldrich (St. Louis, MO). *E. coli* antibodies (bs-2033R/bs-2033R-A555) were purchased from Bioss Antibodies (Woburn, MA). The buffers used in this work were 0.1 M phosphate-buffered saline (PBS) and 0.1 M PBS with 0.1% Tween-20 (PBST). The two antibodies were diluted in PBS before use. Human pooled urine was purchased from Lee BioSolutions (Maryland Heights, MO) and was not subject to IRB approval.

4.2.2 Device Construction

The optimized device consists of five alternating layers of 9984 transparency film and 468 DSA with a reagent glass fiber pad on each end of the device. The device was first assembled with a bottom layer of transparency film, followed by the first DSA layer outlining the fluid channel. The third layer of transparency was placed on top of layer two and was used to seal the fluid channel. Reagent pads were then loaded into the end wells. The following layer of DSA was then placed on top of the reagent pads followed by a final transparency layer to seal the whole device with vent holes on each end. Each layer has a hole in the middle of the device to allow sample to flow down to the bottom fluid channel. Devices were assembled in sets of three and then cut into singular devices before running the assay.

4.2.3 Glass Fiber Membrane Preparation

Glass fiber membrane was first cut into 6 cm x 6 cm squares and loaded into a petri dish. Excess 1% PVP prepared in DI water was added to the petri dish and the glass fiber membrane was soaked for 10 min to fully coat the membrane. Excess PVP was then discarded into waste and membranes were placed onto a mesh for drying. Each membrane square was then dried overnight at 37˚C. Following drying, the membrane was cut into circles using a 4mm biopsy punch. Membrane circles were then stored in a sealed container with silica packets until use.

4.2.4 Imaging Process

Images of each device were taken with a smartphone and imported into ImageJ for data analysis. A white background was used for each image and the smartphone was focused on same part of the TMB reagent pad before each image. Devices were placed in precisely the same spot under a light to control the consistency of the images.

4.2.5 Immunomagnetic Separation (IMS)

Before binding steps, the streptavidin magnetic beads were aliquoted from a stock solution and washed with PBS to remove excess streptavidin not bound to the beads. The DynaMag Magnet was used to remove the magnetic beads from solution to remove the supernatant. The beads were then resuspended in PBS at the desired concentration for each assay.

4.2.6 Biotin Competitive Assay

The 3,3',5,5' - Tetramethylbenzidine (TMB) reagent pad was loaded with 30 µL and dried at 37˚C in an oven for 1 h. The Biotin-HRP reagent pad was loaded with 10 µL at 1 mg/mL and dried at 37˚C for 1 h. Biotin solutions (0.5 mg/mL – 10 mg/mL) were prepared in PBS and

incubated with 1 mg/mL of 0.4 µm streptavidin magnetic beads for 30min while rotating at room temperature. A magnetic separation was conducted after conjugation to remove any unbound biotin and the resulting solution was washed with PBS-Tween (0.1%) and then resuspended into PBS at 1 mg/mL. 60 µL of resulting solutions were then loaded into each device and the device was ran following established protocols.

4.2.7 E. coli Sandwich Immunoassay

The TMB reagent pad was loaded with 30 µL and dried at 37˚C for 1h. 10 µL of the secondary anti-*E. coli*- HRP antibody was loaded onto the second reagent pad at 40 µg/mL and dried at 37˚C for 1h. First, 100 µL of 2.5 mg/mL 0.47 µm streptavidin magnetic beads were vortexed for 30 s at room temperature. Second, the beads were conjugated to 5 µg/mL of biotinylated anti-*E. coli* in a microcentrifuge tube for 20 min on a rotator. Third, IMS was performed using a magnet (DynaMag) to isolate and concentrate the magnetic bead-antibody complex by removing the supernatant and resuspending the content in 100 µL of PBS. Fourth, the bead-antibody complex was added to 1 mL of various concentrations of *E. coli* diluted in PBS and incubated on a rotator for 30 min. Another IMS step was performed to isolate and concentrate the sample, and to remove the supernatant. The complex was washed twice with PBS-Tween (0.1%) to remove any unbound species and blocked with 5% bovine serum albumin (BSA). Finally, 60 µL of the magnetic bead complex at varying concentrations of *E. coli* was then loaded into the device.

4.3 Results and Discussion

4.3.1 Device Design and Assembly

Traditional microfluidic magnetophoresis has demonstrated the ability to perform complex assays.[23-26] However, it is difficult to use in resource limited settings because of the need for external pumps. IFAST offers the advantages of magnetophoresis without the need for external pumps but involves complicated fabrication of a PDMS-glass microchip. We wanted to combine the advantages of IFAST with hybrid capillary devices to improve magnetophoresis μPADs. Previous studies have shown the ability to rehydrate stored reagents on diagnostic membranes to then be sequentially bound.[32, 33] In this work, we have created a simple diagnostic platform, MeSA, that replaces the need for multiple pipetting steps with simply sliding a magnet. We have created a hybrid μPAD that operates by manually sliding a magnet to sequentially bind and wash magnetic complexes. The device is free of any external instrumentation or complex fabrication. The devices are small (80mm x 20mm) and easily portable, making them ideal for POC testing.

The device assembly is shown in Figure 4.1a with blue arrows denoting how the fluid flows through the device**.** First, sample is added into the inlet and fluid flows down through the device until it reaches the bottom fluid channel outlined by the laser cut DSA. Second, capillary action initiates and fills the fluid channel. Third, the fluid flows upward to rehydrate the reagent pads. The reagents stay localized at the pad because after rehydration there is excess sample in the inlet, allowing hydrostatic pressure to prevent fluid flow back toward the inlet (Figure A3.1).[34, 35] Additionally, this keeps the fluid in the channel free of reagents and allows it to act as a wash

buffer during the sliding operation. Vent holes are cut into the top layer of transparency to allow air to escape, preventing air bubbles from forming in the fluid channel.

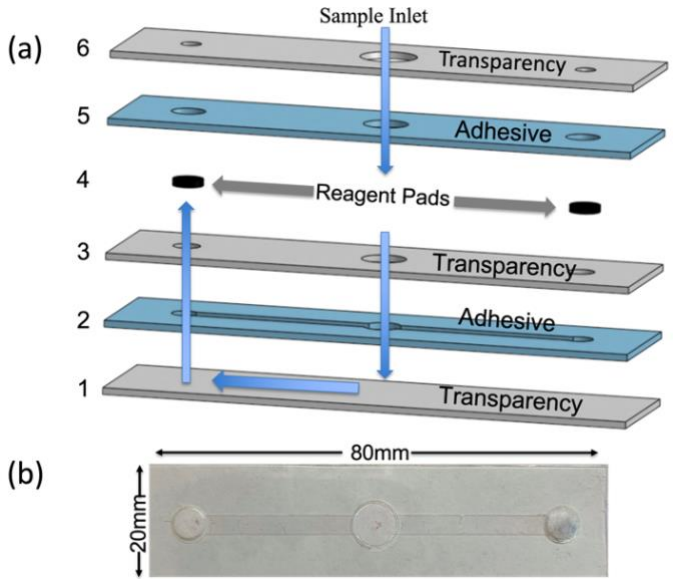

Figure 4.1. (a) CAD rendering of device assembly with alternating transparency and double-sided adhesive layers with blue arrows to indicate the operation of the fluid flow through the device. (b) Photograph of the fully assembled device.

4.3.2 Flow Rate Optimization

In 2018, Channon et al. reported the ability to control flow rate in multi-layer µPADs by varying the channel height.[34, 36] For the MeSA, optimal channel height and flow rate are critical variables to produce consistent flow and elution of reagents from the reagent pads. Two DSA types were investigated to control flow rate, 3M-467 and 3M-468, which have 60 µm and 120 µm thicknesses respectively. Two measurements were taken to determine the optimal channel height and consistency of flow with varying fluid amounts from 40-100 µL. First, the time elapsed until fluid reached the reagent pad was measured and then the time elapsed until the pads were fully rehydrated. Yellow and blue food dye were dried on the reagent pads to visualize flow and the time to rehydrate. (**SI.1**) Devices assembled with 467 DSA with a 60 µm channel height displayed high variability and slower flow to reach/rehydrate the pad. Devices assembled with 468 DSA,

however, displayed smaller error and a decrease in time to reach/rehydrate the pad (Figure 4.2). We hypothesize this is due to the lower surface area to volume ratio with higher channel heights. Following this optimization, devices were assembled using 468 DSA. To reduce sample volume and rehydration time, 60 µL was chosen as the ideal sample volume.. However, we demonstrate a wide range of sample volumes are compatible with this device.

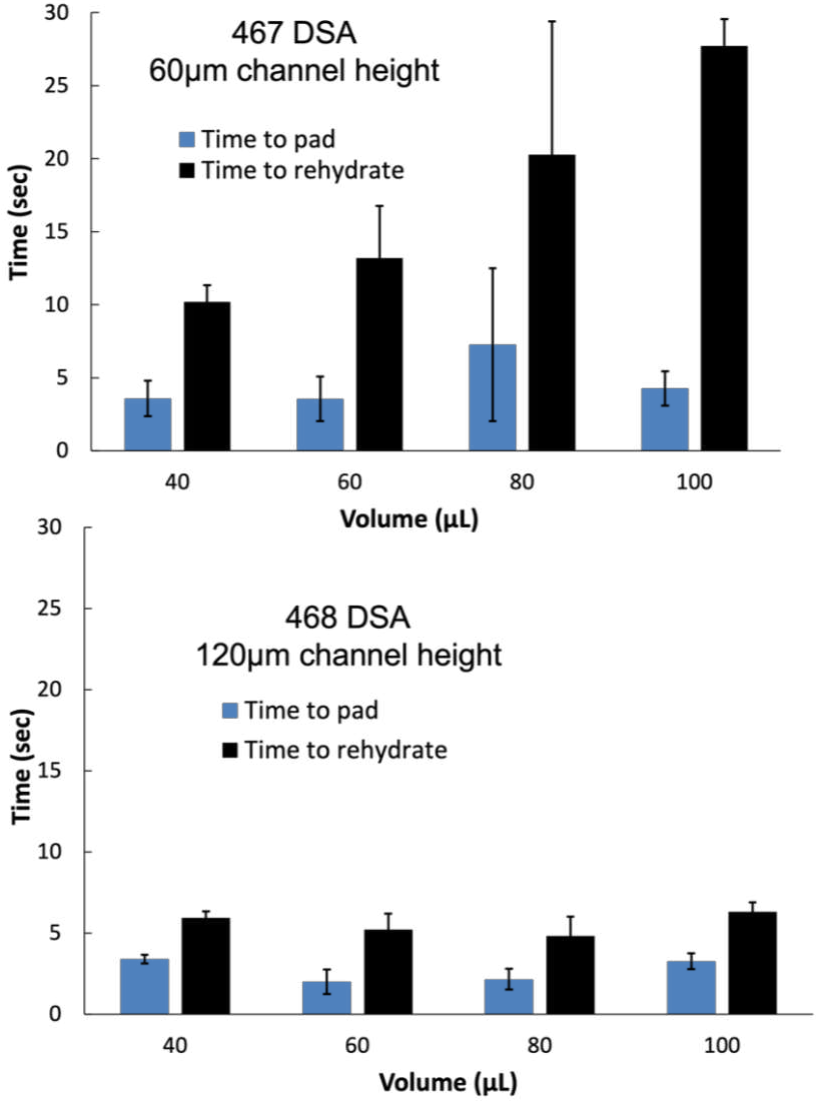

Figure 4.2. Flow rate optimization of varying device channel height with varying sample volume.

4.3.3 MeSA Operation

The MeSA was first demonstrated using the four simple user steps displayed in Figure 4.3 using a competitive biotin assay. First, 60 µL of 1 mg/mL of streptavidin magnetic beads were loaded into the device sample inlet with a 1x peroxide buffer where a permanent magnet was held stationary underneath the device. 15 s was allotted for flow to initiate via capillary action and to rehydrate each of the reagent pads. Second, the magnet was slid to the first reagent pad loaded with biotin-horse radish peroxidase (HRP). When sliding the magnet over the beads, they are held at the high magnetic field of the magnet. The magnet and beads were moved under the reagent pad to allow for the most contact between the beads and the biotin-HRP. Third, the magnetic beads underwent a 1 min incubation to allow conjugation of the biotin-HRP to the streptavidin magnetic beads. Fourth, the magnet and conjugated beads were then moved back across the device to the TMB reagent pad to allow the enzymatic reaction to occur (Figure 4.3). Once the magnetic beads with conjugated biotin-HRP reached the TMB pad, the oxidation of TMB began with the presence of H_2O_2 from the peroxide buffer. TMB oxidized to a blue product; the blue color intensity is dependent to the amount of peroxidase present which can then be correlated to concentration using ImageJ software.[37] After 10 min, images were taken for data analysis for the optimizations and following assays.

Additionally, the speed at which the magnet is slid across in step four was investigated. Here, we were interested to see how fast the end-user can slide the magnet across the device without losing signal. We found that at four seconds was the threshold for the timing of step four

without losing signal. Any amount of time more than four seconds showed similar color intensity (Figure A3.2)

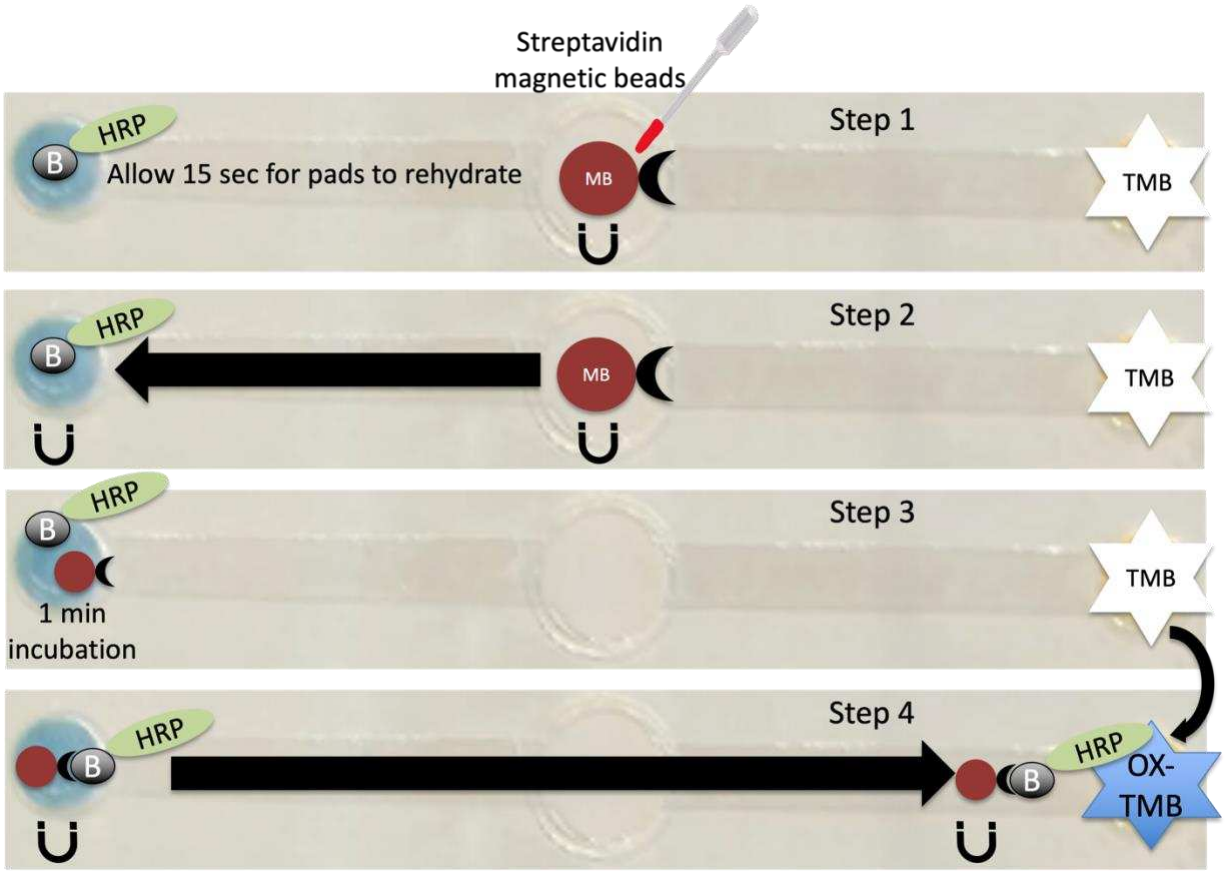

Figure 4.3. Assay operation following four steps. (1) Sample was inserted and within 15s the pads are rehydrated. (2) Magnetic beads were then slid from inlet to Biotin-HRP reagent pad. (3) A one-minute incubation was then allotted for biotin-streptavidin conjugation. (4) Magnetic beads are then slid across the device to the TMB pad for the enzymatic reaction to occur.

4.3.4 Data Evaluation

For each test condition (n=3), the TMB-HRP enzymatic reaction was timed, and images were taken using a smartphone in a controlled light environment. Images were imported into ImageJ, inverted, transferred to 8-bit, and split into RBG channels as described in the experimental section. Mean grey scale intensity measurements were taken following published protocols.[32] The placement of bead complexes under the TMB pad varied slightly, so a consistent circular area was measured in each image where the highest intensity blue oxidized TMB color forms (**Figure A3.1**).

Mean grey scale intensity plots were created for the optimization, biotin, and *E. coli* assay experiments. We found that the red channel provided the largest signal to background difference for the measurement. Quantification of the intensity of the blue formation is then calculated using Equation 6 shown below. The mean grey scale intensity, I_M, is calculated by dividing the test intensity, I_t, by a control intensity, I_c. The control intensity is the same measured area of the blank background. [37, 38]

$$I_M = \frac{I_t}{I_c} \tag{6}$$

4.3.5 Biotin Assay Optimization

To improve the function of the assay, several parameters were modified including PVP, biotin-HRP, and TMB concentrations and incubation time. Previous works demonstrated the ability of PVP to provide sufficient blocking of membranes while allowing for recovery of reagents.[33, 39] 1% PVP blocker of reagent pads yielded the highest blue color intensity and was adopted for subsequent studies (Figure 4.4a). Biotin-HRP optimization demonstrated the ability to show a concentration dependence of peroxidase (Figure 4.4b). Varying volumes of TMB were investigated and 30 µL of TMB was determined to give the strongest blue oxidized TMB intensity (Figure 4.4c). Finally, the incubation time of the streptavidin magnetic beads with biotin-HRP was investigated. It was found that incubation times longer than 60 s did not result in any further increase in signal.

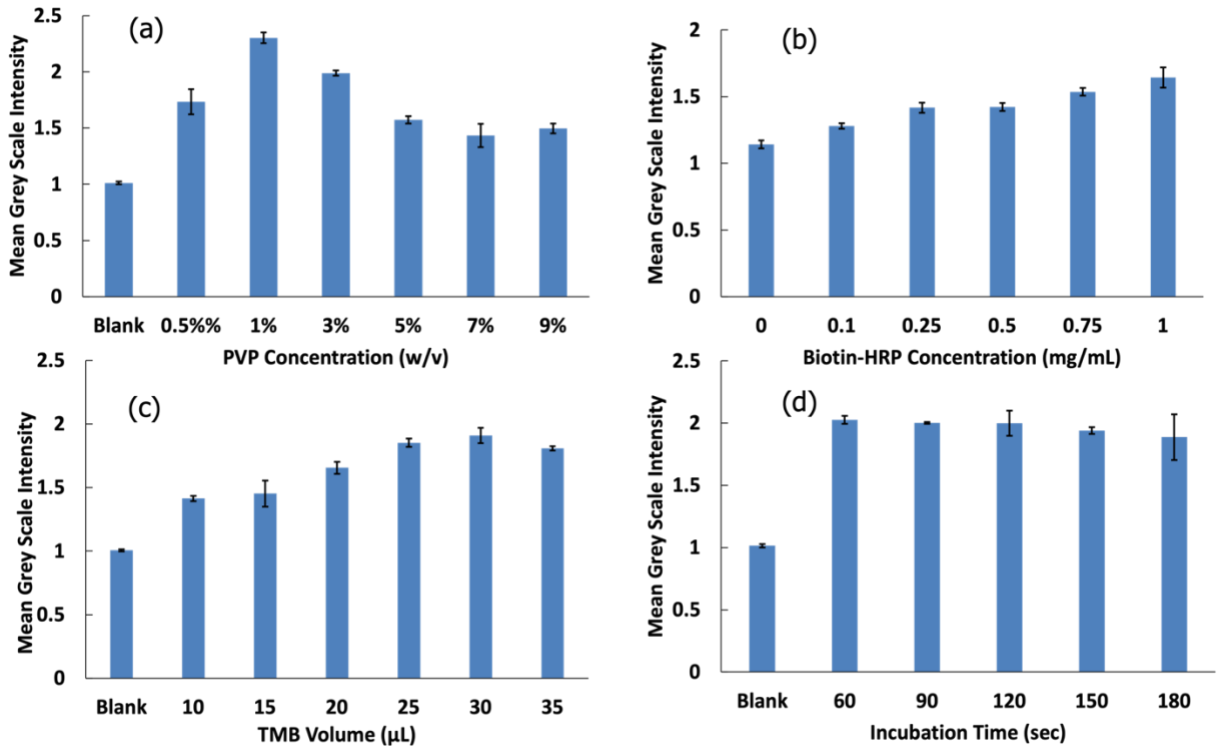

Figure 4.4. Assay optimization experiments. (a) PVP optimization at varying concentrations. (b) Biotin-HRP concentration optimization. (c) TMB volume optimization. (d) Magnetic beads with biotin-HRP incubation time.

4.3.5 Biotin Competitive Assay

A biotin competitive assay was performed as a proof-of-principle demonstration. Competitive assays are widely popular for the detection of small molecules and a common format for at home drug testing kits. These assays are based on the competitive binding between target analytes present in the sample and immobilized antigens that are labeled to detection antibodies. Competitive assays are ideal for the detection of small molecules because there is typically only one epitope available on the antigen to bind.[40] Here, concentrations from 0 to 10 mg/mL of unbound biotin were reacted with 1 mg/mL streptavidin magnetic beads in a microcentrifuge tube for 30 min while rotating. Upon mixing, the streptavidin coated magnetic beads binds to the free biotin. A magnetic separation was then performed to remove any remaining unbound biotin. As

the sample is introduced into the device, the sample is carried *via* capillary action to the reagent pads where the biotinylated horseradish peroxidase is immobilized.

The competitive biotin MeSA was then completed, Figure 4.5 shows the relative colorimetric intensity versus the biotin concentration added to the streptavidin magnetic beads. Here, we demonstrate the competitive assay in PBS and human pooled urine with spiked peroxide buffer to provide H_2O_2 for the enzymatic reaction to occur. Each curve was fit to a four-parameter logistic curve (4PL). A 4PL logistic curve is commonly used for immunoassays because of limiting binding kinetics.[41] Limits of detection (LOD) was calculated for each assay at the low concentration/high-signal end of the curve as the concentration that produced signal two-standard deviations of the zero biotin signal below the zero biotin signal.[42] The LOD was calculated to be 1.3 mg/mL for the assay in PBS and 0.91 mg/mL for the assay in human pooled urine.

For successful operation of this MeSA, magnetic beads need to be visualized to ensure successful transfer of beads across the device. Due to this, a higher concentration of streptavidin magnetic beads is needed. The high concentrations of biotin needed to see a hinderance of signal intensity is due to each streptavidin molecule having four identical binding sites for biotin. To improve sensitivity of this assay, future iterations will focus on starting with biotinylated magnetic beads rather than streptavidin coated magnetic beads. We will create competition between biotinylated magnetic beads and streptavidin-HRP. Varying concentrations of free biotin and streptavidin-HRP will be premixed and then immobilized onto the reagent pad. The free biotin will block binding sites for the biotin magnetic beads on the streptavidin-HRP. By using this format for future experiments, it will allow us to still use a high concentration of magnetic beads to visualize bead transfer and improve sensitivity for this competitive biotin assay.

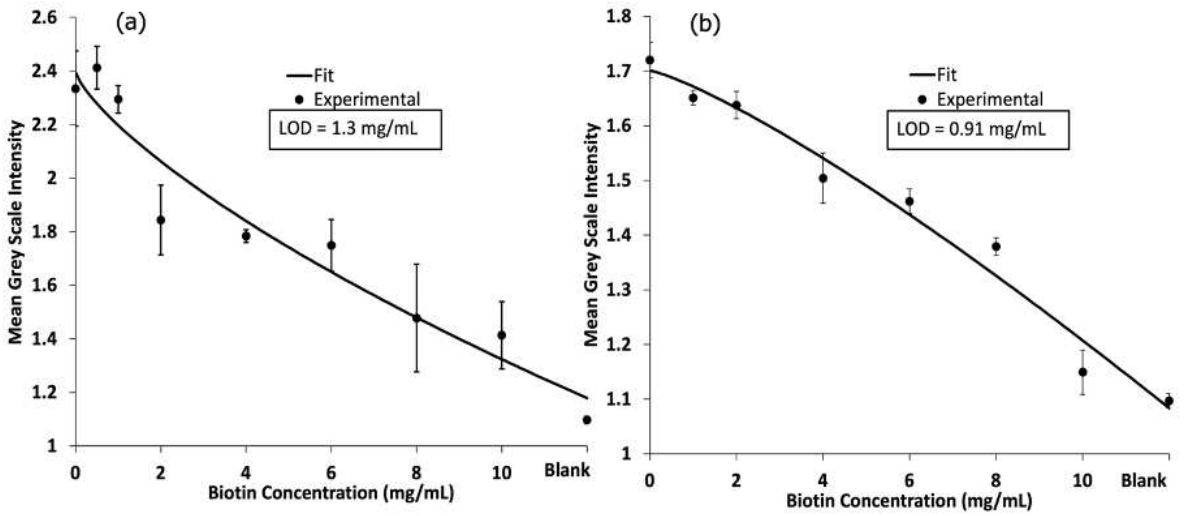

Figure 4.5. (a) 4PL logistic curve of a biotin competitive assay performed in PBS. (b) 4PL logistic curve of biotin competitive assay in human pooled urine.

4.3.6 Sandwich Immunoassay for E. coli Detection

Sandwich immunoassays are also commonly used for the detection of small molecules and pathogens. In a sandwich immunoassay, the target analyte is sandwiched between a capture and detection antibody. The signal intensity is proportional to the concentration of the analyte. Detection of DH5-alpha *E. coli* was conducted using a magnetic sandwich immunoassay to show the versatility of the device described. A biotinylated-*E. coli* antibody was conjugated to the streptavidin magnetic beads in a microcentrifuge tube. Varying concentrations of *E. coli* were then conjugated to the magnetic bead complex. Clinical ranges for *E. coli* in urinary tract infection diagnostic tests are commonly found to be in the range of 10^5 CFU/mL. The data was fit to a 4PL logistic curve and the LOD of 1.62 x 10^3 CFU/mL was calculated demonstrating the assay capability (Figure 4.6).[41, 43]

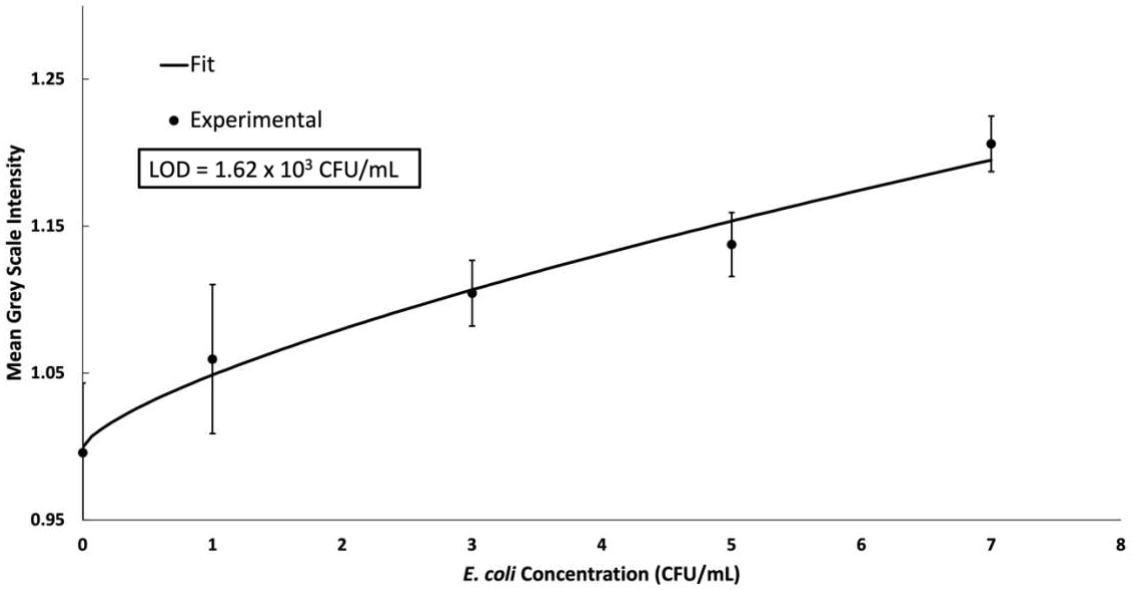

Figure 4.6. 4PL logistic curve of the sandwich *E. coli* assay at varying concentrations.

4.4 Conclusion and Future Work

Many existing diagnostic tests are performed in centralized laboratories, require trained personnel, and are time intensive. POC diagnostic testing such as µPADs has historically been critiqued for low sensitivity however, recent advancements in microfluidics coupled with magnetophoresis has showed promise to improve diagnostics. Here, we have described a novel platform for diagnostic assays using the MeSA. A biotin competitive assay and sandwich immunoassay for *E. coli* detection were completed to demonstrate versatility and functionality. The MeSA is a user-friendly, rapid, and portable platform that we envision to be used for a wide range of POC diagnostics. Future iterations of this device will focus on device optimization to reduce reagent concentrations and improving sensitivity through integration of electrochemical sensors.[44, 45]

REFERENCES

1. Michaud, C., Global burden of infectious diseases. *Encyclopedia of microbiology* **2009**, 444.
2. Organization, W. H. Tuberculosis. https://www.who.int/news-room/fact-sheets/detail/tuberculosis#:~:text=A%20total%20of%201.5%20million,(above%20HIV%2FAIDS).
3. Yager, P.; Domingo, G. J.; Gerdes, J., Point-of-care diagnostics for global health. *Annu. Rev. Biomed. Eng.* **2008,** *10*, 107-144.
4. Organization, W. H., *First WHO Model List of Essential In Vitro Diagnostics: Volume 1017*. World Health Organization: 2019; Vol. 1017.
5. Drain, P. K.; Hyle, E. P.; Noubary, F.; Freedberg, K. A.; Wilson, D.; Bishai, W. R.; Rodriguez, W.; Bassett, I. V., Diagnostic point-of-care tests in resource-limited settings. *The Lancet infectious diseases* **2014,** *14* (3), 239-249.
6. Dye, C., After 2015: infectious diseases in a new era of health and development. *Philosophical Transactions of the Royal Society B-Biological Sciences* **2014,** *369* (1645).
7. Bissonnette, L.; Bergeron, M. G., Diagnosing infections--current and anticipated technologies for point-of-care diagnostics and home-based testing. *Clinical Microbiology and Infection* **2010,** *16* (8), 1044-1053.
8. Yager, P.; Domingo, G. J.; Gerdes, J., Point-of-care diagnostics for global health. *Annual Review of Biomedical Engineering* **2008,** *10*, 107-144.
9. Weissleder, R.; Lee, H.; Ko, J.; Pittet, M. J., COVID-19 diagnostics in context. *Science translational medicine* **2020,** *12* (546), eabc1931.
10. Nasseri, B.; Soleimani, N.; Rabiee, N.; Kalbasi, A.; Karimi, M.; Hamblin, M. R., Point-of-care microfluidic devices for pathogen detection. *Biosensors and Bioelectronics* **2018,** *117*, 112-128.
11. Chin, C. D.; Linder, V.; Sia, S. K., Commercialization of microfluidic point-of-care diagnostic devices. *Lab on a Chip* **2012,** *12* (12), 2118-2134.
12. Lin, Y.; Gritsenko, D.; Feng, S.; Teh, Y. C.; Lu, X.; Xu, J., Detection of heavy metal by paper-based microfluidics. *Biosensors & Bioelectronics* **2016,** *83*, 256-266.
13. Bhardwaj, J.; Devarakonda, S.; Kumar, S.; Jang, J., Development of a paper-based electrochemical immunosensor using an antibody-single walled carbon nanotubes bio-conjugate modified electrode for label-free detection of foodborne pathogens. *Sensors and Actuators B: Chemical* **2017,** *253*, 115-123.
14. Oliveira, N. M.; Vilabril, S.; Oliveira, M. B.; Reis, R. L.; Mano, J. F., Recent advances on open fluidic systems for biomedical applications: A review. *Materials Science and Engineering: C* **2019,** *97*, 851-863.
15. Carrell, C.; Kava, A.; Nguyen, M.; Menger, R.; Munshi, Z.; Call, Z.; Nussbaum, M.; Henry, C., Beyond the lateral flow assay: A review of paper-based microfluidics. *Microelectronic Engineering* **2019,** *206*, 45-54.
16. Fu, E., Paper Microfluidics for POC Testing in Low-Resource Settings. In *Applications of Microfluidic Systems in Biology and Medicine*, Tokeshi, M., Ed. Springer Singapore: Singapore, 2019; pp 325-352.
17. Lei, K. F., Microfluidic systems for diagnostic applications: A review. *Journal of laboratory automation* **2012,** *17* (5), 330-347.

18. Noviana, E.; Ozer, T.; Carrell, C. S.; Link, J. S.; McMahon, C.; Jang, I.; Henry, C. S., Microfluidic paper-based analytical devices: From design to applications. *Chemical Reviews* **2021,** *121* (19), 11835-11885.
19. Ahmed, S.; Bui, M.-P. N.; Abbas, A., Paper-based chemical and biological sensors: Engineering aspects. *Biosensors & Bioelectronics* **2016,** *77*, 249-263.
20. Gong, M. M.; Sinton, D., Turning the Page: Advancing Paper-Based Microfluidics for Broad Diagnostic Application. *Chemical Reviews* **2017,** *117* (12), 8447-8480.
21. Jokerst, J. C.; Emory, J. M.; Henry, C. S., Advances in microfluidics for environmental analysis. *Analyst* **2012,** *137* (1), 24-34.
22. Akyazi, T.; Basabe-Desmonts, L.; Benito-Lopez, F., Review on microfluidic paper-based analytical devices towards commercialisation. *Analytica Chimica Acta* **2018,** *1001*, 1-17.
23. Aimeida, M. I. G. S.; Jayawardane, B. M.; Kolev, S. D.; McKelvie, I. D., Developments of microfluidic paper-based analytical devices (mu PADs) for water analysis: A review. *Talanta* **2018,** *177*, 176-190.
24. Pamme, N.; Manz, A., On-chip free-flow magnetophoresis: Continuous flow separation of magnetic particles and agglomerates. *Analytical Chemistry* **2004,** *76* (24), 7250-7256.
25. Alnaimat, F.; Dagher, S.; Mathew, B.; Hilal-Alnqbi, A.; Khashan, S., Microfluidics Based Magnetophoresis: A Review. *Chem. Rec.* **2018,** *18* (11), 1596-1612.
26. Pamme, N.; Wilhelm, C., Continuous sorting of magnetic cells via on-chip free-flow magnetophoresis. *Lab on a Chip* **2006,** *6* (8), 974-980.
27. Phurimsak, C.; Tarn, M. D.; Peyman, S. A.; Greenman, J.; Pamme, N., On-Chip Determination of C-Reactive Protein Using Magnetic Particles in Continuous Flow. *Analytical Chemistry* **2014,** *86* (21), 10552-10559.
28. Ngamsom, B.; Esfahani, M. M.; Phurimsak, C.; Lopez-Martinez, M. J.; Raymond, J.-C.; Broyer, P.; Patel, P.; Pamme, N., Multiplex sorting of foodborne pathogens by on-chip free-flow magnetophoresis. *Analytica Chimica Acta* **2016,** *918*, 69-76.
29. Berry, S. M.; Alarid, E. T.; Beebe, D. J., One-step purification of nucleic acid for gene expression analysis via Immiscible Filtration Assisted by Surface Tension (IFAST). *Lab on a Chip* **2011,** *11* (10), 1747-1753.
30. Call, Z. D.; Carrell, C. S.; Jang, I.; Geiss, B. J.; Dandy, D. S.; Henry, C. S., Paper-based pump-free magnetophoresis. *Analytical Methods* **2020,** *12* (43), 5177-5185.
31. Mettakoonpitak, J.; Khongsoun, K.; Wongwan, N.; Kaewbutdee, S.; Siripinyanond, A.; Kuharuk, A.; Henry, C. S., Simple biodegradable plastic screen-printing for microfluidic paper-based analytical devices. *Sensors and Actuators B: Chemical* **2021,** *331*, 129463.
32. Link, J.; Carrell, C.; Jang, I.; Panraksa, Y.; Sánchez-Cano, A.; Call, Z.; Noviana, E.; Dandy, D. S.; Geiss, B. J.; Henry, C. S. In *Power-free automated capillary flow assay for SARS-CoV-2 detection*, MicroTAS-Int. Conf. Miniaturized Syst. Chem. Life Sci., 2020; pp 536-537.
33. Martorell, D.; Siebert, S. T. A.; Durst, R. A., Liposome dehydration on nitrocellulose and its application in a biotin immunoassay. *Analytical biochemistry* **1999,** *271* (2), 177-185.
34. Robert B. Channon, M. P. N., Charles S. Henry, David S. Dandy, Multilayered Microfluidic Paper-Based Devices: Characterization,
Modeling, and Perspectives. 2019.
35. Simon, M. G.; Lin, R.; Fisher, J. S.; Lee, A. P., A Laplace pressure based microfluidic trap for passive droplet trapping and controlled release. *Biomicrofluidics* **2012,** *6* (1), 014110.

36. Channon, R. B.; Nguyen, M. P.; Scorzelli, A. G.; Henry, E. M.; Volckens, J.; Dandy, D. S.; Henry, C. S., Rapid flow in multilayer microfluidic paper-based analytical devices. *Lab on a Chip* **2018,** *18* (5), 793-802.
37. Busa, L. S. A.; Maeki, M.; Ishida, A.; Tani, H.; Tokeshi, M., Simple and sensitive colorimetric assay system for horseradish peroxidase using microfluidic paper-based devices. *Sensors and Actuators B: Chemical* **2016,** *236*, 433-441.
38. Busa, L. S. A.; Mohammadi, S.; Maeki, M.; Ishida, A.; Tani, H.; Tokeshi, M., A competitive immunoassay system for microfluidic paper-based analytical detection of small size molecules. *Analyst* **2016,** *141* (24), 6598-6603.
39. Miller-Jaster, K. N.; Petrie Aronin, C. E.; Guilford, W. H., A quantitative comparison of blocking agents in the in vitro motility assay. *Cellular and Molecular Bioengineering* **2012,** *5* (1), 44-51.
40. Zettner, A., Principles of competitive binding assays (saturation analyses). I. Equilibrium techniques. *Clinical chemistry* **1973,** *19* (7), 699-705.
41. Gottschalk, P. G.; Dunn, J. R., The five-parameter logistic: a characterization and comparison with the four-parameter logistic. *Analytical biochemistry* **2005,** *343* (1), 54-65.
42. Murphy, B. M.; He, X.; Dandy, D.; Henry, C. S., Competitive immunoassays for simultaneous detection of metabolites and proteins using micromosaic patterning. *Analytical chemistry* **2008,** *80* (2), 444-450.
43. Carrell, C. S.; Wydallis, R. M.; Bontha, M.; Boehle, K. E.; Beveridge, J. R.; Geiss, B. J.; Henry, C. S., Rotary manifold for automating a paper-based Salmonella immunoassay. *RSC Advances* **2019,** *9* (50), 29078-29086.
44. Santhiago, M.; Wydallis, J. B.; Kubota, L. T.; Henry, C. S., Construction and electrochemical characterization of microelectrodes for improved sensitivity in paper-based analytical devices. *Analytical chemistry* **2013,** *85* (10), 5233-5239.
45. Adkins, J. A.; Boehle, K.; Friend, C.; Chamberlain, B.; Bisha, B.; Henry, C. S., Colorimetric and Electrochemical Bacteria Detection Using Printed Paper- and Transparency-Based Analytic Devices. *Analytical Chemistry* **2017,** *89* (6), 3613-3621.

CHAPTER 5. CONCLUSIONS AND FUTURE WORK

5.1 Chapter Overview

Infectious diseases are the largest health burden for low-income countries and claim millions of lives every year.[1-3] The loss of life in low-income countries is largely due to the lack of access to preventative healthcare and appropriate diagnostic testing.[1, 4] The World Health Organization (WHO) recognizes the need for improved and effective POC diagnostics to reduce infectious disease burden.[5] To maximize impact in low-resource settings, diagnostics should aim to meet the ASSURED criteria outlined by the WHO.[6, 7] Microfluidic devices are a popular approach for diagnostics because they offer reduced assay times, reduced sample volume, and are small (<10 cm). Additionally, microfluidic devices can be used with magnetophoresis to improve sensitivity and specificity. However, traditional microfluidic devices have difficulty translating to the POC because of tedious and expensive fabrication. Microfluidic paper-based analytical devices (μPADs) are a popular alternative to traditional microfluidics due to the natural capillary action through cellulose fibers and simple fabrication. μPADs are portable, low-cost, and do not require external instrumentation making them ideal for POC settings.

Combining microfluidic technology with recent advancement in μPADs offers a promising alternative to improve diagnostic testing. However, traditional microfluidics and μPADs have not yet been successful outside of the laboratory because of limitations such as difficult or expensive fabrication, complicated user-end steps, and insufficient sensitivity or specificity.[8-10] We believe that by combining existing technologies with novel paper-based techniques, we can overcome these challenges to provide diagnostics capable of reducing the burden of infectious diseases. Here we have described advancements in paper-based

technologies that address gaps in current testing and will hopefully lead to improved diagnostics in the long-term.

First, the first example of a pump-free paper-based magnetophoresis device is demonstrated as an alternative to traditional microfluidic magnetophoresis.[11] Traditional magnetophoresis uses external pumps to drive flow and was not coupled with μPADs because the need for sustained high flow velocities to continuously separate magnetic particles. Channon *et al*, demonstrated a 145-fold increase in flow rates with multilayered μPADs over single layer μPADs.[12] Following this work, we hypothesized that multilayered μPADs could enable pump-free magnetophoresis. We created multilayer μPAD using wax-patterned chromatography paper and DSA to create increased fluid flow rates needed to achieve paper-based magnetophoresis. Optimization studies were completed to improve the assay sensitivity and user-end steps. A sandwich immunoassay was completed for the detection of *E. coli* through fluorescence detection with a limit of detection measured at 10^5 CFU/mL. Here, we demonstrated the first example of paper-based magnetophoresis without the need for external instrumentation to drive flow. We envision this work to be used to create more complex POC diagnostics without sacrificing cost or portability. However, moving forward we wanted to improve sensitivity of the assay as well as user steps associated with the assay.

The second project described focuses on improvements of the first device to further this technology to the POC. First, only a portion of the conjugated magnetic beads made it through the first device because particles would become trapped in the cellulose fibers and beads would be left in the sample inlet. To solve this, we added a wash buffer reservoir behind the sample inlet to wash the magnetic beads completely out of the inlet. Additionally, we moved away from wax-patterned paper to a completely transparent device with a burst valve incorporated to establish more

consistent laminar flow. Second, we improved the limit of detection by three orders of magnitude from the first device described in Chapter two. Here, we report an updated pump-free system with improved sensitivity with a simplified operation of microfluidic magnetophoresis for the detection of *E. coli*. Multiple off-chip manipulation steps were still needed for this assay, increasing complexity. For this assay to make a large impact for POC diagnostics, ideally all off-chip manipulation should be done on-chip without multiple user steps.

To make this technology more applicable to POC testing, we took a new approach that simplifies user-end steps through a simple magnet sliding operation. Here, we introduce a Magnetophoresis Slider Assay (MeSA) for sequential binding and washing steps without the need for any external instrumentation. A biotin competitive assay and sandwich immunoassay for *E. coli* detection were completed to demonstrate versatility and functionality. The MeSA builds off previously published work of the IFAST system and sequential binding of traditional magnetophoresis but does not need external pumps or complicated user end steps. Here we demonstrate the ability to a conjugation on-chip that we previously had to do off-chip with multiple pipetting steps. The MeSA is a user-friendly, rapid, and portable platform that can be adapted to incorporate more off-chip conjugation on-chip. Future iterations of this device will focus on device design to perform a complete a full sandwich immunoassay with a simple magnet sliding operation.

5.2 Future Directions

We have demonstrated the ability to perform magnetophoresis in paper, store reagents directly on the device, and conjugate magnetic beads with a simple sliding operation. Future work will aim to eliminate the need for any off-chip manipulations by combining parts of the works described. Work from Jang et al. described in Chapter one demonstrates the ability to rapidly mix

reagents in the main fluid channel. We hypothesize that if we combine the rapid mixer with the work from Chapter three and four, we can minimize off-chip manipulations. Figure 5.1a is a CAD rendering of the proposed device assembly. Figure 5.1b is a top-down view of the device with reagent placement. Here the analyte sample and magnetic beads with bound primary antibody are loaded into the device. Capillary action initiates and the magnetic beads mix with the analyte and the analyte is bound to the primary antibody. The bound magnetic complex is then concentrated at the permanent magnet and the excess unbound analyte will flow into the paper waste pad. The magnetic complex is then slid over to bind the secondary-HRP antibody pad and then finally to the TMB pad for the enzymatic reaction to take place. The device would eliminate any off-chip manipulations if used with commercially available magnetic beads with bound primary antibodies. Additionally, further work will aim for multiplexed detection using electrochemical detection to improve sensitivity over colorimetric detection.

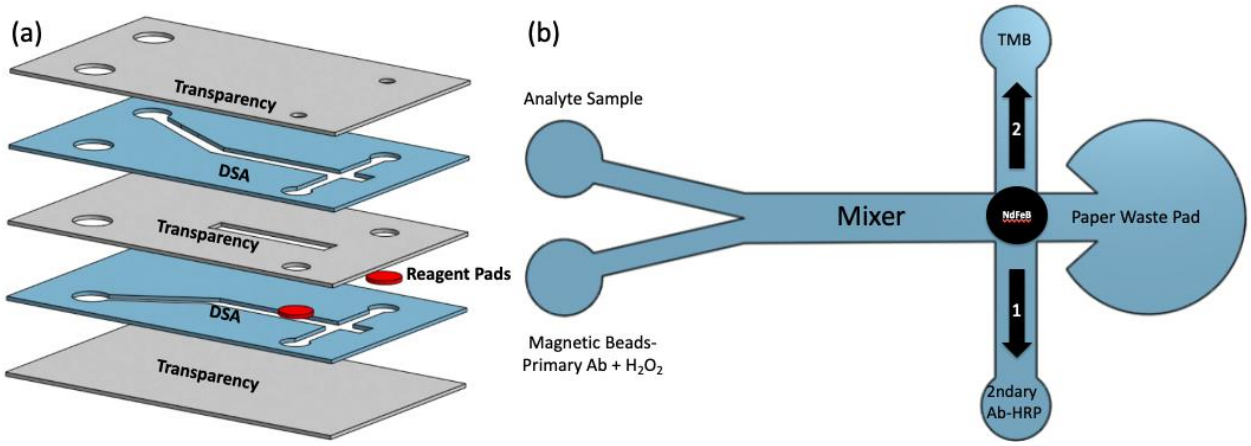

Figure 5.1. (a) CAD rendering of the device assembly with alternating layers of transparency and double-sided adhesive (DSA). (b) Top-down view of the assembled device with corresponding reagent addition and operation of the device.

The work described in this thesis is a step to overcome the shortcomings of traditional microfluidics and µPADs. We report the first example of paper-based magnetophoresis to combine the advantages of microfluidic magnetophoresis with µPADs. By combining these existing

laboratory practices, we can create diagnostics that have a better chance of becoming commercialized and fit the ASSURED criteria.

5.3 Steps to Commercialization

For a device to be commercialized in the United States there are several steps that must be met in accordance with the Federal Drug Administration (FDA) guidance and regulation. Medical devices need to obtain a FDA 510(k) clearance to be marketed legally. To obtain a 510(k) clearance the medical device must choose a predicate device that is substantially equivalent for safety and effectiveness to another legally marketed device through the FDA. When preparing a 510(k) clearance the first step is to determine the type of device to be commercialized. Devices are classified into three types, class I, class II, and class III. Class type is determined based on the risk to the patient/use, the intended use, and indications for use. Class I devices are the lowest risk to the patient/user where class III are the highest risk and come with general controls and also premarket approval (PMA).[13] Following the FDAs code of regulations title 21, the devices described in this thesis are the most similar to *E. coli* serological tests under immunology and microbiology devices with product codes GMZ, GNA, GMY. The *E. coli* serological tests are classified as class I and are subjected to general controls and exempt from PMA.[14] Second, class I devices under a 510(k) notification must have appropriate documentation including technological characteristics and performance testing.[13, 15] Appropriate documentation can be found in the guidance documents database and often will have recognized consensus standards for products. Typical consensus standards will often include, design controls, authorized book keeping, nonclinical testing, clinical comparisons, shelf life data, biocompatibility research, appropriate labelling of devices, and bench performance testing.[13, 15, 16] More specifically, the FDA guidance documents can be referenced on predicated devices to find the applicable performance testing

requirements and recognized consensus standards. However, for GMZ, GNA, and GMY products codes there are no recognized consensus standards linked to these products.[17] The FDA will require similar testing to predicate devices, so to find the appropriate testing needed, the 510(k) summary of predicate devices must be referenced to find the testing completed. For example, for the predicate device ImmunoCard STAT! EHEC (K062546) for *E. coli* EHEC strain detection is a qualitative, rapid and single use test. The performance testing conducted for this predicate device included; clinical sensitivity/specificity, precision/reproducibility, linearity/reportable range, analytical LOD/sensitivity, assay cutoff, and indeterminant range.[18] For the devices described in this thesis, I anticipate all of these tests would need to be completed along with shelf life testing of all the reagents being used. Additionally, the FDA can be contacted directly with questions regarding 510(k) submissions or there are multiple consulting firms for handling 510(k) submissions.[19] Finally, after all of the testing has been completed, the complied information must be submitted to the FDA for review. Review and approval can take up to 180 days, following approval, the device can then be registered and listed with the FDA.[13-16, 20]

As the technology described in this thesis is still in the research and development phase, we are hopeful to progress toward commercializing these devices following FDA guidelines.[13-17] More work needs to be done to further this field; however, I believe these works are a crucial step to demonstrate the possibility of coupling these two technologies. In the future, I hope to continue to work on assay development for diagnostic testing and one day see my work being used to improve healthcare.

REFERENCES

1. Roser, M.; Ritchie, H., Burden of disease. *Our world in data* **2021**.
2. Dye, C., After 2015: infectious diseases in a new era of health and development. *Philosophical Transactions of the Royal Society B-Biological Sciences* **2014,** *369* (1645).
3. Michaud, C., Global burden of infectious diseases. *Encyclopedia of microbiology* **2009**, 444.
4. Yager, P.; Domingo, G. J.; Gerdes, J., Point-of-care diagnostics for global health. *Annu. Rev. Biomed. Eng.* **2008,** *10*, 107-144.
5. Organization, W. H., *First WHO Model List of Essential In Vitro Diagnostics: Volume 1017*. World Health Organization: 2019; Vol. 1017.
6. Smith, S.; Korvink, J. G.; Mager, D.; Land, K., The potential of paper-based diagnostics to meet the ASSURED criteria. *RSC advances* **2018,** *8* (59), 34012-34034.
7. Land, K. J.; Boeras, D. I.; Chen, X.-S.; Ramsay, A. R.; Peeling, R. W., REASSURED diagnostics to inform disease control strategies, strengthen health systems and improve patient outcomes. *Nature Microbiology* **2019,** *4* (1), 46-54.
8. Carrell, C.; Kava, A.; Nguyen, M.; Menger, R.; Munshi, Z.; Call, Z.; Nussbaum, M.; Henry, C., Beyond the lateral flow assay: A review of paper-based microfluidics. *Microelectronic Engineering* **2019,** *206*, 45-54.
9. Ozer, T.; McMahon, C.; Henry, C. S., Advances in paper-based analytical devices. *Annual Review of Analytical Chemistry* **2020,** *13*, 85-109.
10. Noviana, E.; Ozer, T.; Carrell, C. S.; Link, J. S.; McMahon, C.; Jang, I.; Henry, C. S., Microfluidic Paper-Based Analytical Devices: From Design to Applications. *Chemical Reviews* **2021**.
11. Call, Z. D.; Carrell, C. S.; Jang, I.; Geiss, B. J.; Dandy, D. S.; Henry, C. S., Paper-based pump-free magnetophoresis. *Analytical Methods* **2020,** *12* (43), 5177-5185.
12. Channon, R. B.; Nguyen, M. P.; Scorzelli, A. G.; Henry, E. M.; Volckens, J.; Dandy, D. S.; Henry, C. S., Rapid flow in multilayer microfluidic paper-based analytical devices. *Lab on a Chip* **2018,** *18* (5), 793-802.
13. Lynch, M., Five Steps to Medical Device Commercialization. Retrieved January 3, 2017. 2011.
14. Administration, F. D. https://www.accessdata.fda.gov/scripts/cdrh/cfdocs/cfcfr/CFRSearch.cfm?fr=866.3255.
15. Bertrand, A. A.; DeLong, M. R.; Chandawarkar, A.; Robinson, C., The development and commercialization of medical technologies. *Aesthetic Surgery Journal* **2021,** *41* (12), NP2020-NP2029.
16. Volpatti, L. R.; Yetisen, A. K., Commercialization of microfluidic devices. *Trends in biotechnology* **2014,** *32* (7), 347-350.
17. Aministratoin, F. D. https://www.fda.gov/medical-devices/classify-your-medical-device/device-classification-panels.
18. Meridian Bioscience, I. https://www.accessdata.fda.gov/cdrh_docs/pdf6/K062546.pdf.
19. Goldman, S. https://incompliancemag.com/article/medical-device-testing-requirements-for-510k-submissions/.
20. Zuckerman, D. M.; Brown, P.; Nissen, S. E., Medical device recalls and the FDA approval process. *Archives of internal medicine* **2011,** *171* (11), 1006-1011.

APPENDIX 1. SUPPLEMENTARY INFORMATION – PAPER-BASED PUMP-FREE MAGNETOPHORESIS

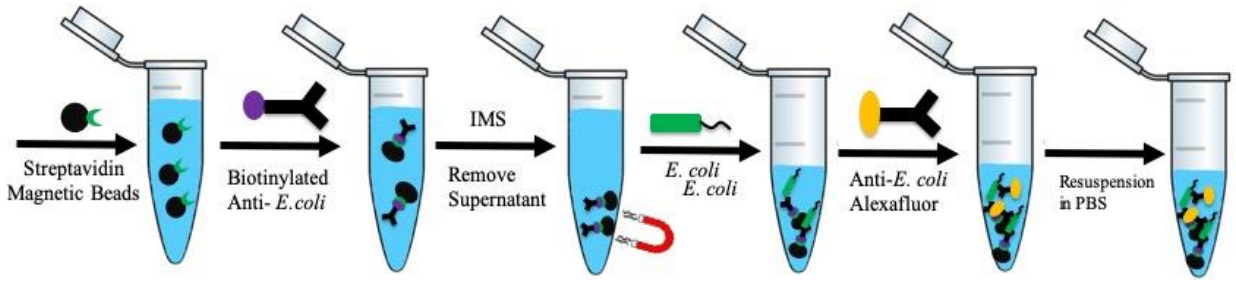

Figure A3.1 Immunomagnetic separation schematic displaying sequential binding and washing steps of the magnetic bead sandwich.

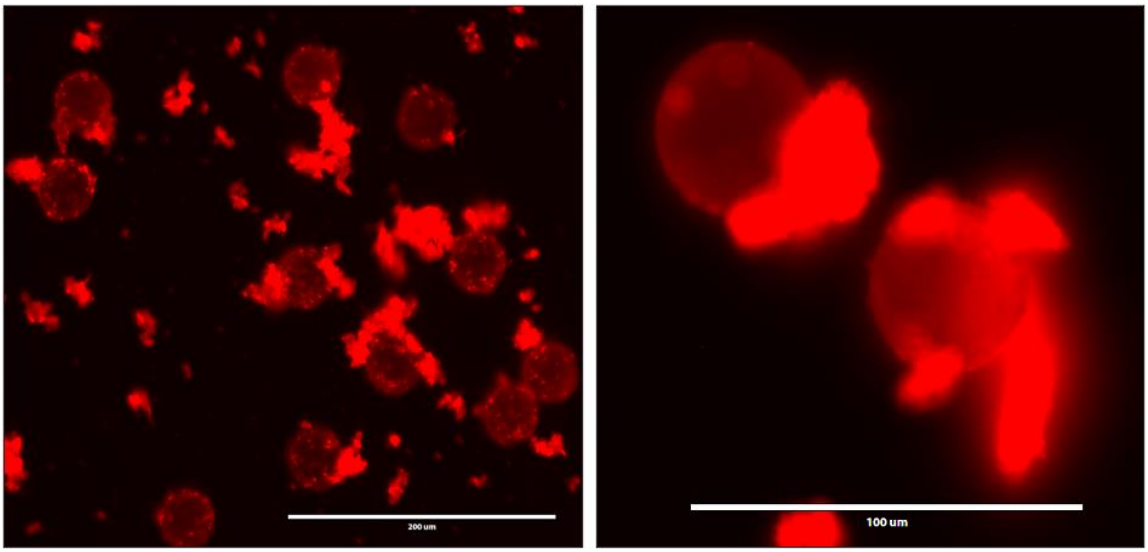

Figure A1.2. Fluorescent microscope image of 44µm magnetic bead sandwich complex with a fluorescent tag conjugated to the *E. coli* bound through immunomagnetic conjugation.

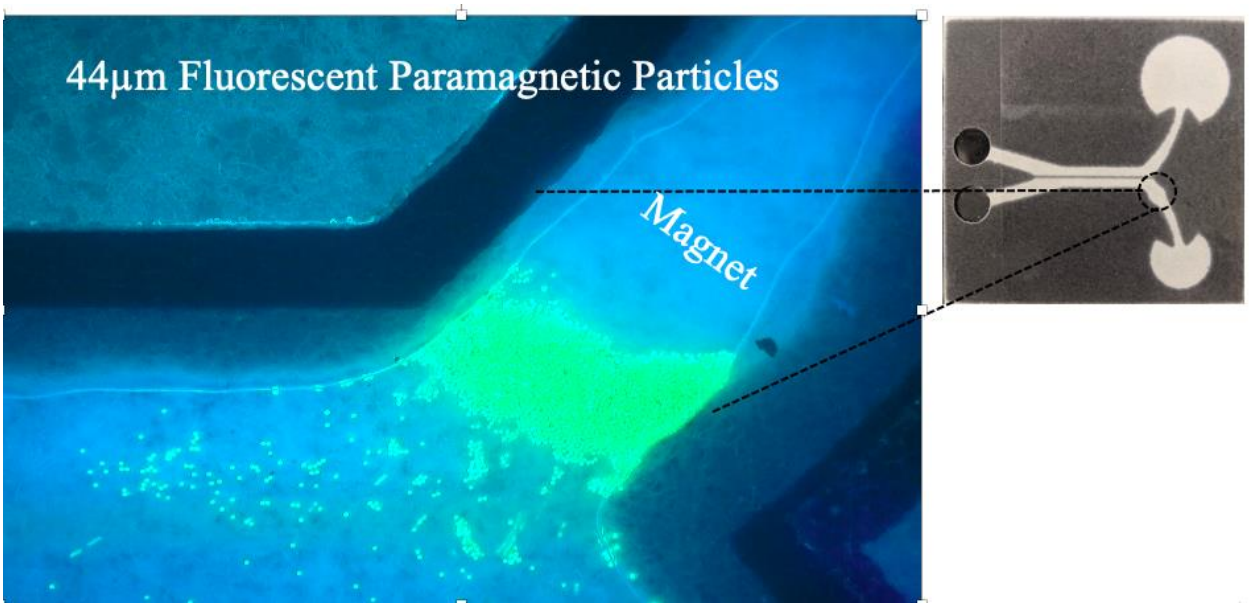

Figure A1.3. Photograph of positive magnetophoresis with 44µm fluorescent magnetic beads.

APPENDIX 2. SUPPLEMENTARY INFORMATION – SIMPLIFIED UTI DIAGNOSTIC: PUMP-FREE MAGNETOPHORESIS FOR *E.* COLI DETECTION

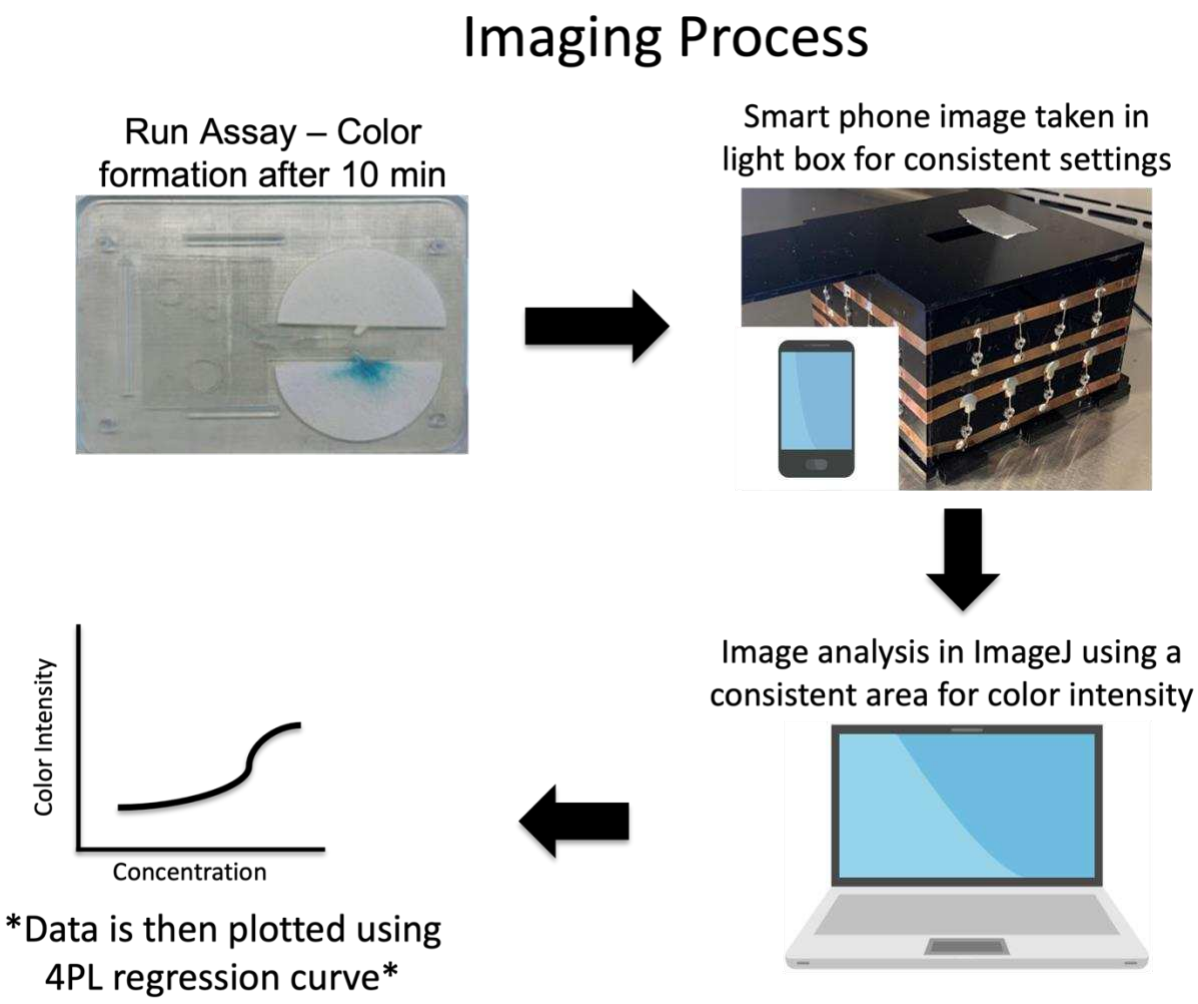

Figure A2.4. Schematic of the imaging process after 10 min elapsed for the enzymatic reaction.

APPENDIX 3. SUPPLEMENTARY INFORMATION – MAGNETOPHORESIS SLIDER ASSAY : A SIMPLE PLATFORM FOR POINT-OF-CARE DIAGNOSTICS

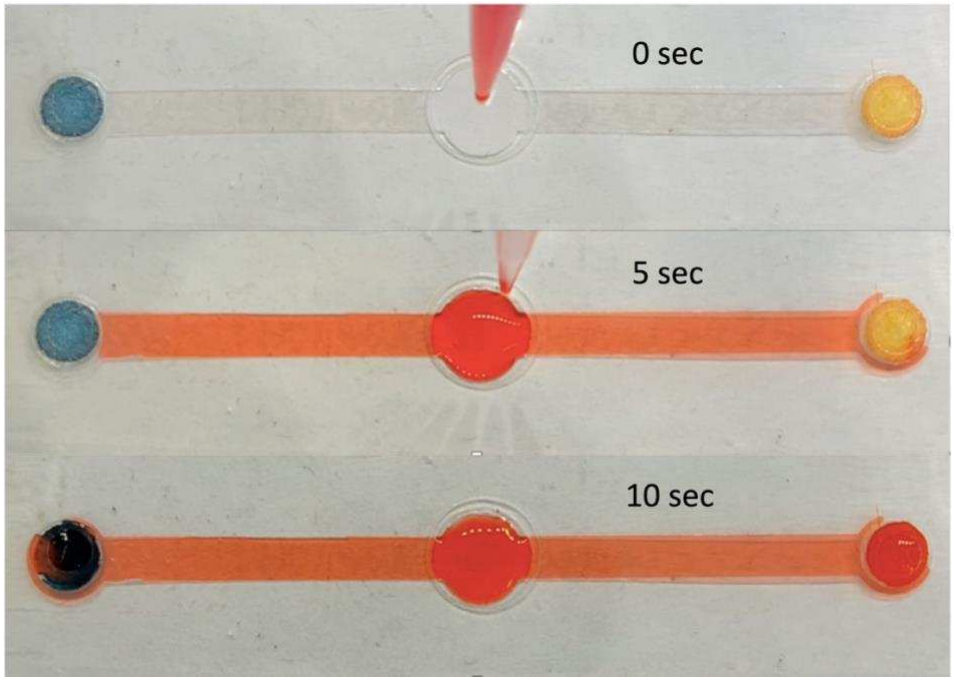

Figure A3.5. Photographs to visualize fluid flow at various time points. Fluid reaches the time point at 5 sec and then pads are rehydrated by 10-15 sec.

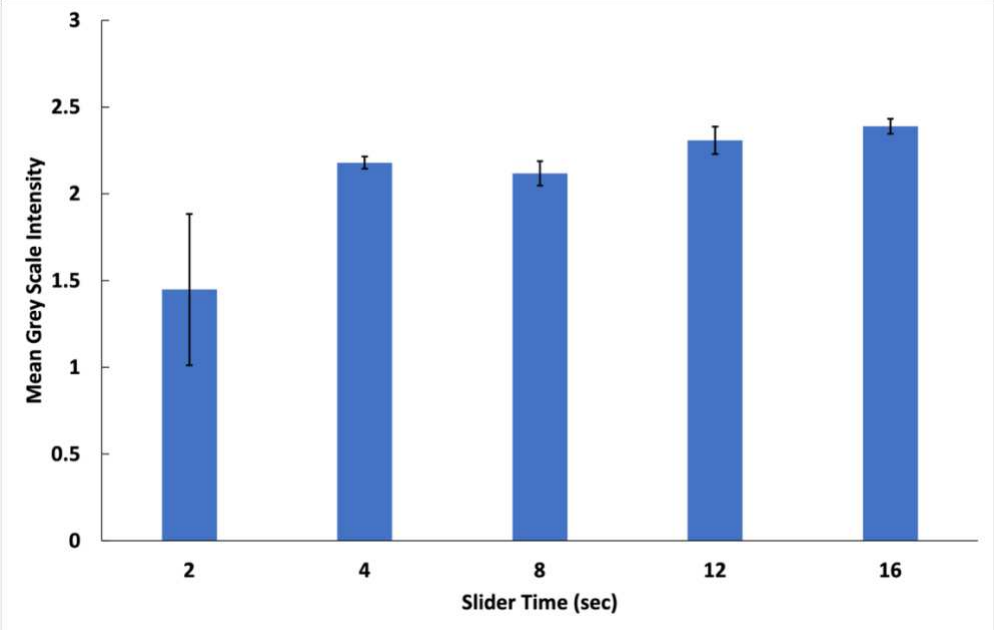

Figure A3.2. The amount of time needed to be allowed for magnetic beads to properly transfer with the magnet across the device.

APPENDIX 4. CAPILLARY DRIVEN IMMUNOASSAY SYSTEM FOR COVID-19

Herein a novel capillary driven immunoassay (CaDI) is described that fully automates the reagent delivery and washing steps of a sandwich enzyme linked immunosorbent assay (ELISA) for the detection of SARS-CoV-2. The device uses a capillary driven microfluidic front end to sequentially supply sample, reagent, and wash buffer to a nitrocellulose test zone to perform an enzymatic sandwich immunoassay. After adding sample all remaining reagents and washing steps are automated and the full assay is run in < 15 min. Reagent storage and drying studies are described to optimize activity of immobilized reagents. Results can be read by eye for a positive/negative answer, or a smart phone image can be analyzed for quantitative results. The assay and device described here demonstrate a novel microfluidic paper-based technology that can be applicable to a range of assays by simply swapping out reagents immobilized in the reagent pads. The details of this work are my contributions to the larger COVID-19 project that involved several people including Dr. Ilhoon Jang, Dr. Cody S. Carrell, Jeremey Link, Elijah Barstis, Rae Bellows and John O'Donnell. These contributions will be part of multiple publications that are in preparation. Contents of this section were taken and combined from a published review article ,in which I was listed as an author, with edits and modifications.[1, 2]

A4.1 Introduction

As of March 2022, more than 433 million people have been infected, and over 5.9 million people have died worldwide from SARS-CoV-2.[3] SARS-CoV-2, the causative agent of COVID-19, is primarily spread in droplets expelled from the mouth, nose, and upper respiratory track.[4, 5] The virus is most infectious directly before and after the onset of symptoms so rapid diagnostics are crucial to properly screen people to reduce transmission. The ideal screening diagnostic would be operational outside of a laboratory, have high clinical specificity and sensitivity (i.e. low

false positive and negative rates), simple enough so that an average untrained user could run the test, and fast enough to screen large numbers of people (<15 min).[6] Laboratory-based well plate Enzyme-Linked Immunosorbent Assays (ELISAs) offer higher sensitivity and specificity than lateral flow assays (LFA), but require expensive instrumentation and trained technicians so rapid, on-site testing is not possible. This work describes a disposable ELISA device that is as simple to use as an LFA, but as sensitive as a well-plate ELISA. The device utilizes capillary-driven flow channels made of transparency films and double-sided adhesive combined with paper pumps to drive flow. As a result, devices are inexpensive (~$1) and can be made in large quantities. The geometry of the channels and storage pads enables automated sequential washing and reagent addition steps with two simple end-user steps. An enzyme label is used to produce a colorimetric signal instead of a nanoparticle label in order to amplify signal and increase sensitivity, while the integrated washing steps decrease false positives and increase reproducibility. Here, we describe a colorimetric assay to detect SARS-CoV-2 using a horseradish peroxidase (HRP) secondary antibody and 3,3,5,5 tetramethylbenzidine (TMB) as a chromogenic substrate.

A4.2 Experimental Procedures

A4.2.1 Drying and Blocking Procedure

A range of blockers were investigated including PBS-Tween 20 (PBST), commercial Stabilguard and Superblock, and aged casein. PBS was used a control as in there were no surfactants, proteins or other detergents added to reduce non-specific binding. Fluorescent-488 anti-IgG was striped on the nitrocellulose at 1 mg/mL and was blocked with corresponding blockers and then dried for 2h, 4h, 6h, and 12h in an oven at 37˚C. Fluorescent measurements were taken before and then after extraction buffer was flowed over the nitrocellulose to determine the amount of antibody left on the nitrocellulose.

A4.3 Results and Discussion

A4.3.1 Assembly and Sequential Binding Operation

The CaDI is designed by stacking alternating layers of patterned hydrophilic polyethylene film and double-sided adhesive to create hollow channels for flow. A nitrocellulose test strip is connected to the outlet of the device and a waste pad is used to create pump-free, capillary driven flow. Immobilized capture antibody is striped onto the test line. The assay uses extraction buffer to dilute nasal swabs and lyse whole virus to expose N Protein for detection. Conjugate release pads embedded in the channels contain the reagents needed for each step of the assay (Figure A4.1). Pad 1 contains the secondary antibody conjugated to HRP and pad 2 contains the chromogenic substrate TMB. After sample containing N protein is added, the N protein first flows over the test line and is bound to the capture antibody. Next, the extraction buffer rehydrates pad 1 and the secondary antibody-HRP flows over the test strip and is bound to the N protein. Finally, the TMB is released into the channel and flows over the test strip for the enzymatic reaction to occur. (Figure A4.1b).

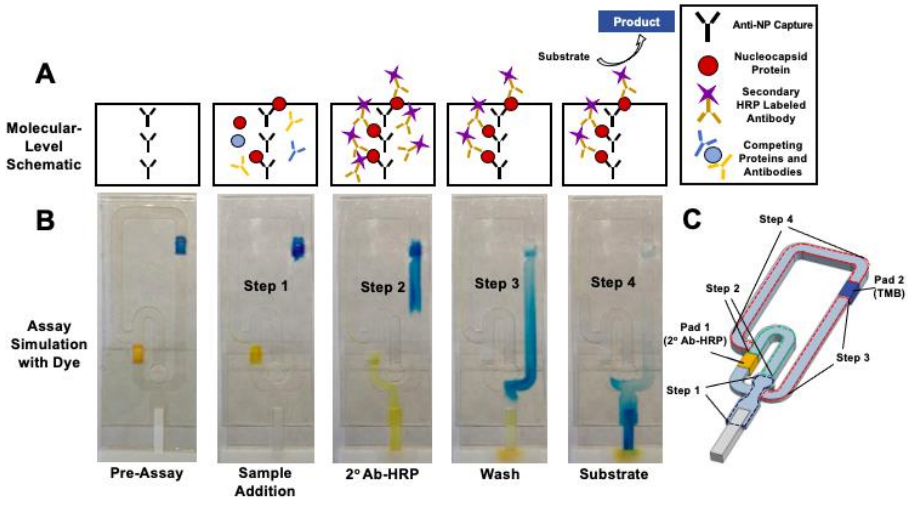

Figure A4.6. (A) Molecular level representation of the immunoassay taking place on the nitrocellulose using an HRP-labeled antibody. (B) Simulation with food dye of the reagent addition and washing steps. The yellow food-dye represents the HRP-labeled antibody, and the blue represents the TMB substrate. (C) 3D rendering of the CaDI channels showing the sequential steps.

A4.3.2 Blocking and Drying Optimization

To prevent non-specific binding of detection antibodies and resulting in false signal the unoccupied sites on the nitrocellulose must be blocked. Blocking buffers and solutions such as highly purified proteins, bovine serum albumin (BSA), and aged casein are commonly used to block membranes and in laboratory well plate ELISA. Commercial blocking solutions are also widely available but the formulations are proprietary. To improve signal-to-noise ratio, and overall stability of immobilized antibodies, a blocking and drying study was conducted. Figure A4.2 displays inverted fluorescent intensity of each blocked nitrocellulose membrane at various time points. Aged casein and superblock showed the highest retention of fluorescent intensity at each time point after reflowing the strips with extraction buffer. Interestingly, Stabilguard and PBST failed to retain most of the antibody on the test line until sufficient drying after 12hr or more. Moving forward after these studies, we were able to adapt our blocking and drying procedures to improve signal. Long-term stability of the activity of the dried antibodies is needed to further conclude the best blocker for this assay, however, the data presented gave us crucial information moving forward to improving the signal of the assay.

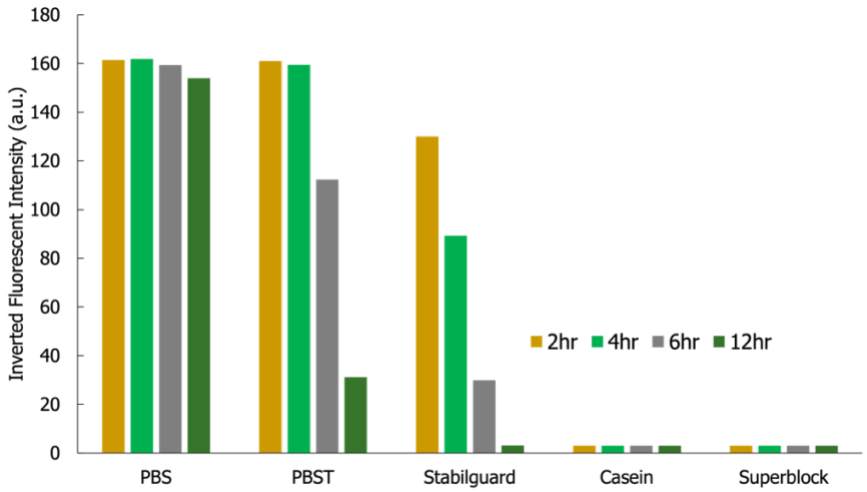

Figure A4.7. Inverted fluorescent intensity of varying drying conditions using multiple blockers.

A4.3.3 Comparison to Traditional ELISA

To test the CaDI as an immunoassay platform we compared the performance of the single-inlet antigen assay to a standard well-plate ELISA. In both formats, the same pair of antibodies were used. Figure A4.3 shows the difference between the well-plate ELISA and the CaDI using serial dilutions of a recombinant N protein. The well-plate ELISA only slightly outperforms the CaDI but the detection limits are on the same order of magnitude at <100 PFU/mL. The small difference between the two can be attributed to the difference in the instrumentation used for quantification: A UV/Vis spectrophotometer with a 0.5 cm path length vs a cell phone image inside a homemade light box. Images of the CaDI test strips are shown in Figure A4.3b. The ELISA requires 15 pipetting steps, over one hour of analysis time, and an expensive instrument for quantification. The CaDI only requires one pipetting step, 15 min from sample addition to result, and can be read by naked eye. The results in Figure A4.3a demonstrate the CaDI's ability to provide the performance of a complex, laboratory-based ELISA with the simplicity of a standard LFA. The nitrocellulose strips in Figure A4.3b were shown to 22 untrained end-users who were asked to list each as positive or negative based on the presence or absence of a test line. Figure A4.3c shows the results of that survey. The concentration where at least 95% of respondents listed a positive result, which is the FDA requirement for naked-eye detection limit, was at 150 PFU/mL, or three times the quantitative detection limit.

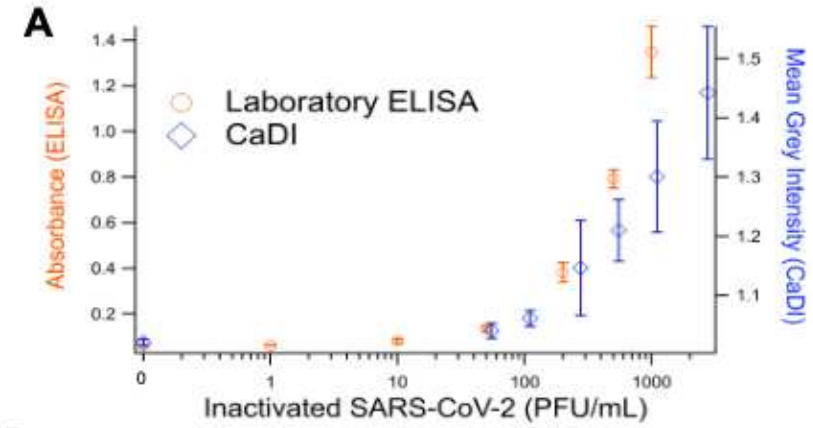

C

Untrained End User Readings				
Concentration (PFU/mL)	0	30	70	150
Number that marked "positive"	0	10	20	22
Total People	22	22	22	22
Percent correct	100%	45%	91%	100%

Figure A8.3. (A) Comparison between CaDI and a well-plate laboratory ELISA. (B) Shows actual images of the nitrocellulose strips shown to 22-untrained users who were asked to list each strip as positive or negative. (C) Percentages from the untrained users correctly identifying a positive or negative strip.

A4.4 Conclusion

Here, we demonstrate a capillary driven immunoassay that fully automates the reagent delivery and washing steps of a sandwich ELISA while retaining the simplicity of an LFA. The CaDI novel design allows for a range of applications where antibodies can easily be swapped out to fit the corresponding assay. Various blockers were investigated to improve assay function and future work will continue to do long-term stability studies. Comparison of the CaDI device to a laboratory ELISA showed the ELISA only slightly outperforming the CaDI system.

REFERENCES

1. Link, J.; Carrell, C.; Jang, I.; Panraksa, Y.; Sánchez-Cano, A.; Call, Z.; Noviana, E.; Dandy, D. S.; Geiss, B. J.; Henry, C. S. In *Power-free automated capillary flow assay for SARS-CoV-2 detection*, MicroTAS-Int. Conf. Miniaturized Syst. Chem. Life Sci., 2020; pp 536-537.
2. Carrell, C.; Link, J.; Jang, I.; Terry, J.; Scherman, M.; Call, Z.; Panraksa, Y.; Dandy, D. S.; Geiss, B. J.; Henry, C., Point-of-Need Disposable ELISA System for COVID-19 Serology Testing. **2020**.
3. Organization, W. H. March 2022 Epidemiological Upate. https://www.who.int/publications/m/item/weekly-epidemiological-update-on-covid-19---8-march-2022 (accessed March 9).
4. Center, J., Coronavirus COVID-19 global cases by Center for Systems Science ad Engineering (CSSE) at Johns Hopkins University 2020 [Available from: https://coronavirus. jhu. edu/map. html. accessed: 2020.
5. Organization, W. H. *COVID-19 and food safety: guidance for food businesses: interim guidance, 07 April 2020*; World Health Organization: 2020.
6. Weissleder, R.; Lee, H.; Ko, J.; Pittet, M. J., COVID-19 diagnostics in context. *Science translational medicine* **2020,** *12* (546), eabc1931.

APPENDIX 5. 3D PRINTED PARTS FOR MICROFLUIDCS AT THE POINT-OF-CARE

Here, I described 3D printed parts for microfluidic device housings and flow cells. The works describes methods and applications for 3D printing. Device housings are described for the CaDI work described in Appendix 4 and magnetophoresis work from Chapter three. Additionally, a 3D printed microfluidic flow cell with integrated microelectrodes for pathogen detection is described. The works described were solely designed and optimized by me with assistance from Dr. Cynthia McCord for integrating the electrodes into the final part described in this appendix.

A5.1 Introduction

3D printing offers a wide range of applications from the aerospace industry to the food industry.[1, 2] Multiple types of 3D printers are commercially available and generally classified into seven categories, including binding jetting, directed energy deposition, material extrusion, material jetting, powder bed fusion, sheet lamination, and photopolymerization.[3-5] In the last two decades 3D printing has become increasingly popular for the field of microfluidics for flow cells and device housings.[6] Here, I will be describing 3D printed parts for microfluidics using a stereolithography (SLA) printed classified under photopolymerization. SLA printers cure liquid photopolymer resin into solid parts through UV light exposure.[7] A light source produces a 405nm laser and then is focused by a mirror to cure one layer at time (Figure A5.1).[8] 3D printed parts can be designed in computer assisted drawing (CAD) software and then directly uploaded to the printer. SLA printers provide high surface resolution making it ideal for microfluidics.

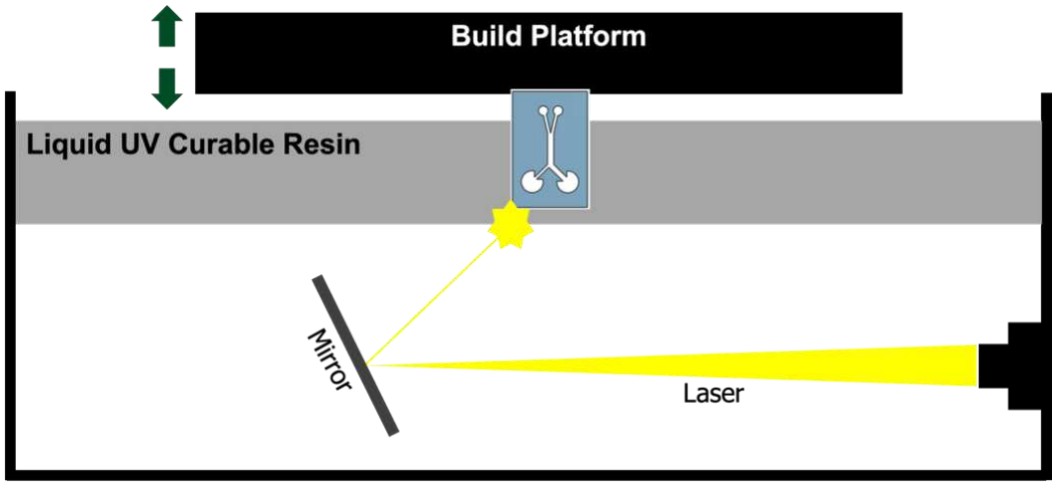

Figure A5.9. Schematic of normal SLA printer.

Device housings for point-of-care (POC) diagnostics are critical to develop assays for commercialization.[9] Current commercially POC test incorporate housings to enhance user-friendliness.[9] For traditional LFAs containing a test and control line, housings or cassettes will have a viewing window for the user to easily read results. The most common example, being the home pregnancy test (Figure A5.2a).[10] Housings are often simple snap fitting plastic pieces to seal the device from contamination, and to avoid improper use. Additionally, housings have been developed to incorporate nasal swaps with LFAs (Figure A5.2b).[11]

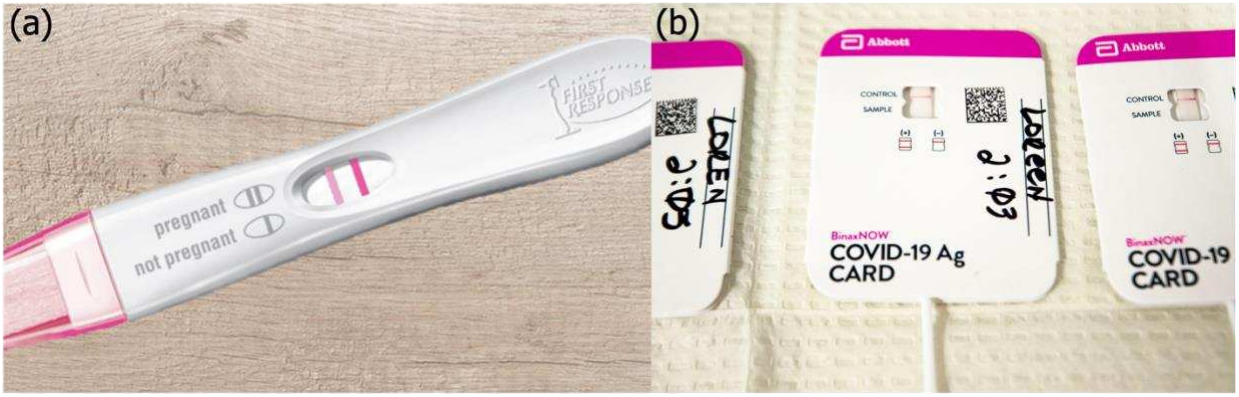

Figure A5.10. (a) Image of a home pregnancy test with housing. (b) Photograph Binax COVID-19 home test kit with integrated nasal swap.

A5.2 3D Printed Parts

A5.2.1 Capillary-Driven Immunoassay (CaDI) Housing

In appendix 4, we discuss a novel technology for the detection of SARS-COV-2 by sequential delivery of reagents. To further this technology towards commercialization, I developed a device housing. Here, I designed key features in the housing to improve user friendliness and reproducibility of the assay. The housing is a two-part design with a top and bottom that push together using friction boss fittings for a tight seal. A test-viewing window and sample inlet port were added to the top part. Device alignment features were added into the bottom part to ensure consistent device placement. Pull tabs were added onto each end of the bottom part to allow for two parts to be separated if needed (Figure A5.3).

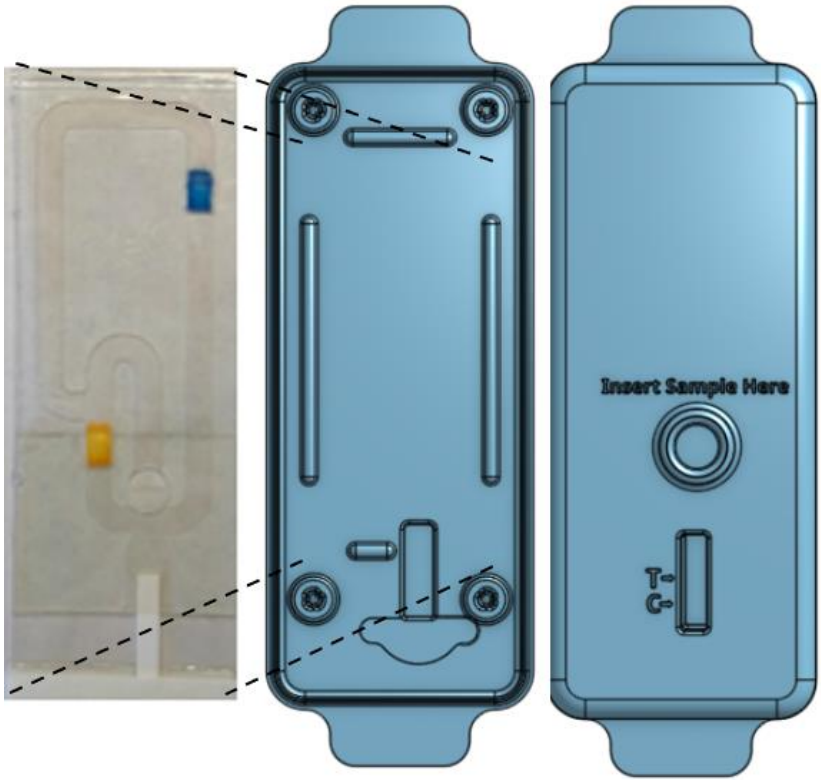

Figure A5.11. Photograph of CaDI device and CAD rendering of the device housing.

A5.2.2 Manetophoresis Device Housing

In Chapter three, I describe a capillary driven pump-free magnetophoresis device that addressed improvements from the device discussed in Chapter 2. A housing was designed to improve user-friendliness and create more reproducible magnetophoresis. The housing is designed similar to the housing described above with sample inlets, viewing window, alignment features and friction boss fittings. Additionally, a magnet hole was designed to fit the ¼" NdFeB permanent magnet used for this assay perfectly. By placing the magnet in the exact right orientation every time, the magnetic particles will be attracted to the high magnetic field in the same flow path every time increasing assay consistency. Figure A5.4 shows a CAD rendering of the device housing and a photograph of the device in the housing.

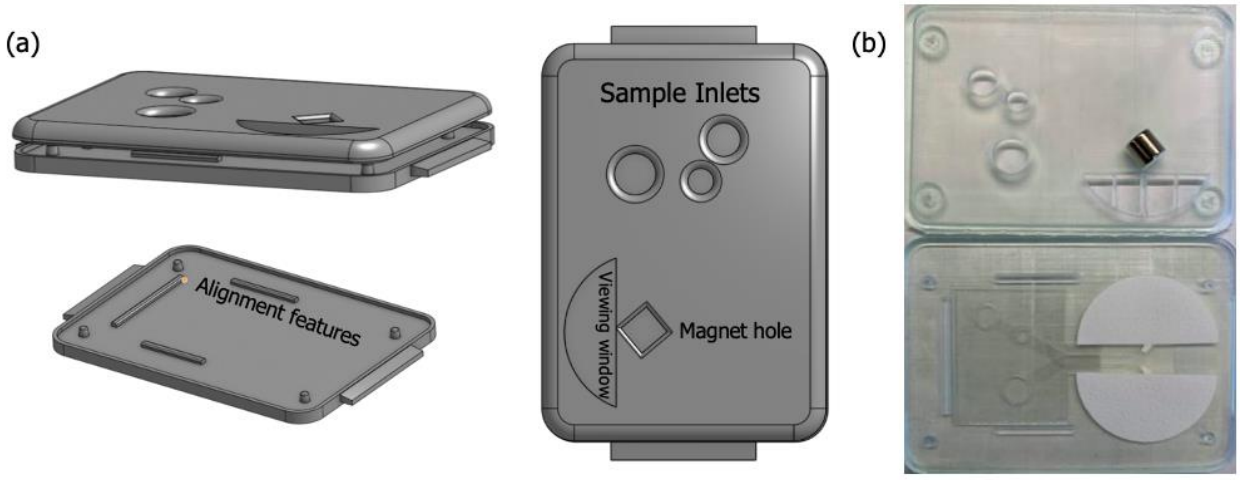

Figure A5.12. (a) CAD rendering of magnetophoresis device housing. (b) Photograph of microfluidic magnetophoresis device assembled with device housing.

A5.2.3 Microfluidic Flow Cell with Electrochemical Detection

3D printed microfluidics have become a widely popular alternative to traditional microfluidics. 3D printing microfluidic devices eliminates the need for tedious fabrication techniques with traditional microfluidics. In 2000, Renaud *et al* reported the first SLA printed

microfluidic cell for rapid mixing. [12] Many groups have expanded to bacterial detection using fluorescence and electrochemical methods.[2, 13] The Henry group has recently investigated cheap thermoplastic electrodes (TPEs) as an alternative to expensive commercial electrodes.[14] TPEs have been integrated with ePADs discussed earlier for pathogen detection and can be heat-pressed into polymethylmethacrylate (PMMA) to create electrode arrays.[15-17]

Here, I describe unpublished work for a microfluidic flow cell with integrated TPEs for pathogen detection. The device is a two-part design with a 3D printed top and a PMMA bottom with an integrated TPE array (Figure A5.5). The TPE array was designed with eight working electrodes with a corresponding counter and reference electrode. The two parts are sealed together using six NdFeB permanent magnets. A gasket is used to outline the fluid channel and is compressed to seal the fluid channel when the device is assembled. The top part was designed with a sample inlet and outlet that can be drill tapped to fit a syringe pump to drive flow. After flow is initiated through the syringe pump, the fluid follows the outlined channel and flows over the electrode array for pathogen detection. The device was tested and able to handle 1mL/min of solution without any leaking occurring resulting in high throughput of sample.

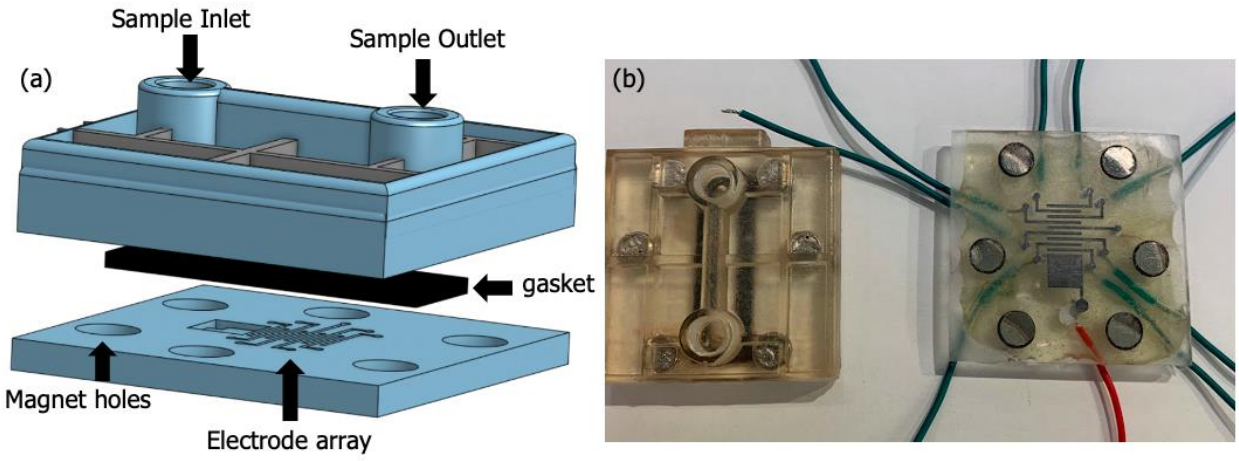

Figure A5.13. (a) CAD rendering of the 3D printed flow cell assembly. (b) Photograph of actual device with copper wire for connections to TPE array.

A5.3 CONCLUSIONS

3D printed microfluidics is a rapidly growing field to fabricate cheap alternatives to traditional methods. SLA 3D printing allows for rapid prototyping with high surface resolution making it an ideal choice for microfluidics. Here, I demonstrate the ability to create 3D printed parts for microfluidic flow cells and device housings. The work described can be adapted for multiple device designs for point-of-care diagnostics.

REFERENCES

1. Waheed, S.; Cabot, J. M.; Macdonald, N. P.; Lewis, T.; Guijt, R. M.; Paull, B.; Breadmore, M. C., 3D printed microfluidic devices: enablers and barriers. *Lab on a Chip* **2016,** *16* (11), 1993-2013.
2. Ho, C. M. B.; Ng, S. H.; Li, K. H. H.; Yoon, Y.-J., 3D printed microfluidics for biological applications. *Lab on a Chip* **2015,** *15* (18), 3627-3637.
3. Shahrubudin, N.; Lee, T. C.; Ramlan, R., An overview on 3D printing technology: Technological, materials, and applications. *Procedia Manufacturing* **2019,** *35*, 1286-1296.
4. Yan, Q.; Dong, H.; Su, J.; Han, J.; Song, B.; Wei, Q.; Shi, Y., A review of 3D printing technology for medical applications. *Engineering* **2018,** *4* (5), 729-742.
5. Bhattacharjee, N.; Urrios, A.; Kang, S.; Folch, A., The upcoming 3D-printing revolution in microfluidics. *Lab on a Chip* **2016,** *16* (10), 1720-1742.
6. Au, A. K.; Huynh, W.; Horowitz, L. F.; Folch, A., 3D-printed microfluidics. *Angewandte Chemie International Edition* **2016,** *55* (12), 3862-3881.
7. Nielsen, A. V.; Beauchamp, M. J.; Nordin, G. P.; Woolley, A. T., 3D printed microfluidics. *Annual Review of Analytical Chemistry* **2020,** *13*, 45-65.
8. Ma, X. L. In *Research on application of SLA technology in the 3D printing technology*, Applied mechanics and materials, Trans Tech Publ: 2013; pp 938-941.
9. Hnasko, R. M.; Jackson, E. S.; Lin, A. V.; Haff, R. P.; McGarvey, J. A., A rapid and sensitive lateral flow immunoassay (LFIA) for the detection of gluten in foods. *Food Chemistry* **2021,** *355*, 129514.
10. Response, F. https://www.google.com/search?q=home+pregnancy+test&tbm=isch&ved=2ahUKEwjM6cfTwrD2AhVCCZ0JHV_MBogQ2-cCegQIABAA&oq=home+pregnancy+test&gs_lcp=CgNpbWcQAzIHCCMQ7wMQJzIICAAQgAQQsQMyBQgAEIAEMgUIABCABDIFCAAQgAQyBQgAEIAEMgUIABCABDIFCAAQgAQyBQgAEIAEMgUIABCABDoICAAQsQMQgwE6BAgAEAM6BAgAEEM6BwgAELEDEEM6BggAEAgQHlDaBViNMmCHM2gDcAB4AIABvwGIAecXkgEEMy4yMJgBAKABAaoBC2d3cy13aXotaW1nwAEB&sclient=img&ei=aickYsyMI8KS9PwP35ibwAg&bih=785&biw=1573#imgrc=rRw4xSGByyV-fM.
11. Radio, C. P. https://www.cpr.org/2021/12/31/if-you-take-an-at-home-covid-test-and-its-positive-youre-supposed-to-report-it-to-colorado-officials-heres-how/ (accessed March 3).
12. Bertsch, A.; Bernhard, P.; Vogt, C.; Renaud, P., Rapid prototyping of small size objects. *Rapid Prototyping Journal* **2000**.
13. Lee, W.; Kwon, D.; Choi, W.; Jung, G. Y.; Au, A. K.; Folch, A.; Jeon, S., 3D-printed microfluidic device for the detection of pathogenic bacteria using size-based separation in helical channel with trapezoid cross-section. *Scientific reports* **2015,** *5* (1), 1-7.
14. Klunder, K. J.; Nilsson, Z.; Sambur, J. B.; Henry, C. S., Patternable solvent-processed thermoplastic graphite electrodes. *Journal of the American Chemical Society* **2017,** *139* (36), 12623-12631.
15. Ozer, T.; McCord, C.; Geiss, B. J.; Dandy, D.; Henry, C. S., Thermoplastic Electrodes for Detection of Escherichia coli. *Journal of The Electrochemical Society* **2021,** *168* (4), 047509.
16. McCord, C. P.; Summers, B.; Henry, C. S., Redox behavior and surface morphology of polystyrene thermoplastic electrodes. *Electrochimica Acta* **2021,** *393*, 139069.

17. Noviana, E.; McCord, C. P.; Clark, K. M.; Jang, I.; Henry, C. S., Electrochemical paper-based devices: Sensing approaches and progress toward practical applications. *Lab on a Chip* **2020,** *20* (1), 9-34.

APPENDIX 6. RAPID DETECTION OF CHRONIC WASTING DISEASE PROPOSAL

Specific Aims:

Chronic Wasting Disease (CWD) is a fatal and highly contagious neurological disease that affects cervid species including deer, moose, and elk. Since its discovery in 1967 in Larimer Country, Colorado, CWD has spread to 25 states as of January, 2021.[1] CWD is classified as a transmissible spongiform encephalopathy (TSE) or prion disease, meaning normal cellular prions will misfold abnormally. CWD is similar to other prion diseases such as Alzheimer's and Parkinson's disease where abnormal prions replicate using normal cellular proteins.[2, 3] Unfortunately, similar to Alzheimer's and Parkinson's, there is no cure for CWD so early detection is currently the best way for disease mitigation. Current diagnostic approaches rely on the isolation of misfolded prions found in brain tissue of the infected animals. Common detection approaches include real-time quaking-induced conversion (RT-QuIC), immunohistochemistry (IHC), and enzyme immunoassay (EIA). [1, 4-7] These methods are expensive, time and labor intensive, and require trained personnel in a laboratory setting. Sampling is done by taking retropharyngeal lymph nodes (RLN) or orbex (OB) tissue which must be removed from the animals post-mortem. The samples are then sent for testing where results can take weeks. During this time, the hunters will process the animal, which wastes time and resources on a potentially inedible animal. In 2020 alone, the state of Colorado spent 75 dollars per CWD test totaling to over one million. CWD mitigation is not only a major problem for Colorado but also for 24 other states. A rapid diagnostic for CWD that hunters can use post-harvest would save state agencies millions of dollars and allow hunters to accurately diagnose infected meat in the field before processing and consuming. Here, we will describe a rapid and portable enzyme immunoassay for CWD detection. We are aiming to take a simplistic approach to detect prions sensitively and accurately. The assay utilizes three well

known concepts: prions binding to stainless steel; heparan sulfate affinity to prions; and the enzyme-substrate reaction of horseradish peroxidase and 3,3',5,5' Tetramethylbenzidine (TMB). Firstly, a stainless-steel probe will be directly inserted into lymph node tissue to collect prions onto the surface of the probe. A RLN tissue will be selected because it is the first place prions replicate and has the highest infectivity.[8] The infectious, abnormal prions are protease resistant while the normal cellular prions are not. This allows us to insert the probe into proteinase K for the digestion step of the normal cellular prions, leaving only the abnormal form left on the probe. Following the digestion step, a heparan sulfate-HRP label will be conjugated to the abnormal prions. Once the abnormal prions are labeled with an enzyme, we will use TMB to produce a blue colorimetric signal (Figure A6.1). If there are no infectious abnormal prions present, then there will be no blue color formation. Results can be read by eye for a positive/negative answer, or a smart phone image can be analyzed for quantitative results. I am the sole writer of this work and this proposal is in preparation for future grant submissions.

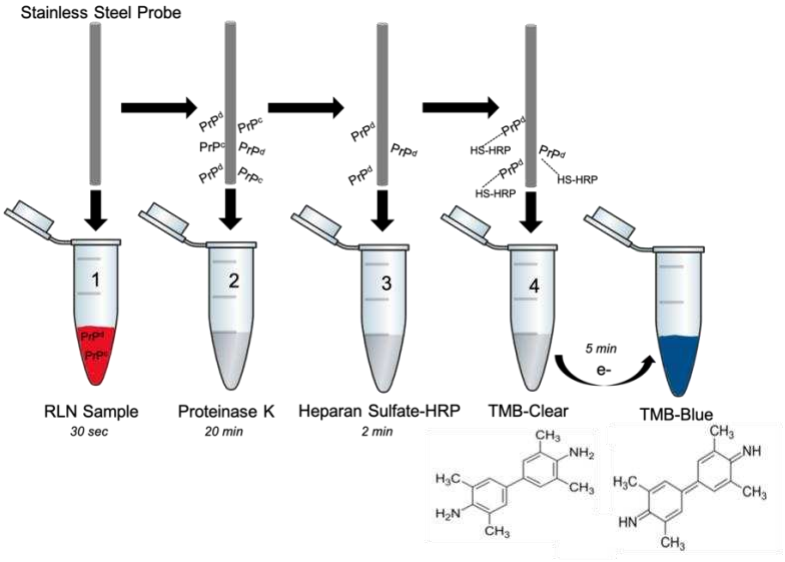

Figure A6.1. Schematic of the sequential binding process of the assay with the colorimetric detection of TMB-Blue in the presence of PrP^{Sc}.

Aim 1: Develop a proof-of-concept assay with CWD infected mice

The Henry lab will optimize the three steps of the assay using samples derived from mice. Stainless steel binding conditions, PrP^C digestion, and heparan sulfate affinity will all be studied and optimized.

Significance: Current methods for CWD can take up to 4 hours to complete and sometimes weeks for results to be returned. The proposed system will greatly impact data collection of infected cervid herds, time-to-answer for hunters and save money for local agencies. We will start with testing CWD infected mice tissue to establish proof-of-concept for the assay and a baseline for a limit of detection.

Innovation: Current testing for CWD is performed in a laboratory setting using IHC or RT-QuIC assays. Current detection methods are not field deployable and cannot be operated by untrained users. The system described will be able to translate to the point-of-need (PON) to be operated by untrained users.

Aim 2: Demonstrate accurate testing of CWD using RLN samples from deer

Significance: Following the development of a working CWD assay using infected mice tissue, we will transfer to testing for CWD levels in deer RLN samples. This will demonstrate assay capability to field testing. This assay will help hunters easily and accurately test their own sample in the field, removing any guess work and consumption of infected meat.

Innovation: To the best of our knowledge there are no portable diagnostics to rapidly and accurately detect CWD.

Significance: We are aiming to create a simple, rapid, and portable diagnostic assay from a RLN sample for CWD detection. CWD is a fatal neurological disease that is rapidly affecting the cervid

population across North America and has now been found in South Korea and Europe.[1, 9] To slow the spread of CWD, rapid diagnostics are needed to properly diagnose infected cervids. The most promising CWD diagnostic assays are RT-QuIC and a traditional enzyme linked immunosorbent assay (ELISA). RT-QuIC assays involve amplifying prion proteins using quaking-induced conversion of normal cellular prion proteins (PrP^{C}) to the infectious abnormal scrapie prion protein (PrP^{Sc}).[10] Whereas a laboratory well-plate ELISA uses capture and detection antibodies specific to PrP^{Sc}. Both assays are expensive, require trained personnel, complex instrumentation, and are unsuitable for field testing.[4, 11, 12] To improve CWD diagnostics to the PON, the assays must become portable, easy to use and provide faster results without relinquishing limits of detection (LOD).

In this project, we will adapt proven analytical methods to create rapid detection of CWD that will be able to translate to the PON. To our knowledge, there are currently no portable and rapid CWD diagnostics.[11, 12] The proposed system will translate to the PON, eliminating the need for trained personnel and complex instrumentation. The PrP^{C} and PrP^{Sc} prions have a strong affinity to bind to stainless steel.[13, 14] Herein, a stainless-steel probe will be inserted into a RLN tissue sample to bind PrP^{C} and PrP^{Sc}. The PrP^{C} will then be degraded using Proteinase K (PK) while leaving the PrP^{Sc} intact and bound to the probe.[15] After degradation of the PrP^{C}, the probe will be incubated with Heparan Sulfate (HS) conjugated to horseradish peroxidase (HRP). We will use 3,3',5,5' Tetramethylbenzidine (TMB) to provide a rapid colorimetric reaction from clear to blue in the presence of HRP and H_2O_2. The assay proposed here will eliminate the need for instrumentation used in RT-QuIC assays and ELISAs such as thermal cyclers, fluorometers and other expensive laboratory instrumentation. The assay described will be an easy-to-read, PON diagnostic test that the untrained user can operate. **We hypothesize a stainless-steel probe**

method with colorimetric detection can be used to detect PrPSc sensitively and specifically from a RLN tissue sample in 30 min or less.

Innovation: Our proposal in innovative in the following ways:

- Creating the first portable CWD diagnostic to be used by untrained users at the PON.
- The current gold standard methods for detecting CWD are labor intensive and involve complicated instrumentation. The assay described will be cost effective and provide timely answers for hunters.

Approach:

Overview: Portable detection of CWD from a RLN will be performed by completing two aims. The first aim will focus on determining if this novel assay will work with the proposed sequence of binding steps using infected mice tissue. In this aim, the focus will be on optimizing the conjugation conditions for each step of the assay starting with the conjugation of prions to the probe. pH, reagent concentrations and incubation times will be investigated and optimized to ensure proper binding and detection. In the second aim, we will focus on transferring the assay from infected mice tissue to deer RLN samples. The second aim will provide useful information and data to show the ability of the assay to perform at the PON.

Team: The Henry, Giess and Zabel labs at Colorado State University are well versed in creating portable diagnostics. The Henry and Giess labs have successfully collaborated on 22 publications aimed at detecting infectious diseases with enzyme detection at the point-of-care.[12, 16-23] The Zabel lab is a part of the Prion Research Center here at Colorado State University and has 43 publications surrounding prion research. Dr. Zabel utilizes novel mouse models for CWD that

have led to numerous publications surrounding prion replication, disease progression and transmission.[23-26]

Background and theoretical basis:

Abnormal prions replicate by the recruiting and denaturing the normal cellular proteins, turning the PrP^{C} into the PrP^{Sc} form. The PrP^{Sc} form takes the normal PrP^{C} and uses it as a substrate to propagate itself. [27] CWD is classified as a spongiform brain disorder because PrP^{Sc} degrades the tissue around them and forms holes in the brain (like a sponge). Misfolded prions don't degrade and are resistant to proteinase digestion, so they remain on any surface that a deer licks, sniffs etc. This includes materials, such as wood, soil, cement, and stainless steel making the spread of the prions very prevalent.[14] Once a cervid is infected with CWD it is always fatal but can take several years for symptoms to develop. Symptoms include weight loss, stumbling, lethargy, and other neurological conditions. While the incubation time of the disease can be up to several years, cervids can spread the disease as soon as they become infected making early detection of CWD important. Early detection is difficult because sampling is currently done post-mortem by removing the lymph nodes. Antemortem testing is difficult because prion levels in blood and urine are relatively low compared to concentration levels in lymph nodes. Post-mortem testing of lymph nodes has since become the standard to achieve the best limits of detection. Creating a field-deployable test capable of testing antemortem and post-mortem is ideal to improve current diagnostic testing.

We will develop an assay using the knowledge that prions bind well to stainless steel while the PrP^{Sc} form is resistant from proteinase while the cellular PrP^{C} form will completely degrade in the presence of proteinase K. This allows for detection of the PrP^{Sc} separate from the PrP^{C} form.

The following results are relevant to this proposal and demonstrate the capabilities of our laboratories and the science of the proposed system. *(1) Infectivity of scrapie prions bound to stainless steel surface.* In a 1999 publication, scrapie prions were found to bind and retain activity on a 0.15 x 5mm stainless steel wire through extensive washes.[28] The binding of prions to stainless steel has since become commonplace for diagnostics.[14, 29] For our assay, we will use this practice to initially bind prions to a small stainless steel probe. *(2) Efficient prion disease transmission through common environmental materials.* A study in 2017, found that prions will bind quickly and efficiently to several surfaces. Stainless steel, wood, cement, and glass were all found to find prions to the surface within minutes and retain activity after multiple washes. [14] *(3) Protease-sensitive scrapie prion protein in aggregates of heterogeneous sizes.* A 2002 publication showed that prion infected tissue contains protease sensitive prions. By incubating the tissue for 30 min at 37˚C the infectious scrapie prion protein was retained while the normal prion protein was eliminated from the tissue. Herein, this incubation step will allow us to cleave off the normal prion PrP^{C} and only leave the infectious form present on the stainless-steel probe to then label. *(4) Identification of the Heparan Sulfate Binding Sites in the Cellular Prion Protein.* In 2002, a publication reported that by using biosensor and enzyme-linked immunosorbent assay they showed direct heparin and HS-binding activity in recombinant cellular prion protein.[30] Once our assay has gone through the PK incubation step to cleave off the normal prion form, only the PrP^{Sc} will be left to be labeled with HS-HRP conjugate. The HS-HRP conjugate can then be incubated with H_2O_2 and TMB to provide a colorimetric reaction yielding the blue oxidized TMB product.

Proposed Experiments:

Aim 1: **In this aim, we will create a novel CWD diagnostic to detect PrP^{Sc} by a colorimetric label to be read by the naked eye.**

The goal of this aim to develop the full assay conditions in laboratory-controlled settings to optimize each reagent addition and conjugation steps. In this aim, each conjugation step will be done with appropriate washing steps in a well plate following published conditions to ensure proof-of-concept.[12, 31]

Objective 1: Optimize binding conditions for prions to a stainless-steel probe

A thin stainless-steel wire will be optimal for field testing to make it easier for hunters to insert into the lymph nodes and recover prions bound to probe. Samples of PrP^{Sc} infected tissue will be collected from infected mice from the Zabel lab. Prions have a high affinity to bind to the surface of stainless steel and this process happens quickly. [28, 32] Probe size will be investigated along with washing procedures and the incubation times of the probes into the infected tissue. Incubation times will be optimized starting with 30 seconds and up to 2 min. The binding efficiency will be tested with enzyme-substrate amplification of HS-HRP and TMB. By using the HRP-TMB interaction we will be able to correlate the amount of prions bound at each time point to the color intensity formed. The color intensity at each time point will be analyzed with UV-Vis; absorbance measurements will be correlated to concentration. The lowest incubation time yielding the blue oxidized form of TMB will be adopted into the next objective.

Objective 2: Optimize degradation conditions of PrP^{c} using PK

Following the binding of prions to the stainless-steel probe, the PrP^{C} form needs to be degraded to test for the presence of the protease resistant PrP^{Sc} form. PK has been shown to effectivity degrade PrP^{c}. [33, 34] After PK digestion, only the PrP^{Sc} will be left bound to the stainless-steel probe enhancing the specificity of the assay. Standard conditions that will be investigated include incubation time, washing steps, PK concentration, temperature range, and pH. Initial

conditions will follow standard procedures and be optimized from them to meet the needs of the portable assay. [34-36] After the PK digestion, the samples will be analyzed to determine degradation via western blot. [37, 38]

Objective 3: Optimize the binding conditions of HS-HRP to PrP^{Sc}.

Following objective 2 and 3, the binding conditions of HS-HRP to PrP^{Sc} will be investigated to optimize the enzyme-substrate reaction from TMB clear to TMB blue. HS has been shown to bind well to prions, and after the PK digestion only the PrP^{Sc} will be left for conjugation. [30, 39, 40] Washing procedures, concentration and incubation times of the conjugate will be investigated and optimized. Non-specific binding of the heparan sulfate to the probe will be investigated and can be mitigated by use of commercially available blockers. Colorimetric results will be determined by adding TMB to the samples and analyzing color intensity with ImageJ software.

Objective 4: Optimize the TMB conditions and time-to-answer for the assay

After the previous conjugation steps have been optimized, the TMB conditions will be investigated to produce the optimal TMB color formation in the presence of HS-HRP bound to PrP^{Sc}. The Henry lab and Geiss lab have experience with traditional well-plate ELISAs using HRP-TMB for a detection scheme. A commercially available Ultra TMB substrate solution will be used that requires no pretreatment steps before use. When oxidized, TMB will turn from a clear solution into a blue solution after one electron loss. Traditional color formation is set to be analyzed at 30 min; Color formation starts in as little at 10 seconds at high concentrations of HRP. For this simple yes/no diagnostic test, the user can read the test as soon as color forms cutting down the time to answer.

Objective 5: Comparison of detection limit with IHC to working assay

Comparison of the detection limits from the stainless-steel probe assay will be compared to IHC or RT-QuIC for validation in collaboration with the Zabel lab. Current LODs for standard methods using RLN samples range from 10^{-6} to 10^{-8} µg/g of sample. We anticipate a LOD of 10^{-5} µg/g initially based on reported ELISA LODs.[1, 7]

Potential Pitfalls and Workarounds:

(1) PK digestion has been shown to completely degrade PrP^{C} after 30 min – 1 hr incubation time at 37˚C of the probe and leave only the PrP^{Sc}.[34, 37, 38] To make this test as rapid and portable as possible, we will need to optimize the digestion to decrease the time it will take for digestion. This diagnostic would also be deployed during the hunting season, which occurs in the fall/winter resulting temperatures lower than 37˚C. Small portable precision heaters have been shown to be an effective alternative to expensive laboratory equipment.[41, 42] Here we will look to deploy one of these portable heater options. The digestion time and multiple temperature ranges will be investigated to determine the best combination, while still translating to the PON. *(2)* Heparan sulfate and Heparin promote prion replication by binding to normal and abnormal prion proteins.[43] A potential pitfall could be the nonspecific binding of the HS to the normal prions. If nonspecific binding occurs, then it would lead to false positives with the TMB colorimetric substrate. In this case we can work around this by using an anti-PrP^{Sc} antibody labeled with HRP (Figure A6.2). Commercial blockers would be used in addition with the antibody to ensure no nonspecific binding occurs. *(3)* Our target LOD is 10^{-2} to be competitive with IHC and RT-QuIC, however, if sensitivity is too low then we will investigate the following approaches to improve sensitivity. First, concentration of HS-HRP will be optimized by investigating varying concentrations to ensure the most enzyme turnover as possible with TMB-Clear into TMB-Blue. Second, longer

incubation times and/or agitation of the probe into the tissue may be needed to coat the probe sufficiently with prions. Third, the probe material will be investigated, by testing how well the probe binds prions initially and retains prions after multiple washing and binding steps. Results published by Pritzkow et al. showed that wooden tooth picks and cement bound and retained the highest prion levels onto the surface after multiple washing steps.[14] More porous materials like wood or cement might increase false positives so we anticipate PK digestion to be more efficient on a stainless steel.

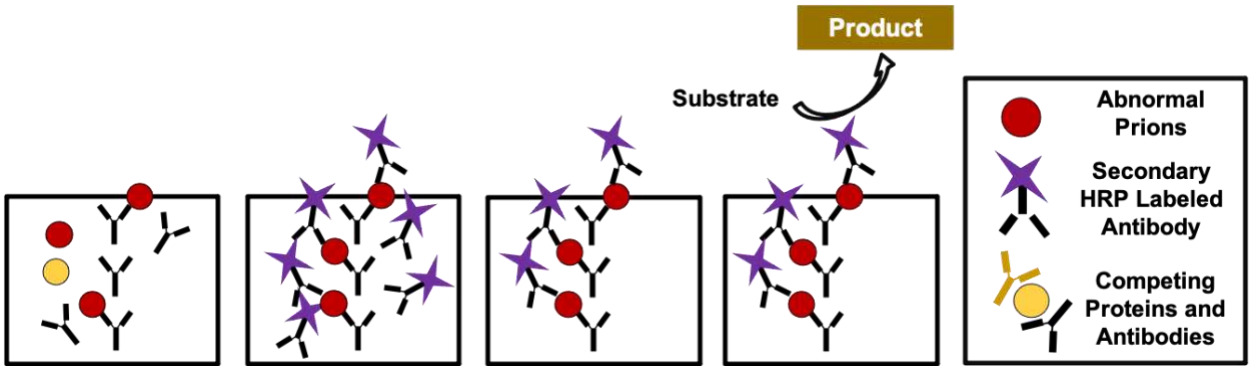

Figure A6.2. Molecular level schematic of the stepwise conjugation steps of reagents using PrP^{Sc} specific antibody. with enzyme and substrate reaction.

Aim 2: **In this aim we will investigate testing RLN samples from post-mortem cervids for CWD detection**

The goal of this aim is to translate the working assay from aim 1 with mice infected tissue to cervid RLN samples. We will first test harvested RLN samples from CWD positive deer in a laboratory setting and then will transfer to field testing cervid with the collaboration of Colorado Parks and Wildlife. We will investigate LODs with cervid tissue and the ability of the assay to be portable for untrained users to operate.

Figure A6.3. Schematic of the stepwise workflow from mice to RLN harvested samples to field testing of cervids.

Objective 1: Confirm assay conditions from infected mice tissue to cervids

The mice tissue that will be used in aim 1, will be inoculated with the PrP^{Sc} protein harvested from captive mule deer in collaboration with the Zabel lab and Colorado Parks and Wildlife. In this aim, we will focus on ensuring the translation from the infected mice tissue to direct sampling of the RLN tissue of captive mule deer. This objective will focus on investigating each binding step outlined in aim 1 to ensure sufficient binding and detection of the PrP^{Sc} form from cervid RLN samples.

Objective 2: Investigate RLN tissue viability from cervid samples

RLN tissue starts to degrade less than 1 min after death, so it is advantageous to sample immediately after harvest. In this objective, we will investigate the maximum lifetime of CWD positive tissue that is still able to be detected with our assay. We will start by testing RLN immediately after harvest and subsequent testing every week until no signal is present while the tissue is kept at 4˚C. Additional viability tests will be conducted with frozen RLN tissue to determine a lifetime when tissue is kept at -20˚C.

Objective 3: Determine the LOD using cervid RLN samples

The goal of this objective will be to replicate the sensitivity of the assay found in aim 1. The work in this objective will be completed in a laboratory setting and results will be compared

against RT-QuIC and IHC. The heterogeneity of cervids will be investigated to understand the sensitivity and specificity of the assay.

Objective 4: Develop Standard Operating Procedures (SOPs) for each binding step and fabrication

Improper use of well vetted home diagnostic kits is common and have been well documented.[44] Creating an easy-to-use diagnostic kit is critical for when developing POM diagnostics. The test may work perfect in the laboratory by trained users, however if it cannot be operated by untrained users then it will fail to translate to the PON. In this objective a full SOP will be created and tested to ensure easy comprehension and use for all users.

Objective 5: Field testing on post-mortem cervids with collaboration of Colorado Parks and Wildlife

In collaboration with the Zabel lab, and the Colorado Parks and Wildlife we will conduct field testing on post-mortem cervids as earliest as the 2022-2023 hunting season. In the initial sample testing, we hope to test 100 deer and/or elk to collect a large enough sample size to show the viability of the working assay.

Potential Pitfalls and workarounds:

(1) Contamination of probe with competing proteins is a potential pitfall that we will investigate. After the initial binding of prions to the stainless-steel probe, competing proteins may also be present on the probe. In this case, the PK digestion is a crucial step in the assay to ensure only the PrP^{Sc} form is left to bind to HS-HRP. If we do encounter non-specific binding from competing proteins, we will investigate two workarounds. First, by using blockers to restrict binding sites on the competing proteins. Second, use of a monoclonal anti-PrP^{Sc}-HRP in the place

of HS-HRP, could improve selectivity because the monoclonal antibody will be specific to the antigen epitope. *(2)* The heterogeneity of cervids and sensitivity with varying levels of infectivity is a potential pitfall. To translate to the PON the assay will need be able to handle a wide range of prion levels in a consistent manner. Longer incubation times, washing steps and concentrations of reagents will be investigated to produce consistent results from low infection levels to high infection levels. During aim 2, we will optimize the assay to be performed in a timely manner but also remaining consistent for low levels of CWD. *(3)* Temperature is a potential pitfall that can impact the assay working correctly. The PK, HS-HRP and TMB will need to be kept cooled before use to avoid degradation. The temperature of the tissue sample will also need to be cooled quickly if analysis does not happen directly after harvest. This will be a concern when this assay is ready for portable detection. For portable detection we will develop an assay kit that is packed with ice packs to keep the reagents cold until use.

Summary:

This proposal aims to demonstrate a rapid, portable, and inexpensive CWD assay using a novel diagnostic assay. CWD is spreading rapidly through free ranging and captive cervids creating a need for portable diagnostics to slow or stop disease transmission. We will combine proven techniques to create a working portable assay. The assay will be run via PrP^{Sc} binding to stainless steel probe followed by labeling with an enzyme to produce a colorimetric signal that can be read by eye. Importantly, this proposed assay could dramatically change the detection for CWD and help mitigate the spread of CWD. There are several innovations presented in this proposal. First, there are no current rapid and portable diagnostic tests for CWD detection. The method described will enhance time to answer for hunters and state agencies for CWD in cervids. Second, the current gold standard methods for detecting CWD are labor intensive and involve complicated

instrumentation. We will create a user-friendly assay that will cut down on time to answer from weeks to minutes. Finally, this proposal will create a portable CWD diagnostic that could potentially save millions of dollars in testing and refund fees, not only in Colorado but across the United States. We are hopeful that the proposed assay can provide the type of CWD screening needed to slow the spread of CWD and eventually protect cervid herds from a fatal disease.

REFERENCES

1. Haley, N. J.; Carver, S.; Hoon-Hanks, L. L.; Henderson, D. M.; Davenport, K. A.; Bunting, E.; Gray, S.; Trindle, B.; Galeota, J.; LeVan, I., Detection of chronic wasting disease in the lymph nodes of free-ranging cervids by real-time quaking-induced conversion. *Journal of clinical microbiology* **2014,** *52* (9), 3237-3243.
2. Prusiner, S. B., Prions. *Proceedings of the National Academy of Sciences* **1998,** *95* (23), 13363-13383.
3. Prusiner, S. B., Neurodegenerative diseases and prions. *New England Journal of Medicine* **2001,** *344* (20), 1516-1526.
4. Hibler, C. P.; Wilson, K. L.; Spraker, T. R.; Miller, M. W.; Zink, R. R.; DeBuse, L. L.; Andersen, E.; Schweitzer, D.; Kennedy, J. A.; Baeten, L. A., Field validation and assessment of an enzyme-linked immunosorbent assay for detecting chronic wasting disease in mule deer (Odocoileus hemionus), white-tailed deer (Odocoileus virginianus), and Rocky Mountain elk (Cervus elaphus nelsoni). *Journal of Veterinary Diagnostic Investigation* **2003,** *15* (4), 311-319.
5. Keane, D. P.; Barr, D. J.; Keller, J. E.; Hall, S. M.; Langenberg, J. A.; Bochsler, P. N., Comparison of retropharyngeal lymph node and obex region of the brainstem in detection of chronic wasting disease in white-tailed deer (Odocoileus virginianus). *Journal of Veterinary Diagnostic Investigation* **2008,** *20* (1), 58-60.
6. Rivera, N. A.; Brandt, A. L.; Novakofski, J. E.; Mateus-Pinilla, N. E., Chronic wasting disease in cervids: Prevalence, impact and management strategies. *Veterinary Medicine: Research and Reports* **2019,** *10*, 123.
7. Tewari, D.; Steward, D.; Fasnacht, M.; Livengood, J., Detection by real-time quaking-induced conversion (RT-QuIC), ELISA, and IHC of chronic wasting disease prion in lymph nodes from Pennsylvania white-tailed deer with specific PRNP genotypes. *Journal of Veterinary Diagnostic Investigation* **2021**, 10406387211021411.
8. Ferreira, N. C.; Charco, J. M.; Plagenz, J.; Orru, C. D.; Denkers, N. D.; Metrick, M. A.; Hughson, A. G.; Griffin, K. A.; Race, B.; Hoover, E. A., Detection of chronic wasting disease in mule and white-tailed deer by RT-QuIC analysis of outer ear. *Scientific Reports* **2021,** *11* (1), 1-9.
9. Benestad, S. L.; Mitchell, G.; Simmons, M.; Ytrehus, B.; Vikøren, T., First case of chronic wasting disease in Europe in a Norwegian free-ranging reindeer. *Veterinary research* **2016,** *47* (1), 1-7.
10. Kal'nov, S.; Verkhovsky, O.; Tsibezov, V.; Alekseev, K.; Chudakova, D.; Filatov, I.; Grebennikova, T., Problems of ante mortem diagnostics of prion diseases. *Voprosy Virusologii* **2021,** *65* (6), 326-334.
11. Schwabenlander, M. D.; Rowden, G. R.; Li, M.; LaSharr, K.; Hildebrand, E. C.; Stone, S.; Seelig, D. M.; Jennelle, C. S.; Cornicelli, L.; Wolf, T. M., Comparison of Chronic Wasting Disease Detection Methods and Procedures: implications for free-ranging white-tailed deer (Odocoileus virginianus) surveillance and management. *bioRxiv* **2021**.
12. Carrell, C. S.; Wydallis, R. M.; Bontha, M.; Boehle, K. E.; Beveridge, J. R.; Geiss, B. J.; Henry, C. S., Rotary manifold for automating a paper-based Salmonella immunoassay. *RSC Advances* **2019,** *9* (50), 29078-29086.
13. Williams, K.; Hughson, A. G.; Chesebro, B.; Race, B., Inactivation of chronic wasting disease prions using sodium hypochlorite. *Plos one* **2019,** *14* (10), e0223659.

14. Pritzkow, S.; Morales, R.; Lyon, A.; Concha-Marambio, L.; Urayama, A.; Soto, C., Efficient prion disease transmission through common environmental materials. *Journal of Biological Chemistry* **2018,** *293* (9), 3363-3373.
15. Barria, M. A.; Libori, A.; Mitchell, G.; Head, M. W., Susceptibility of human prion protein to conversion by chronic wasting disease prions. *Emerging infectious diseases* **2018,** *24* (8), 1482.
16. Adkins, J. A.; Boehle, K.; Friend, C.; Chamberlain, B.; Bisha, B.; Henry, C. S., Colorimetric and Electrochemical Bacteria Detection Using Printed Paper- and Transparency-Based Analytic Devices. *Analytical Chemistry* **2017,** *89* (6), 3613-3621.
17. Channon, R. B.; Yang, Y.; Feibelman, K. M.; Geiss, B. J.; Dandy, D. S.; Henry, C. S., Development of an Electrochemical Paper-Based Analytical Device for Trace Detection of Virus Particles. *Analytical Chemistry* **2018,** *90* (12), 7777-7783.
18. Srisa-Art, M.; Boehle, K. E.; Geiss, B. J.; Henry, C. S., Highly Sensitive Detection of Salmonella typhimurium Using a Colorimetric Paper-Based Analytical Device Coupled with Immunomagnetic Separation. *Analytical Chemistry* **2018,** *90* (1), 1035-1043.
19. Carrell, C.; Kava, A.; Nguyen, M.; Menger, R.; Munshi, Z.; Call, Z.; Nussbaum, M.; Henry, C., Beyond the lateral flow assay: A review of paper-based microfluidics. *Microelectronic Engineering* **2019,** *206*, 45-54.
20. Pierson, T. C.; Sánchez, M. D.; Puffer, B. A.; Ahmed, A. A.; Geiss, B. J.; Valentine, L. E.; Altamura, L. A.; Diamond, M. S.; Doms, R. W., A rapid and quantitative assay for measuring antibody-mediated neutralization of West Nile virus infection. *Virology* **2006,** *346* (1), 53-65.
21. Wang, L.; Veselinovic, M.; Yang, L.; Geiss, B. J.; Dandy, D. S.; Chen, T., A sensitive DNA capacitive biosensor using interdigitated electrodes. *Biosensors and Bioelectronics* **2017,** *87*, 646-653.
22. Haley, N. J.; Mathiason, C. K.; Zabel, M. D.; Telling, G. C.; Hoover, E. A., Detection of sub-clinical CWD infection in conventional test-negative deer long after oral exposure to urine and feces from CWD+ deer. *PloS one* **2009,** *4* (11), e7990.
23. Haley, N. J.; Seelig, D. M.; Zabel, M. D.; Telling, G. C.; Hoover, E. A., Detection of CWD prions in urine and saliva of deer by transgenic mouse bioassay. *PloS one* **2009,** *4* (3), e4848.
24. Zabel, M. D.; Avery, A. C., Prions—not your immunologist's pathogen. *PLoS pathogens* **2015,** *11* (2), e1004624.
25. Hoover, C. E.; Davenport, K. A.; Henderson, D. M.; Denkers, N. D.; Mathiason, C. K.; Soto, C.; Zabel, M. D.; Hoover, E. A., Pathways of prion spread during early chronic wasting disease in deer. *Journal of virology* **2017,** *91* (10), e00077-17.
26. Osterholm, M. T.; Anderson, C. J.; Zabel, M. D.; Scheftel, J. M.; Moore, K. A.; Appleby, B. S., Chronic wasting disease in cervids: implications for prion transmission to humans and other animal species. *MBio* **2019,** *10* (4), e01091-19.
27. Baskakov, I. V.; Breydo, L., Converting the prion protein: what makes the protein infectious. *Biochimica et Biophysica Acta (BBA)-Molecular Basis of Disease* **2007,** *1772* (6), 692-703.
28. Zobeley, E.; Flechsig, E.; Cozzio, A.; Enari, M.; Weissmann, C., Infectivity of scrapie prions bound to a stainless steel surface. *Molecular medicine* **1999,** *5* (4), 240-243.
29. Haley, N. J.; Siepker, C.; Walter, W. D.; Thomsen, B. V.; Greenlee, J. J.; Lehmkuhl, A. D.; Richt, J. A., Antemortem detection of chronic wasting disease prions in nasal brush

collections and rectal biopsy specimens from white-tailed deer by real-time quaking-induced conversion. *Journal of clinical microbiology* **2016,** *54* (4), 1108-1116.
30. Warner, R. G.; Hundt, C.; Weiss, S.; Turnbull, J. E., Identification of the heparan sulfate binding sites in the cellular prion protein. *Journal of Biological Chemistry* **2002,** *277* (21), 18421-18430.
31. Call, Z. D.; Carrell, C. S.; Jang, I.; Geiss, B. J.; Dandy, D. S.; Henry, C. S., Paper-based pump-free magnetophoresis. *Analytical Methods* **2020,** *12* (43), 5177-5185.
32. Flechsig, E.; Hegyi, I.; Enari, M.; Schwarz, P.; Collinge, J.; Weissmann, C., Transmission of scrapie by steel-surface-bound prions. *Molecular medicine* **2001,** *7* (10), 679-684.
33. Tzaban, S.; Friedlander, G.; Schonberger, O.; Horonchik, L.; Yedidia, Y.; Shaked, G.; Gabizon, R.; Taraboulos, A., Protease-sensitive scrapie prion protein in aggregates of heterogeneous sizes. *Biochemistry* **2002,** *41* (42), 12868-12875.
34. Pastrana, M. A.; Sajnani, G.; Onisko, B.; Castilla, J.; Morales, R.; Soto, C.; Requena, J. R., Isolation and characterization of a proteinase K-sensitive PrPSc fraction. *Biochemistry* **2006,** *45* (51), 15710-15717.
35. Sajnani, G.; Requena, J. R., Prions, proteinase K and infectivity. *Prion* **2012,** *6* (5), 430-432.
36. Silva, C. J.; Vázquez-Fernández, E.; Onisko, B.; Requena, J. R., Proteinase K and the structure of PrPSc: The good, the bad and the ugly. *Virus research* **2015,** *207*, 120-126.
37. Meyerett, C.; Michel, B.; Pulford, B.; Spraker, T. R.; Nichols, T. A.; Johnson, T.; Kurt, T.; Hoover, E. A.; Telling, G. C.; Zabel, M. D., In vitro strain adaptation of CWD prions by serial protein misfolding cyclic amplification. *Virology* **2008,** *382* (2), 267-276.
38. Pulford, B.; Spraker, T. R.; Wyckoff, A. C.; Meyerett, C.; Bender, H.; Ferguson, A.; Wyatt, B.; Lockwood, K.; Powers, J.; Telling, G. C., Detection of PrPCWD in feces from naturally exposed Rocky Mountain elk (Cervus elaphus nelsoni) using protein misfolding cyclic amplification. *Journal of wildlife diseases* **2012,** *48* (2), 425-434.
39. Callender, J. A.; Sevillano, A. M.; Soldau, K.; Kurt, T. D.; Schumann, T.; Pizzo, D. P.; Altmeppen, H.; Glatzel, M.; Esko, J. D.; Sigurdson, C. J., Prion protein post-translational modifications modulate heparan sulfate binding and limit aggregate size in prion disease. *Neurobiology of disease* **2020,** *142*, 104955.
40. Pan, T.; Wong, B.-S.; Liu, T.; Li, R.; Petersen, R. B.; Sy, M.-S., Cell-surface prion protein interacts with glycosaminoglycans. *Biochemical Journal* **2002,** *368* (1), 81-90.
41. Buser, J.; Diesburg, S.; Singleton, J.; Guelig, D.; Bishop, J.; Zentner, C.; Burton, R.; LaBarre, P.; Yager, P.; Weigl, B., Precision chemical heating for diagnostic devices. *Lab on a chip* **2015,** *15* (23), 4423-4432.
42. Jeong, S.; Lim, J.; Kim, M.-Y.; Yeom, J.; Cho, H.; Lee, H.; Shin, Y.-B.; Lee, J.-H., Portable low-power thermal cycler with dual thin-film Pt heaters for a polymeric PCR chip. *Biomedical microdevices* **2018,** *20* (1), 1-8.
43. Imamura, M.; Tabeta, N.; Kato, N.; Matsuura, Y.; Iwamaru, Y.; Yokoyama, T.; Murayama, Y., Heparan sulfate and heparin promote faithful prion replication in vitro by binding to normal and abnormal prion proteins in protein misfolding cyclic amplification. *Journal of Biological Chemistry* **2016,** *291* (51), 26478-26486.
44. Grispen, J. E.; Ickenroth, M. H.; de Vries, N. K.; van der Weijden, T.; Ronda, G., Quality and use of consumer information provided with home test kits: room for improvement. *Health Expectations* **2014,** *17* (5), 741-752.